2009

CRITICAL ROLE OF CX40 CARBOXYLIC TAIL IN REDUCED ELECTRICAL COUPLING BETWEEN MICROVASCULAR ENDOTHELIAL CELLS IN SEPSIS

Mohammad F. Siddiqui

CRITICAL ROLE OF CX40 CARBOXYLIC TAIL IN REDUCED ELECTRICAL COUPLING BETWEEN MICROVASCULAR ENDOTHELIAL CELLS IN SEPSIS

(Spine title: Cx40 carboxylic tail and endothelial cell coupling during sepsis)

(Thesis format: Monograph)

by

Mohammad F. Siddiqui

Graduate Program in Medical Biophysics

A thesis submitted in partial fulfillment
of the requirements for the degree of
Master of Science

The School of Graduate and Postdoctoral Studies
The University of Western Ontario
London, Ontario, Canada

Abstract

Electrical coupling between endothelial cells of the inner surface of arterioles is required for the arteriolar conducted response that coordinates microvascular function along the vascular tree. Gap junction proteins, connexins (Cx), form inter-endothelial channels, which facilitate exchange of metabolites and electrical signals between cells. Our lab has reported that, among the connexins found in endothelial cells, Cx40 is the target protein responsible for lipopolysaccharide (LPS) - and hypoxia/reoxygenation (H/R)-induced reduction in electrical coupling between mouse microvascular endothelial cells (MMEC) was assessed. LPS is an initiating factor in sepsis and its effect could be aggravated by H/R present in septic tissue. Using electrophysiology the role of the Cx40 cytoplasmic carboxylic tail in LPS-, H/R-, and LPS+H/R-induced reduction in coupling between MMEC was assessed. LPS, H/R or LPS+H/R reduced coupling in WT cells and in Cx40 knock-out (KO) cells infected with adenovirus carrying Cx40 cDNA (AdV-Cx40). Reduction in coupling was larger after LPS+H/R than after LPS or H/R alone. No change in coupling was seen in Cx40KO cells and in Cx40KO cells infected with AdV-Cx40$_{\Delta 237\text{-}358}$ (Cx40 without its cytoplasmic carboxylic tail) or with AdV-Cx40$_{\Delta 345\text{-}358}$ (Cx40 without its tail tip). It is concluded that the Cx40 tail tip is crucial in Cx40 function during inflammatory conditions, including compromised arteriolar conducted response during sepsis.

Keywords: Electrical cell coupling in sepsis, lipopolysaccharide, hypoxia / reoxygenation, connexin40.

Acknowledgements

My special thanks to my supervisor, Dr. Karel Tyml, for his continuous support and encouragement in successfully seeing through this project of an extensive nature. I also would like to thank my co-supervisor Dr. Tom Forbes and advisory committee members, Drs. Richard Potter, Douglas Jones and Qingping Feng, that helped shaping up the work periodically.

I also would like to bring to notice all the people who, by sharing their expertise, contributed to the project as and when required. In doing so, I would like to acknowledge the efforts of Michael Bolon, who introduced to me the core techniques of electrophysiology and cell culture. Contributions of Dr. Tianqing Peng in assisting establish the adenoviral titration and infection protocols are considered crucial throughout the project. I would like to go further in thanking Fuyan Li for her help in genotyping and mice breeding and Hong-xing Wang for his role in the immunohistochemistry work. Moreover, I thank all the members of Dr. Tyml's lab for their useful discussions relevant to the research.

Finally, I would like to acknowledge my family, especially my wife, Sumaira, whom I am extremely grateful to for her enduring love and support. Needless to mention, my greatest source of inspiration and blessings have always been my dad, Dr. M.K.Hasnuddin Siddiqui and my mom, Mrs. Kausar Nishat Siddiqui.

Financial support was provided by the Heart and Stroke Foundation of Ontario.

Table of Contents

List of Figures

List of Tables

Citation List

ACh	Acetylcholine
ADP	Adenosine diphosphate
AdV	Adenovirus
AdV- β-gal	Adenovirus carrying β-gal
AdV-Cx40	Adenovirus carrying wild-type Cx40
AdV-Cx40$_{\Delta 237\text{-}358}$	Adenovirus carrying Cx40, truncated at position 236
AdV-Cx40$_{\Delta 345\text{-}358}$	Adenovirus carrying Cx40, truncated at position 344
ATP	Adenosine triphosphate
β-gal	Beta-galactosidase
bp	Base pairs
BSA	Bovine serum albumin
C- terminal / tail	Carboxylic terminal / tail
cAMP	Cyclic adenosine monophosphate
cDNA	Complementary DNA
CPE	Cytopathic effects
Ct	No. of cycles taken to cross a threshold of fluorescence in RT-PCR
Cx	Connexins
DMEM	Dulbecco's Modified Eagle's Medium
DSM	Dialyzed serum medium
E_m	Cell membrane potential
ΔE_m	Change in E_m

FBS	Fetal bovine serum
GJIC	Gap junctional intercellular communication
HEK293 cells	Cell line from human embryonic kidney
HEPES	N-[2-hydroxethyl]piperazine-N'-[2-ethane sulfonic acid]
H/R	Hypoxia followed by reoxygenation
IFU	Infectious unit (equivalent to PFU)
I/R	Ischemia followed by reperfusion
kDa	Kilo daltons
λ (lambda)	Space constant, length constant
LPS	Lipopolysaccharide
MΩ	Mega ohms
MAPK	Mitogen-activated protein kinase
MOI	Multiplicity of infection
MMEC	Mouse microvascular endothelial cells
mRNA	Messenger RNA
N- terminal	Amino terminal
NADPH oxidase	Nicotinamide adenine dinucleotide phosphate-oxidase
PBS	Phosphate buffered saline
PCR	Polymerase chain reaction
PFU	Plaque forming units
PKA	Protein kinase A
PKC	Protein kinase C
r_i	Intercellular resistance

R_m	Membrane resistance
RMEC	Rat microvascular endothelial cells
RNA	Ribonucleic acid
ROS	Reactive oxygen species
RT-PCR	Real-time PCR
Ser / S	Serine
TLR-4	Toll-like receptor 4
WT	Wild type

Chapter 1: Introduction

1.1 Gap junction intercellular communication in microvasculature

1.1.1 Vascular function in microcirculation:

Within the microcirculation, the distribution and magnitude of blood flow represent a coordinated interplay between arteriolar, capillary, and venular segments (Figure 1A) according to local and regional metabolic demand. Large variation in blood flow is required as the tissue needs change substantially in relation to cellular function (Pittman, 2005). Consequently, prerequisites for the delivery of large increases in oxygen and for the manifold enhancements of blood flow are a considerable capacity of the vessels to increase their diameter and coordinating mechanisms which serve to change vascular diameter simultaneously over large distances. Wide spread control of blood flow is modulated by resistance vessels, including arterioles and venules (Melander and Johansson, 1968; Secomb and Pries, 2002). Capillaries are thought to sense metabolic changes in their surroundings and transfer this information to the resistance vessels (Song and Tyml, 1993; Secomb and Pries, 2002). Endothelial cell-to-cell communication has been recognized as an important participant in this conducted response (Secomb and Pries, 2002).

The synchronized behavior of arterioles in the microcirculation is easily studied and appreciated by stimulating an isolated vessel *in vitro* or an arteriole in the microcirculation *in vivo* in a localized manner because such a focal stimulation does not only induce a dilation or constriction at the site of stimulation but also at remote distant sites (Segal and Duling, 1986; Emerson and Segal, 2000a; Dora et al., 2003). Such a response is termed conducted or ascending response although it spreads to up- as well as downstream sites. The distances covered by a

conducted response varies between tissues and eliciting stimulus but can reach up to several millimeters. The remote response could not be explained by direct diffusion, thus it was suggested that a signal could be transmitted along the vascular wall (Dietrich and Tyml, 1992). Whereas a small amount of norepinephrine (NE) to a capillary temporarily reduced the blood flow due to upstream constriction of the feeding arteriole (Dietrich, 1989), acetylcholine (ACh), could also elicit a remote response in a feeding arteriole (i.e., increased flow) when applied to a downstream capillary (Song and Tyml, 1993). The remote conducted responses are thought to rely on the spread of membrane potential from the site of agonist application through gap junctions connecting cells of the vessel wall (Gustafsson and Holstein, 1999). Electrical stimulation has been used to study conducted vasomotor responses in arterioles, but the pathways and modes of activation of the responses induced by electrical stimulation remain to be determined. In 1993, Song and Tyml proposed that signal communication along a capillary could be the result of the conduction of a receptor-mediated change in membrane potential. Based on direct electrophysiological measurement within the arterial wall, it has been demonstrated that the principal pathway of the conducted vasomotor response is propagation of hyper/depolarizing electrical currents along the endothelial cell (EC) layer of the blood vessel (Emerson and Segal, 2001; Yamamoto et al., 2001). Intercellular electrical coupling is mediated by gap junctions (Haefliger et al., 2004), which have a low electrical resistance (Goodenough et al., 1996; Kumar and Gilula, 1996).

1.1.2 Electrical coupling between endothelial cells:

All blood vessels are lined with an inner layer of endothelial cells that come into direct contact with the blood. The endothelial cell layer is surrounded by a layer of elastic lamina

which is not continuous and allows for the endothelial cells to come into contact with the smooth muscle layer below (Yamamoto et al., 2001). The endothelium may allow the spread of conducted dilations which travel further distances along the vessel than conducted constrictions that may rely on the smooth muscle as a conducting pathway. Conduction of signals between endothelial cells and smooth vessel cells is facilitated by the presence of gap junction channels (Figure 1B).The endothelial cell layer may provide a more efficient pathway because of the anatomical shape and the length of a single cell that may serve as a distinct pathway to coordinate vascular behavior (Haas and Duling, 1997).

The endothelial cell layer plays an important role in the coordinated response that matches blood flow to demand of the tissue. In a study using the hamster cremaster muscle, the application of ACh to the capillary network triggered vasodilation of the feeding vessel, resulting in increased perfusion of the capillary bed (Segal, 1991). Similarly, a study using rat mesentery arteries showed that constrictive responses are also conducted from the capillary network to the supplying arteriole in response to the application of epinephrine onto capillaries (Dietrich, 1989). Direct electrophysiological measurements have demonstrated that electrical currents travel through both the endothelial and smooth muscle cell layers (Welsh and Segal, 1998), but that electrical coupling between endothelial cells mainly underlies arteriolar conduction (Emerson & Segal, 2000a & 2001; Yamamoto et al., 2001). Further study of this phenomena showed that it is endothelial cells that govern smooth muscle cell tone. In isolated hamster feed arteries, it was found that hyperpolarization or depolarization of an endothelial cell (by current injection) caused either relaxation or constriction of smooth muscle cells resulting in dilation or constriction of the vessel (Emerson and Segal, 2000a). Not only was this seen locally, these signals were conducted along the blood vessels to points distal from the site of injection as well (Emerson and Segal,

2000a). Indeed, the importance of endothelial cells is underscored by studies on mouse cremaster muscle that showed that on selective disruption of endothelium, the conducted vasodilation in response to ACh was nearly abolished (Robin et al., 2004). However, when smooth muscle cell layer was damaged, hyperpolarization and vasodilation was conducted along the vessel without attenuation (Emerson and Segal, 2000b). It is also demonstrated that endothelium and smooth muscle are electrically coupled to each other by myoendothelial coupling (gap junctions present between endothelial cells and smooth vessel cells, Figure 1B) which plays a key role in coordinating vasomotor activity (Emerson and Segal, 2000a).

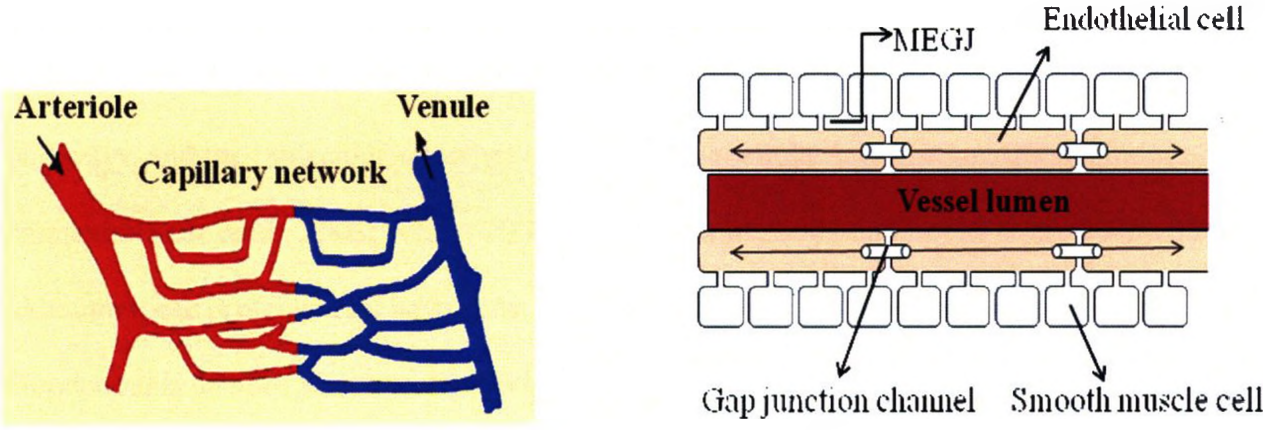

A B

Figure 1. **(A)** Network of microvascular blood vessels namely arteriole, capillary and venule. Arrow indicate direction of blood flow. **(B)** Endothelial cells lining inner surface of blood vessel and smooth vessel cells lying outer to endothelial cells. Gap junction channels present between endothelial cells, smooth vessel cells and inbetween both the cell type (myoendothelial gap junction-MEGJ).

1.1.3 Connexins – structure & expression:

The coordination of cellular events in tissues and organs is mediated by intercellular communication across gap junctions, tightly packed cluster of channels directly connecting the cytoplasm of adjacent cells (Figure 1C). Gap junctions are constructed of a multigene family of integral membrane proteins, the connexins (Cx) that provide a direct pathway for ions, second messengers, and small metabolites between cells and allow for electrical coupling (Paul, 1986; Bennett, 1994; Goodenough et al., 1996). Since Paul and colleagues cloned and sequenced the first connexin (Cx) Cx32 in 1986 (Paul, 1986), the connexin family has grown to 21 members in mammals (Willecke et al., 2002) and one cell type often expresses more than one connexin (Saez et al., 2003). However, the expression of several connexins in one cell is not redundant. Gap junctions are not just simple channels that offer a low-resistance intercellular pathway for exchange of small solutes. Rather, the connexins mediate specific cell-to-cell signaling pathways, and the molecular selectivity as well as subcellular localization differs among connexin (Saez et al., 2003; White, 2003; Figueroa et al., 2004 and Locke et al., 2005). Thus, although these proteins may have some overlap in function, they work in concert (Simon and Goodenough, 1998b; Simon and McWhorter, 2002; Figueroa et al., 2006; Haefliger et al., 2006) and in many cases the function of one connexin cannot be replaced by other connexin isoform (White, 2003; Haefliger et al., 2006; Wolfle et al., 2007 and Zheng et al., 2007). All vertebrate gap junctions are composed of connexins (Bruzzone, 1996) that are distinguished by molecular mass in kilo daltons (kDa) as predicted from their cloned cDNA. For example, a connexin with the predicted molecular mass of 40 kDa is referred to as Cx40.

The connexin protein has four transmembrane domains with two extracellular loops, one cytoplasmic loop and a cytoplasmic amino (N) and carboxylic (C) terminal region (Figure 1C)

(Saez et al., 2003; Evans et al., 2006). The transmembrane domains and the two extracellular loops are highly conserved among connexins with the cytoplasmic loop and C-terminal showing the greatest diversity (Simon and Goodenough, 1998). Six connexins form a connexon and when two connexons from adjacent cells dock together, they form a gap junction. Connexons not opposed by any other connexon are known as hemichannels. Connexons and hemichannels are predicted to have all six identical connexins (homomeric) or different connexins (heteromeric). Furthermore, two homomeric hemichannels join to form a homotypic channel and two heteromeric hemichannels join to form a heterotypic channel.

Connexins are synthesized mainly by membrane-bound ribosomes and are transported through Golgi apparatus (Laird et al., 1995) to the plasma membrane as connexons in membrane vesicles that transit along the cell's secretory pathway (Evans et al., 1999). Cx43 and possibly Cx46 do not appear to oligomerize into connexons while in the endoplasmic reticulum but most likely in the trans Golgi network (Musil et al., 1993; Koval et al., 1997). However, substantial evidence also exists that at least Cx32 and Cx26 can oligomerize within endoplasmic reticulum membranes (Falk et al., 1997; Falk and Gilula, 1998). To ensure the integrity of the compartments involved in connexin secretion connexons would be closed while retained within the Golgi apparatus and during their transport to the cell surface where they appear as hemichannels (Jordan et al., 1999). While cell surface hemichannels can be gated open (Harris, 2001), they are expected to primarily exist in a closed state. In co-ordination with intercellular adhesion (Jongen et al., 1991; Meyer et al., 1992), connexons from one cell would pair with connexons from a neighboring cell to form intercellular gap junction channels. These channels cluster to form tightly packed arrays of gap junction channels referred to as gap junction plaques. Formation and degradation of gap junctions is a very dynamic process with reports of half-lives

of less than 2h in cultured cells and tissues (Crow et al., 1990; Musil et al., 1990; Laird et al, 1995; Lampe, 1994; Beardslee et al., 1998). Therefore, the regulation of gap junction assembly and turnover is likely to be critical in the control of intercellular communication.

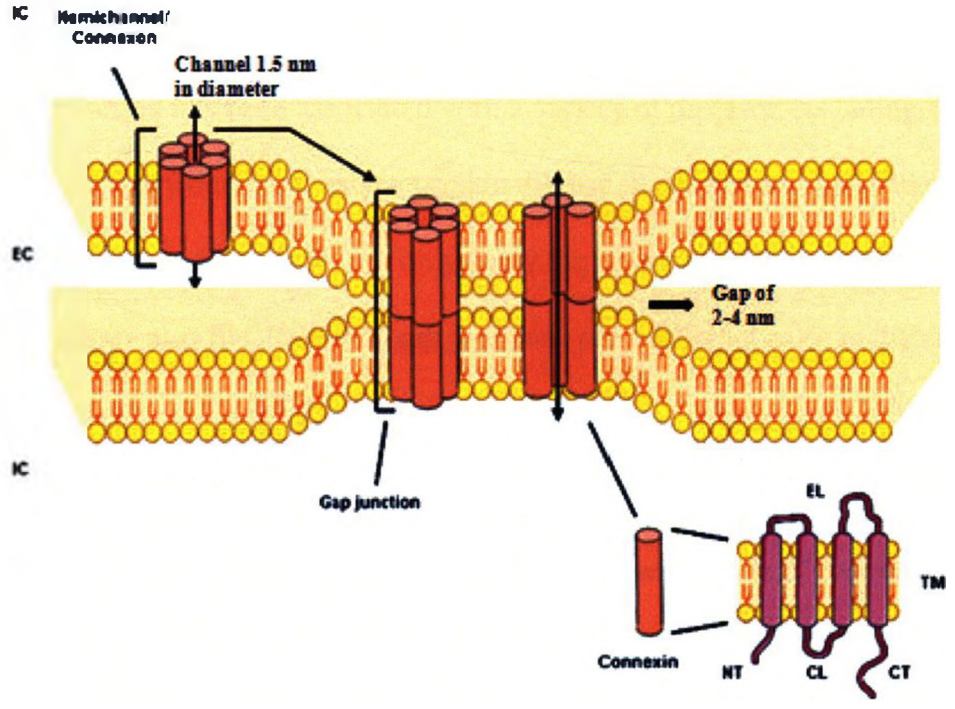

Figure 1C. Molecular architecture of gap junctions. Gap Junctions are grouped in plaques at the membrane surface of two apposed cells, and are composed of twelve connexin proteins, organized as two hexameric hemichannels. The connexin protein is organized as four membrane-spanning domains (TM1-4), two extracellular loops (EL1 and EL2), one cytoplasmic loop (CL), one cytoplasmic amino tail (NT) and one cytoplasmic carboxylic tail (CT) (EC, extracellular; IC, intracellular)
(Modified figure from: Decrock E. et al., *Cell Death and Differentiation,* (2009), **16,** 524–536).

Gap junctions composed of different connexin isoforms have unique permeability and conductance properties, allowing for the passage of molecules of specific size and charge (Elfgang et al., 1995; Valiunas et al., 2002). Connexins are differentially expressed in tissues with some being significantly expressed in only a few tissues and some, like Cx43, being more widespread. Gap junctions play significant regulatory roles in embryonic development, electrical coupling, apoptosis, differentiation, tissue homeostasis and metabolic transport in non-vascularized tissue (Willecke et al., 2002; Goodenough and Paul, 2003). Deficient or improper gap junction function has been associated with a variety of diseases, including some forms of neuropathy, hereditary deafness, cataracts, skin disease, heart disease, and cancer (Saez et al, 2003). These disparate phenotypes not only show the diversity of the expression pattern of connexins, but they also illustrate that gap junctions play different roles in different tissues.

1.1.4 Connexins in vasculature – significance of Cx40:

The vascular gap junctions are assembled from one or more of four connexin proteins: Cx37, Cx40, Cx43, and Cx45 (Severs et al., 2001; Evans and Martin, 2002; Figueroa et al., 2004; Haefliger et al., 2006). However, only three of these are expressed in adult mammalian vascular endothelium: Cx37, Cx40 and Cx43 (Larson et al., 1990; Bruzzone et al., 1993; Reed et al., 1993), and these are thought to play a key role in coordinating the behavior of smooth muscle and endothelial cells (Dora et al., 1997; Yashiro and Duling, 2000; Segal and Jacobs, 2001; Isakson and Duling, 2005). Connexin expression is also modified in a variety of pathologies, including hypertension and atherosclerosis (Davies et al., 2001; de Wit et al., 2003; Haefliger et al., 2004). Thus the expression patterns for connexins suggest that they may be involved in control of vascular function as well as the genesis of vascular diseases.

The expression of connexins in the vascular wall is dependent on vessel type and tissue. Cx40 and Cx37 are abundantly expressed in endothelial cells, whereas Cx43 and possibly to a lesser extent Cx45 are expressed in smooth muscle cells (van Kempen and Jongsma, 1999; de Wit et al., 2006b). The expression varies especially in arterioles and small arteries. In these vessels depending on their origin, Cx43 has been found in the endothelium and Cx37 in smooth muscle cells. Interestingly, in some vascular beds Cx43 cannot be found at all. Moreover, it suggests specific functions of different connexins within the vascular tree and possibly even within different organs. The function of gap junctional coupling in the vasculature has been suggested to control upstream regulation of vascular tone (de Wit et al., 2000). Consistent with the importance of gap junctions for the vascular homeostasis, it has been found that selective ablation of connexin genes results in severe vascular malformations. Cx45 knockout (KO) mice die at early embryonic stages and exhibit major defects in remodeling and organization of blood vessels (Kruger et al., 2000). In addition, these animals fail to form a smooth muscle layer surrounding the major arteries (Kruger et al., 2000). Deletion of Cx43 modifies the expression of many genes known to be involved in the differentiation and function of vascular cells, and cell-signaling pathways important for the regulation of vasculogenesis and angiogenesis (Walker et al., 2005), which produces several alterations in the pattern of coronary artery development, and the embryos die at birth of blockage of the right ventricular outflow tract (Reaume et al., 1995; Clauss et al., 2006). Although Cx40-deficient embryos exhibit small septational defects, deletion of one allele of Cx43 increases the cardiac malformations of Cx40KO mice and leads to neonatal death. In contrast, haplo- insufficiency of Cx40 did not affect the Cx43KO phenotype (Kirchhoff et al., 2000). Deletion of Cx37 is not lethal and has not been shown to produce any particular vascular phenotype. However, simultaneous ablation of Cx37 and Cx40 results in severe

vascular abnormalities in skin, testis, intestine, stomach, and lung, and the animals do not survive past the first postnatal day (Simon and McWhorter, 2002), which highlights the role of the endothelial cell–gap junction communication in the development of the vasculature. Taken together, these data indicate that individual connexin isoforms are differentially involved in vascular development and emphasize the notion that although these gap junction proteins may be co expressed, they basically work in concert.

The main focus of my study will be on Cx40 since Cx40 has been reported to play the central role in the conducted response (de Wit et al., 2000; Figueroa et al., 2003). Our lab has also discovered that Cx40 critically participates in the vascular pathophysiology during inflammation, since reduced electrical coupling between microvascular endothelial cells caused by lipopolysaccharide (LPS) or hypoxia / reoxygenation (H/R) was found to be Cx40 - dependent (Bolon et al., 2005 & 2007). Connexin40 has recently been suggested to be the key protein in the decrease in endothelial coupling following initiation of sepsis or hypoxia/reoxygenation. It has been shown in a mouse model of sepsis that decreased endothelial dye coupling correlated with decreased Cx40 protein expression at 18 h post-LPS (Simon et al., 2004). Additionally, recovery of impaired endothelium-dependent relaxation 12–24 h after the onset of sepsis correlated with increased Cx40 protein expression (Rignault et al., 2005). Cx40 was also shown to be solely responsible for more pronounced reduction in electrical coupling between mouse microvascular endothelial cells when simultaneously exposed to LPS and H/R and that also show that both protein kinase A (PKA) and protein kinase C (PKC) are involved in a signaling cascade that ultimately targets Cx40, with PKA acting directly on Cx40 (Bolon et al., 2008). Cx40 seems to play a key role in the control of microvascular network function, because deletion of Cx40 has been associated with irregular vasomotion (de Wit et al., 2003) and a

reduced conduction of vasodilator responses induced by ACh, bradykinin (de Wit et al., 2000, Wolfle et al., 2007), or electrical stimulation (Figueroa et al., 2003) in mouse cremaster arterioles. Recently, Cx40 was found to be essential for the efficient, nondecremental propagation of the vasodilator response activated by ACh (Figueroa and Duling, 2008). Also, Cx40-deficient mice display an elevated mean arterial pressure, suggesting that Cx40-depending gap junctional coupling is necessary to regulate vascular behavior and peripheral resistance (de Wit et al., 2006b).

1.2 Regulation of gap junctional channel conductance

Gap junction channels allow intercellular communication between contiguous cells in a tissue and half gap junction channels, or hemichannels, may permit direct communication between the cytoplasm and extracellular milieu. Gap junctional intercellular communication (GJIC) is driven by the passive diffusion of small (<1–1.5 kDa) hydrophilic molecules such as glucose, glutamate, glutathione, cyclic adenosine monophosphate (cAMP), adenosine triphosphate (ATP), inositol trisphosphate (IP3) and ions (e.g., Ca^{2+}, K^{+}, Na^{+}) (Alexander and Goldberg, 2003). The permeability of gap junction channels is acutely regulated in response to various stimuli, including protein phosphorylation / dephosphorylation, intracellular pH, calcium concentrations, voltage and also various chemicals. As channel close, cells uncouple from each other electrically and metabolically. Uncoupling is mainly a protective device for isolating healthy cells from damaged neighbours, but in some cells there is evidence for channel gating sensitivity to nearly physiological [Ca^{2+}], and [H^{+}], suggesting that modulation of channel permeability by these ions may be relevant to normal cell function as well (Peracchia et al., 2000).

1.2.1 Phosphorylation of connexins:

Protein phosphorylation is the primary means of switching the activity of a cellular protein rapidly from one state to another. Thus, protein phosphorylation is considered as being a key event in many signal transduction pathways of biological systems. Phosphorylation of substrate sites at serine, threonine or tyrosine residues is performed by members of the protein kinase family, the second largest family in the human genome. Protein phosphorylation is a fundamental regulatory cellular mechanism. Biochemically, this includes a transfer of a phosphate moiety from adenosine triphosphate (ATP) to the acceptor residue, thereby generating adenosine diphosphate (ADP). It is a post-translational event which normally occurs in either the cytosol or the nucleus of the cell. Protein kinases catalyze the phosphorylation events that are essential for the regulation of cellular processes like metabolism, proliferation, differentiation and apoptosis (Johnson et al., 1996 & 1998; Kolibaba and Druker, 1997; Hunter, 1998).

As an ubiquitous post-translation modification process, protein phosphorylation has proven to be a key mechanism in regulating the function of gap junction channels. Connexins have long been reported by many investigators to be regulated by numerous protein kinases, including those that phosphorylate serine, threonine and tyrosine residues (Lampe and Lau, 2004; Warn-Cramer et al., 2004). The activation of protein kinases (Tenbroek et al., 2001; Cottrell et al., 2003) and protein phosphatases (Warn-Cramer et al., 1998; John et al., 2003) have been correlated with a reduction or increase of junctional communication. Therefore, since those first reports (Kanno et al., 1984; Azarnia et al., 1988), it has been reasonable to speculate that phosphorylation induces channel gating. Gating has been defined as the mechanism by which the movement of ionic or non-ionic species becomes physically restricted due to the alteration of the molecular structure of the channel itself (Hille, 2003).

Many of the connexins not only contain consensus phosphorylation sequences for protein kinases, but have also been demonstrated to be phosphorylated by kinases in vitro and in some cases in cell culture or tissues. In addition, many connexins (Cx31, Cx32, Cx37, Cx40, Cx43, Cx45, Cx46, Cx50, and Cx56) have been shown to be phosphoproteins by either a shift in their electrophoretic mobility or direct incorporation of ^{32}P (Saez et al., 1998; Lampe and Lau, 2000). The carboxylic terminal region of the connexin proteins appears to be the primary region that becomes phosphorylated (Lampe and Lau, 2000). No reports of phosphorylation of the N-terminal region of connexins have been presented. However, Cx26 is the only connexin that has been reported to not be phosphorylated (Traub et al., 1989) which may be due to the fact that it is the shortest connexin and only has a few C-terminal tail amino acids after the fourth transmembrane domain that could interact with cytoplasmic signaling elements. Since Cx26 can form functional channels, connexin phosphorylation clearly is not necessary for the formation of gap junction channels.

Protein kinase activators and inhibitors have been used extensively to modulate and study gap junction function. However, it appears that the similar phosphorylating conditions can affect cells containing different connexins to a variable extent (Kwak et al., 1995). A brief overview on the phosphorylation of Cx32, Cx40, Cx43, and Cx45 is mentioned here as much of the current and past efforts to understand the importance of phosphorylation on connexin function have involved these four connexins.

Cx32 is phosphorylated *in vitro* by the serine/threonine protein kinases: cAMP-dependent protein kinase (PKA), calcium/calmodulin- dependent protein kinase, and PKC (Saez et al., 1998). PKC and PKA can phosphorylate ser233 *in vitro,* which is the only phosphorylation site that has been identified in Cx32 to date (Saez et al., 1990). Mutation of this site did not lead to a

change in the macroscopic conductance of gap junctions formed from the mutant protein expressed in *Xenopus* oocytes (Werner et al., 1991), but whether lack of this phosphorylation event affected events such as gap junction formation or turnover was not reported. Several studies have shown that increasing cAMP levels or treating cells with PKC activators increases the extent of Cx32 phosphorylation, which can affect channel properties (Saez et al, 1998).

Cx43 is the most widely expressed connexin in tissues and cell lines and, thus, it has received the most attention by investigators. Several phosphospecific antibodies against Cx43 have been developed thus helped revealing some specific roles of Cx43 phosphorylation in gap junction function. Several consensus sites for serine/threonine phosphorylation by protein kinases A, C, & G and Mitogen-activated protein kinase (MAPK) have been identified (Saez et al., 1993; Kwak and Jongsma, 1996; Lau et al., 1996; Warn-Cramer et al., 1998). Phosphorylation of Cx43 by tyrosine protein kinases mediates disruption of gap junction communication (Lin et al., 2006; Solan and Lampe, 2008). MAPK appeared to phosphorylate Cx43 directly in EGF (receptor tyrosine kinase) - treated cells (Kanemitsu and Lau, 1993). PKC-mediated phosphorylation of S368 in Cx43 is one major mechanism by which phorbol ester tumor promoter, TPA, which stimulates PKC, disrupts gap junctional communication (Martinez et al., 2002). Although purified PKA did not appear to phosphorylate Cx43 efficiently *in vitro* (Tenbroek et al., 1998), agents that upregulate endogenous cAMP levels generally resulted in an increase in gap junctional communication (Traub et al., 1987; Darrow et al., 1996). Therefore, like PKC, regulation of gap junctional communication by PKA will likely be a complex event that may involve multiple signal transduction cascades. However, Cx43 is a relatively poor substrate for PKA compared to PKC or MAPK (Shah et al., 2002; Yogo et al., 2002). Thus,

considerable evidence indicates that Cx43 is a highly phosphorylated and a highly regulated protein.

In Cx45, reagents that increased cAMP levels had no effect in HEK293 and BHK21 cells (Butterweck et al., 1994), but induced subtle effects on HeLa cells transfected with Cx45 (van Veen et al., 2000). Increasing cAMP levels appeared to increase Cx45 expression in neonatal rat ventricular myocytes (Darrow et al., 1996). Increased gap junctional communication in a pancreatic cell line expressing Cx45 was observed only when a functional cAMP-gated chloride channel (CFTR) was present (Chanson et al., 1999). Mouse Cx45 has 9 serine residues in the 23 amino acids of the C-terminus and mutation of all nine serine sites led to a reduced half-life of Cx45, which suggested a role for phosphorylation of some of these sites in the stabilization of the protein (Hertlein et al., 1998). Thus, phosphorylation of Cx45 may play a regulatory role in gap junctional communication.

1.2.2 Connexin 40 phosphorylation:

Cx40 is thought to have multiple phosphorylation sites for both PKA and PKC. On the basis of neural network study used to predict kinase-specific protein phosphorylation sites (Blom et al., 2004), Cx40 protein contains residues having consensus phosphorylation sequence for PKA. PKA activation has been shown to increase Cx40 phosphorylation and gap junctional conductance (van Rijen et al., 2000). Reduced PKA activity has been shown to dephosphorylate Cx40 and reduce inter-endothelial electrical coupling after hypoxia / reoxygenation (H/R) treatment (Bolon et al., 2005). Similar study has shown that lipopolysaccharide (LPS) reduced electrical coupling in mouse microvascular endothelial cells by targeting Cx40 in a tyrosine-, ERK1/2-, PKA-, and PKC – dependent manner (Bolon et al., 2007). Later study by Bolon (Bolon

et al., 2008) showed for the first time that phosphorylation of serine residues of Cx40 correlates with changes in coupling caused by experimental manipulation of the various components of LPS + H/R – induced signaling (protein tyrosine kinase, ERK1/2 inhibition, PKA activation/inhibition) (Bolon et al., 2008). Since activated PKA can phosphorylate Cx40 and subsequently increase Cx40 conductance, it is possible that baseline phosphorylation of Cx40 maintains the gap junctions in an open state via baseline PKA and PKC activation. LPS and hypoxia / reoxygenation (H/R) treatment reduces this activation and thus yields reduced Cx40 conductance. Thus, these studies suggest that the phosphorylation and dephosphorylation events triggered by various stimuli regulate gap junction permeability.

1.2.3 Carboxylic tail tale of connexins:

The carboxylic (C) - terminal, which varies significantly in both length and composition, is nearly unique to each type of connexin. The C-terminal regions of the connexins are thought to contain most of the regulatory and protein-protein interaction domains. For most connexins studied so far, the C - terminal is a substrate for specific kinases and/or protein partners, acting as a regulatory domain to modulate the activity of gap junction channels in response to appropriate biochemical stimuli (Duffy et al., 2002; Thomas et al., 2002). The carboxylic tail, which is located in the cytoplasm, contains multiple phosphorylatable serine, threonine, and tyrosine residues, and has been considered as an intrinsic part of the voltage and low pH gate for various gap junction channels. Therefore, if this domain is involved in the mechanism by which phosphorylation drives channels to gate, it is valuable to consider that phosphorylation-induced gating may be intrinsically linked to changes in the channel's molecular structure that reversibly affects permeability to ions or uncharged molecules. Moreover, alterations in the net charge of

connexin's C- terminal domain, induced by phosphorylation, could also modulate the kinetics of either voltage- or low pH-regulated gating.

Since the C- terminal region of connexin proteins contains the most pronounced sequence diversity among different connexins, as well as a large number of potential phosphorylation sites, it appears to be the primary region that becomes phosphorylated with the exception of Cx56 that can be phosphorylated within the cytoplasmic loop region, in addition to its C - terminal domain (Berthoud et al., 1997), and Cx26 which is the only connexin that has been reported as not to be phosphorylated for the formation of gap junction channel (Traub et al., 1989). This may be due to the fact that it is the shortest connexin and has a few C-terminal tail amino acids that could interact with cytoplasmic signaling domains.

A physiological example of the importance of the C-terminal domain of connexins was demonstrated by a Cx32 mutant that is truncated at position 219, resulting in the deletion of the C-terminus. Although this mutant Cx32 was functional when expressed in *Xenopus* oocytes, it has been associated with Charcot–Marie–Tooth disease (Rabadan-Diehl et al., 1994). Taken together, these studies suggest that the C-terminal domain of connexins, which contains multiple phosphorylation sites, functions as a vital regulatory element of not only channel gating, but perhaps, may also influence the rate of connexin trafficking and gap junction assembly and turnover.

Mice that are engineered to lack the C-terminus of Cx43 die shortly after birth (Maass et al., 2004), and removal of the C-terminal domain leads to prevention of PDGF (platelet-derived growth factor)-induced cell growth (Moorby, 2000). The critical influence of the C-terminal domain in Cx43 on channel function was illustrated by the expression of the truncated Cx43 mutant in *Xenopus* oocytes or SKHep1 cells, where the resulting channels exhibited different

permeability and electrophysiological properties than those formed by wild-type Cx43 (Dunham et al., 1992; Fishman et al., 1991). Moreover, the ability of the C-terminal domain to modulate the activity of gap junctions was evident in experiments demonstrating that the expression of the separate C-terminal region of Cx43 restored the ability of the v-src tyrosine kinase and cytoplasmic acidification to disrupt the activity of channels formed by truncated Cx43 in *Xenopus* oocytes (Dunham et al., 1992; Calero et al., 1998; Zhou et al., 1999). Several consensus sites for serine / threonine phosphorylation by protein kinases A, C, & G and MAP kinases have also been identified at the end of the carboxyl-terminus tail in Cx43 (Saez et al., 1993; Kwak and Jongsma, 1996; Lau et al., 1996; Warn-Cramer et al., 1998).

In Cx45, after exchange or deletion of nine carboxylic terminal serine residues, phosphorylation was decreased by 90%. When the C-terminus of Cx45 was truncated by 26 amino acid residues, the remaining protein was not transported to the plasma membrane. Moreover, phosphorylation of the double serine motif near the carboxylic terminus of Cx45 prevented accelerated degradation of mouse Cx45 protein (Hertlein et al., 1998).

Cx40 is thought to have multiple phosphorylation sites, having the consensus sequences for both PKA and PKC, in close proximity to each other in its carboxylic tail (Blom et al., 2004; Hjerrild et al., 2004). Later, Bolon et al has reported PKA - specific serine phosphorylation of Cx40 and its correlation to Cx40 gap junction conductance (Bolon et al., 2008). However, little work has been reported to determine the functional role of the carboxylic tail of Cx40 in the regulation of the gap junction intercellular communication.

1.3 Effect of lipopolysaccharide on cell coupling

1.3.1 Sepsis:

Sepsis describes a complex clinical syndrome that results from the host inability to regulate the inflammatory response against infection (Ulloa et al., 2009). It can be defined as a systemic inflammatory response to a local infection (Nguyen and Smith, 2007). Sepsis is considered an uncontrolled, unregulated, and self-sustaining intravascular inflammation, resulting from an imbalance between systemic proinflammatory reaction and excessive anti-inflammatory response. The former includes endothelial damage, microvascular dysfunction, impaired tissue oxygenation and multiple organ failure (Bauer, 2002). Here, impaired microvascular blood flow is critical in the development of this failure (Vincent and De Backer, 2005) and has therefore been extensively studied in animal models of sepsis (Cryer et al., 1987; Lam et al., 1994; Piper et al., 1996) as well as in humans (Boerma et al., 2007). Importantly, impaired microvascular blood flow results in episodes of micro-regional ischemia and reperfusion (I/R), i.e. intermittent capillary blood flow (Motterlini et al., 1998; Armour et al., 2001; Bateman et al., 2001), potentially aggravating the microvascular impairment.

Sepsis reduces arteriolar responsiveness to vasoactive stimuli (Wu et al., 2003; Lidington et al., 2007), and thus could contribute to the development of microvascular blood flow impairment. A key function of the arteriole is to control the hemodynamic resistance to blood flow via its ability to conduct electrical signals along its length (Welsh and Segal, 1998; Emerson and Segal, 2001; Tyml et al., 2001).

1.3.2 Lipopolysaccharide – a model for sepsis:

Endotoxin, lipopolysaccharide (LPS) is a major constituent of Gram-negative bacteria causing sepsis (Bone, 1991). LPS is termed as "endotoxin" because it is not actively secreted by bacteria into the surrounding environment. However, when bacterial cell lysis (e.g., during phagocytosis of bacteria or antibiotic – induced bacterial cell lysis) occurs, endotoxins are released and exert their deleterious effects on the host. With the wider understanding of the role of endotoxin (LPS) in the etiology of sepsis, the vast majority of research has focused on this bacterial product rather than other infection – related toxins. Once in the circulation, LPS can bind to LPS – binding protein (LBP) to form a complex. This complex then binds with high affinity to a monocyte/macrophage cell surface receptor, CD14. A transmembrane signal is then generated by a transmembrane protein resulting in cellular activation of NFkappa B and secretion of inflammatory cytokines. Soluble CD14 can also bind LPS/LBP and can thus activate endothelial cells, which do not express surface CD14 (Horn, 1998).

Activation of endothelial cells by LPS leads to altered endothelial function, including increased expression of adhesion molecules, cytoskeletal rearrangement and altered activity of various kinases (Yang et al., 1994; Arditi et al., 1995; Lidington et al., 2000; Peng et al., 2005; Rose et al., 2005; Bolon et al., 2006 & 2008). Significantly, many of these kinases have previously been associated with control of intercellular communication.

Several studies have reportedly used LPS to mimic the effect of sepsis. For example, as an *ex vivo* model of sepsis, human blood was stimulated with LPS to study the kinetics of proinflammatory cytokines (Ertel et al., 1995). LPS model of sepsis was also used in addressing the communication deficit in the skeletal muscle microvasculature during sepsis (Lidington et al., 2000). Mouse microvascular endothelial cells (MMEC) were treated with LPS to study the role

of connexin 40 in the reduction of electrical coupling between the cells during sepsis (Bolon et al., 2006 & 2008).

1.3.3 Inter-endothelial cell coupling response to lipopolysaccharide – role of Cx40:

Of the connexins found in the vasculature, there is evidence in the literature to suggest a key role for Cx40 in endothelial cell coupling after LPS treatment. Decrease in endothelial cell communication due to LPS was correlated with decrease in Cx40 protein expression (Simon et al., 2004). Recovery of compromised endothelium - dependent relaxation, in a model of sepsis, was found to be co-related to increased Cx40 protein expression (Rignault et al., 2005). It is also shown that Cx40 plays a key role in LPS-induced decrease in electrical coupling in mouse microvascular endothelial cells and that this decrease in coupling is tyrosine kinase-, ERK1/2-, PKC, - and PKA-sensitive (Bolon et al., 2007). LPS is also shown to cause serine dephospho-rylation of Cx40 in a PKA - dependent manner (Bolon et al., 2008).

1.4 Effect of hypoxia/reoxygenation (H/R) on cell coupling

1.4.1 H/R – as the basic elements of ischemia/reperfusion (I/R):

In context of this study, hypoxia can be defined as a deficit in atmospheric oxygen. In vivo, hypoxia may occur as a part of ischemia, cessation of blood flow within an organ, which results in a decrease in blood and tissue oxygen levels and build up of metabolic wastes. It is reported that acute ischemic episodes rapidly activate endothelial cells to release inflammatory mediators such as cytokines and thereby promote the recruitment and adherence of neutrophils to the endothelium (Michiels et al., 2000). This recruitment may ultimately prove fatal to these cells

due to the tissue damage that results from an intense inflammatory reaction (Pohlman and Harlan, 2000).

Reperfusion after ischemia induces a sequence of events ultimately leading to cellular damage and organ dysfunction. By definition, reperfusion injury begins after the restoration of oxygen and metabolic substrates to energy-deprived and metabolically perturbed tissue. A large body of experimental literature supports the notion of free radical-generated reperfusion injury when oxygen is reintroduced to ischemic tissue (Hess and Manson, 1984; McCord et al., 1985; Ambrosio and Tritto, 1999; Li and Shah, 2004). Excess formation of reactive oxygen species (ROS), including superoxide ion (O^{-2}), during reperfusion is usually associated with the term "oxidative stress" which was, perhaps, most appropriately redefined as "an imbalance between oxidants and antioxidants in favor of oxidants, leading to disruption of redox signaling & control and/or molecular damage" (Jones, 2006). Potential enzymatic sources of ROS include the mitochondrial respiration, arachidonic acid pathway enzymes lipoxygenase and cyclooxygenase, cytochrome p450s, xanthine oxidase, NADH/NADPH oxidases, nitric oxide synthase (NOS), peroxidases, and other hemoproteins (Hua and David, 2000).

Although each of the above-mentioned enzymes can produce ROS in vascular cells, it is generally recognized that NADPH oxidases are predominant sources of ROS in the vasculature (Kukreja et al., 1986; Mueller et al., 2005; Wolin et al, 2005; Wolin, 2009). The increase in ROS is thought to contribute to vascular dysfunction involving numerous signaling pathways, including activation / inactivation of certain enzymes. For example, H/R-induced increase in oxidative stress is reported to reduce PKA activity (Hastie et al., 1997; Bolon et al., 2005). In addition to the modulation of PKA activity, H/R has been shown to affect protein tyrosine kinase (PTK) and MAP kinase signaling (Seko et al., 1996; Zhang et al., 1999; Mottet et al., 2003).

1.4.2 Effect of hypoxia /reoxygenation on cell coupling – role of Cx40:

Gap junctions in endothelial cells that are exposed to hypoxia plus reoxygenation show various responses. Most importantly it has been observed that cells show reduced gap junctional communication - GJIC (Masamichi et al., 2000). Oxidative stress induced by the addition of oxygen radical generating agents decreased GJIC (Ruch and Klaunig, 1988; Brad et al., 1997). This decrease in communication is thought to be mediated by phosphorylation of the gap junction proteins (Oh et al., 1991) in response to oxidative stress, which appears to activate specific protein kinases in the endothelial cells (Barchowsky et al., 1994). H/R was shown to reduce interendothelial electrical coupling via increase in superoxide production and decrease in PKA activity (Bolon et al., 2005). In addition to the modulation of PKA activity, H/R has been shown to affect protein tyrosine kinase (PTK) and MAP kinase signaling (Seko et al., 1996; Zhang et al., 1999 & 2000; Mottet et al., 2003; Rose et al., 2005).

Connexin 40 was shown to participate critically in the vascular pathophysiology during inflammation, since reduced electrical coupling between microvascular endothelial cells caused by H/R was found to be Cx40 - dependent (Bolon et al., 2005). This reduction in coupling between microvascular endothelial cells after H/R was found to be associated with elevated ROS production and reduced PKA activity. In another study, H/R was shown to cause PKA – dependent serine dephosphorylation of Cx40, thereby, effecting the reduced communication between the cells (Bolon et al., 2008). Since Cx40 has been shown to have the highest conductance of the vascular connexins (Traub et al., 1994), it suggests that Cx40 plays the largest role in dictating the baseline inter-endothelial coupling and could be responsible for the effect of reduced coupling after H/R insult.

1.5 Effect of LPS+H/R on cell coupling

1.5.1 Clinical relevance of the study:

Microcirculation, the network of blood vessels <100 μm in diameter throughout the body, is an integrated functional system that is the principal site of oxygen transport from blood to underlying tissues and the chief regulator of tissue oxygen delivery to meet cellular oxygen demands. There is an abundant data that microcirculatory homeostasis is profoundly disrupted in sepsis, and microcirculatory failure is a hallmark of the septic state (Bateman et al., 2003, Trzeciak et al., 2008). Severe endotoxemic sepsis is characterized by inadequate tissue oxygenation and altered oxygen distribution, leading to reduced oxygen extraction in different organs (Lam et al., 1994; Ellis et al., 2002). Thus, impaired microvascular blood flow results in episodes of micro-regional ischemia and reperfusion (I/R) potentially aggravating the microvascular impairment. The pathogenesis of impaired oxygen extraction in septic states is related to a cascade of responses including capillary blockage by activated neutrophils and platelets, release of cytokines and vasoactive substances, and the consequent damage to the vascular tissue (Cipolle et al., 1993). Vascular endothelial cell injury and increased permeability caused by oxygen free radicals appear to be major determinants in organ dysfunction mediated by endotoxin.

1.5.2 Effect of LPS plus H/R on cell coupling – role of Cx40:

Oxidative stress, induced under a variety of conditions including I/R, is known to prime inflammatory cells for increased responsiveness to subsequent stimuli, such as LPS, leading to enhanced liberation of proinflammatory chemokines and cytokines (Khadaroo et al., 2003). Shock/resuscitation - induced oxidative stress in alveolar macrophages recovered from

resuscitated animals exhibited exaggerated LPS responsiveness with excessive generation of proinflammatory molecules (Powers et al., 2006; Cuschieri and Maier, 2007). Toll-like receptor 4 (TLR-4), a major upstream sensor for LPS, expression was upregulated following LPS and hemorrhagic shock

The scenario of "concurrent hit" involving an enhanced effect of I/R during sepsis has been recently examined (Bolon et al., 2008). This study showed, for the first time, that in a more physiologically relevant model of sepsis, where mouse microvascular endothelial cells were simultaneously exposed to LPS and H/R, the reduction in electrical coupling was significantly more pronounced than reduction following H/R or LPS stimulus alone. It was further demonstrated that this pronounced reduction depends solely on the gap junction protein Cx40 and that both PKA and PKC are involved in a signaling cascade that ultimately targets Cx40. PKA was found to act directly on Cx40 since following LPS+H/R treatment, both total serine residues and PKA-substrate-dependent serine residues on Cx40 were dephosphorylated, but the PKC-dependent-serine residues were not. Since a prominent feature of sepsis seen at the tissue level is impaired capillary blood flow, including micro-regional H/R, the study suggests that LPS+H/R lead to synergistic impairment of vascular function.

Chapter 2 : Rationale, Hypothesis and Objectives

2.1 Rationale of thesis

Regulation of blood flow distribution depends on the well-integrated regulation of vasomotor tone along the length of arterioles and on the coordination of different microvessel segments (de Wit et al., 2000; Figueroa et al., 2003). Vascular endothelial cell coupling plays an important role in the conduction of vasomotor responses in both arterioles and arteries (Segal, 2005). This conducted vasomotor responses have been associated with the propagation of electrical signals (Figueroa et al., 2003), usually attributed to electrotonic spread of changes in membrane potential via gap junctional connection between adjacent cells (Gustafsson and Holstein-Rathlou, 1999). Gap junction protein, Cx40, which is predominantly located in the endothelial cells (Gabriel and Paul, 1998; van Kempen and Jongsma, 1999), seems to play a key role in the control of microvascular network function (de Wit et al., 2003; Wolfle et al., 2007; Figueroa and Duling, 2008).

Sepsis not only involves primary signaling of LPS, an initiating factor of sepsis, but also H/R signaling as compromised microcirculation in sepsis is associated with micro-regional I/R (De Backer et al., 2002). Our lab has reported that LPS, H/R and LPS+H/R treatments reduced electrical coupling between mouse microvascular endothelial cells (MMEC) and that Cx40 stands out as a target gap junction protein in their signaling pathways (Bolon et al., 2005, 2007 & 2008 respectively). According to these findings, the reduction in intercellular coupling (increase in intercellular electrical resistance) between MMEC subjected to H/R and /or LPS is Cx40 dependent and that this reduction is associated with reduced PKA/PKC activity and PKA-dependent serine dephosphorylation of Cx40. Others have also shown that PKA activation

increases both Cx40 gap junctional conductance and Cx40 phosphorylation (van Rijen et al., 2000).

It has also been shown that PKA/PKC consensus sequences where phosphorylation could occur are present in close proximity to each other in the carboxylic tail of Cx40 (Blom et al., 2004; Hjerrild et al., 2004). Therefore, it is possible that baseline phosphorylation of Cx40 maintains the gap junction in an open state via baseline PKA/PKC activation (Bolon et al; 2005), and that H/R- and/or LPS-induced signaling closes Cx40 gap junctions via dephosphorylation of one or more of the 17 serine residues present along the carboxylic tail of Cx40, composed of residues 236 – 358. The rationale for my thesis is to address this possibility.

2.2 Hypothesis and Objectives

2.2.1 Hypothesis 1:

Carboxylic tail of intracellular domain of Cx40 is involved in the reduced inter- endothelial cell electrical coupling after LPS treatment.

Rationale: Cx40 is known to be directly involved in the reduction of interendothelial cell electrical coupling under the effect of LPS, an initiating factor of sepsis, and that this response is correlated to PKA/PKC activity (Bolon et al., 2007) and PKA-dependent serine dephospho-rylation (Bolon et al, 2008). Since it is also known that potential phosphorylation sites with consensus sequences for PKA/PKC is predicted to be present in the carboxylic tail of Cx40 (Blom et al., 2004; Hjerrild et al., 2004), it is very likely that serine residue/s present along the carboxylic tail (residues 236-358), could be the potential target in the LPS-induced reduction of intercellular electrical coupling. Moreover, as the end region of the Cx40 carboxylic tail

(residues 345-358) is more serine- rich (5 out of 14 residues) than the remaining tail (12 out of 108 residues), the likelihood of finding the target serine residue/s in this region, hence, increases. Therefore, along with wild-type Cx40 (Figure 2), I proposed to investigate on Cx40 with its carboxylic tail deleted, separately, at positions 236 (devoid of residues 237-358, deletion 1; Figure 3) and 344 (devoid of residues 345-358, deletion 2; Figure 4). Functional response to the deletion 1 will indicate the target serine residue/s to be present in the tail region, whereas response elicited by deletion 2 along with that of deletion 1 will indicate their presence in the end region of the carboxylic tail. But, if the response is elicited in deletion 1 but not in deletion 2, then this will indicate the target serine residue/s to be present in-between position 237-344.

Objectives:

I. To establish an infection procedure to deliver adenovirus (AdV) carrying Cx40 cDNA into mouse microvascular endothelial cells.

II. To infect endothelial cells obtained from Cx40KO mice, with AdV carrying wild type Cx40 (AdV-Cx40), with AdV carrying Cx40 with carboxylic tail residues deleted from 237 to 358 (AdV-Cx40$_{\Delta 237\text{-}358}$), and with AdV carrying Cx40 with carboxylic tail residues deleted from 345 to 358 (AdV-Cx40$_{\Delta 345\text{-}358}$).

III. To examine Cx40 protein expression in infected endothelial cells by using immuno-cytochemistry.

IV. To determine electrical coupling in wild type, Cx40KO, and infected Cx40KO cells exposed to LPS by electrophysiological technique.

2.2.2 Hypothesis 2:

Carboxylic tail of intracellular domain of Cx40 is involved in the reduced interendothelial cell electrical coupling after H/R treatment.

Rationale: It is known that during sepsis compromised microcirculation is associated with episodes of I/R (De Backer et al., 2002). It is also known that H/R, basic elements of I/R, reduce intercellular electrical coupling. For example, H/R - induced reduction in coupling is reported both in HUVEC (Zhang et al, 1999, 2000a & 2000b) and rat cortical astrocytes (Martinez et al., 2000). Subsequently, our laboratory reported similar outcome in rat microvascular endothelial cells (Rose et al., 2005) as well as mouse microvascular endothelial cells (Bolon et al., 2005). Bolon et al also showed that this reduction in coupling after H/R is via oxidant - and PKA - dependent signaling that targets Cx40. Others have also shown that PKA activation increases both Cx40 gap junctional conductance and Cx40 phosphorylation (van Rijen et al., 2000). More recently our lab has shown PKA-specific serine phosphorylation of Cx40 (Bolon et al., 2008). Based on these findings and the neural network studies (Blom, 2004; Hjerrild, 2004) that predicted PKA - specific phosphorylation sites to be in the carboxylic tail of Cx40, I sought to investigate the role of Cx40 carboxylic tail with respect to the serine residue/s as potential target therein. Although the effect of H/R on intercellular electrical coupling and PKA-dependent phosphorylation status of serine is similar to that of LPS, the serine residues targeted by H/R-induced signaling may be different than in the case of LPS. Therefore, the strategy of testing Cx40 with its carboxylic tail separately deleted at positions 236 and 344, for the reasons as discussed in the case of LPS, was adopted.

Objectives:

I. To infect endothelial cells obtained from Cx40KO mice, with AdV carrying wild type Cx40 (AdV-Cx40), with AdV carrying Cx40 with carboxylic tail residues deleted from 237 to 358 (AdV-Cx40$_{\Delta 237\text{-}358}$), and with AdV carrying Cx40 with carboxylic tail residues deleted from 345 to 358 (AdV-Cx40$_{\Delta 345\text{-}358}$).

II. To determine electrical coupling in wild type, Cx40KO, and infected Cx40KO cells exposed to LPS by electrophysiological technique.

2.2.3 Hypothesis 3:

Synergistic reduction of interendothelial cell electrical coupling after LPS+H/R treatment occurs in Cx40KO cells infected with Adv-Cx40 .

Rationale: Oxidative stress is known to prime inflammatory cells for increased responsiveness to subsequent stimuli, such as LPS. An aggravated effect has been shown for the "two-hit" scenario of circulatory shock followed by infection, where I/R-induced oxidative stress primes/enhances the innate immune response (Khadaroo et al., 2003; Powers et al., 2006). In a model of sepsis involving both LPS and H/R, our lab has recently reported that that concurrent LPS+H/R results in a significant decrease in microvascular endothelial cell communication and that Cx40 is most likely the sole target connexin (Bolon et al., 2008). This study further demonstrated, for the first time, that this decrease in coupling is due to the direct PKA-dependent serine dephosphorylation of Cx40. Moreover, based on neural network it was predicted that PKA substrate is present in the carboxylic tail of Cx40 (Blom et al., 2004; Hjerrild et al., 2004). These

findings, in combination, provide a solid ground to investigate the potential role of the carboxylic tail of Cx40 in gap junctional conductance under the influence of LPS+H/R.

Objectives:

I. To infect endothelial cells obtained from Cx40KO mice, with AdV carrying wild type Cx40 (AdV-Cx40).

II. To determine electrical coupling in wild type, Cx40KO, and infected Cx40KO cells exposed to LPS+H/R by electrophysiological technique.

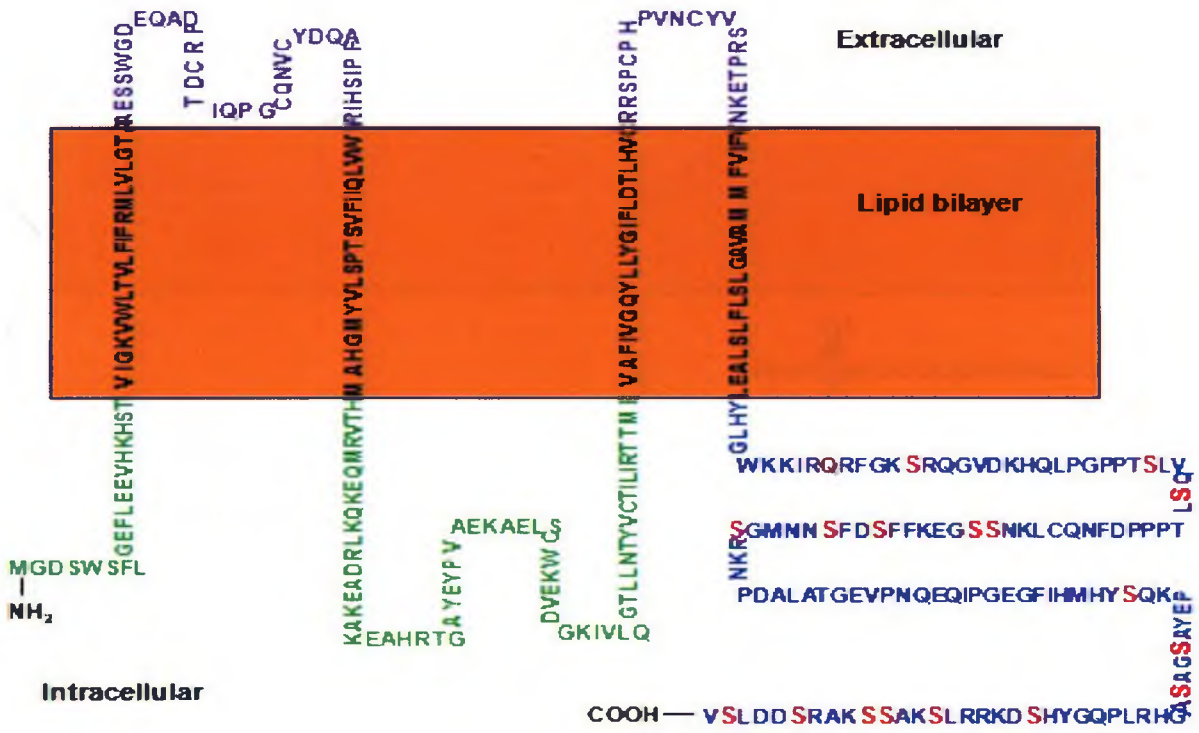

Figure 2. Schematic representation of the primary structure of the mouse Cx40 protein showing all the 358 residues. The intracellular folding of Cx40 is drawn arbitrarily. Serine residues present in the carboxylic tail (residues 236-358) are marked in bold red.

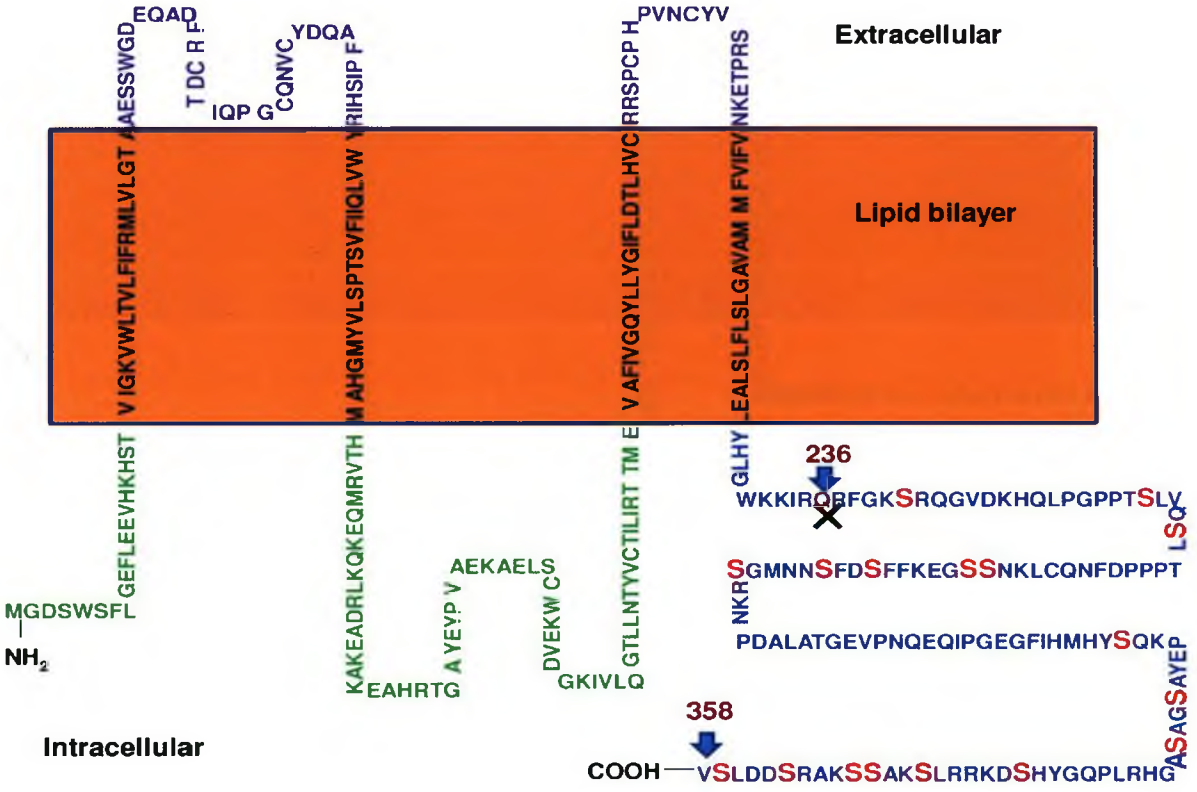

Figure 3. Schematic representation of primary structure of Cx40 protein indicating the site of deletion of its carboxylic tail at residue 236. The missing portion of Cx40 (residues 237-358) have 108 residues including 12 serine residues, marked in bold red.

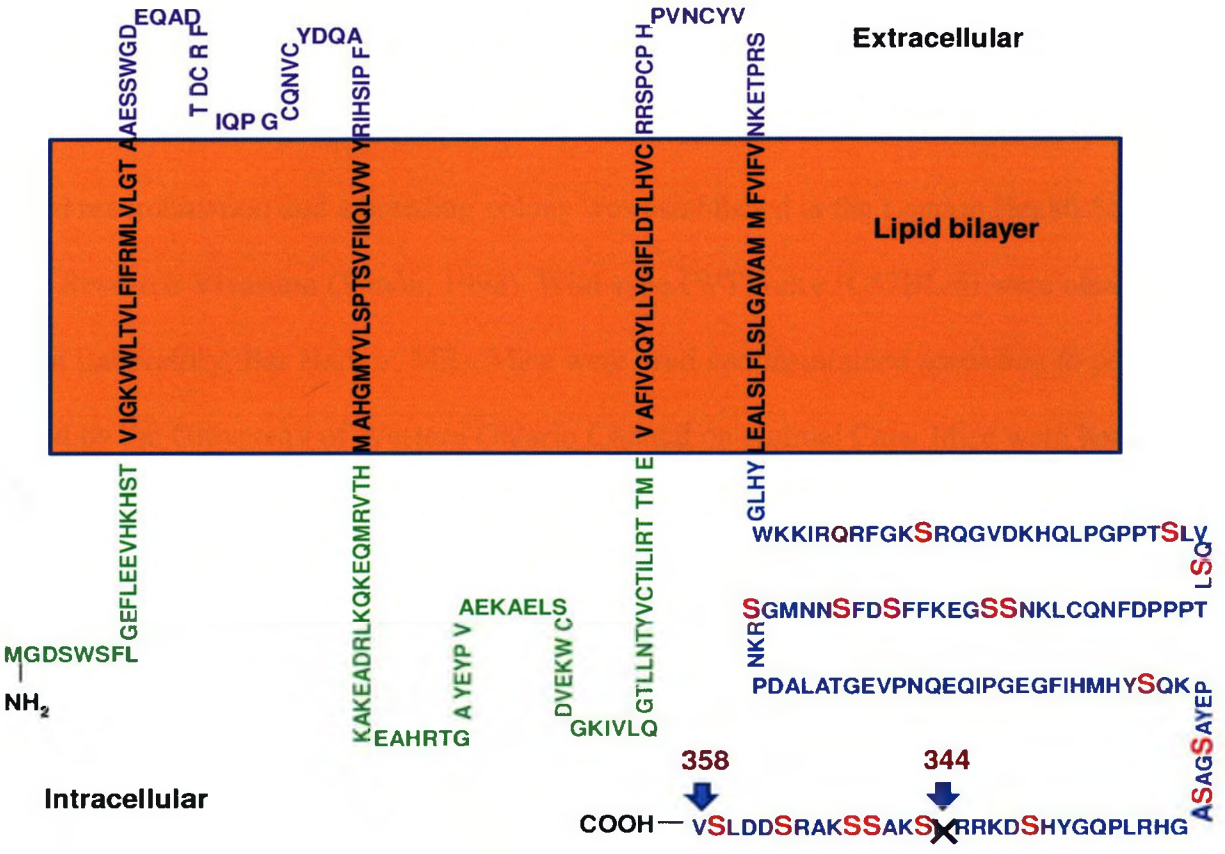

Figure 4. Schematic representation of primary structure of Cx40 protein indicating the site of deletion of its carboxylic tail at residue 344. The missing portion of Cx40 (residues 345-358) have 14 residues including 5 serine residues, marked in bold red.

Chapter 3 : Materials and Methods

3.1 Genotyping

The Cx40 knockout mouse (*Gja5* $^{-/-}$) was created in Dr. D. Paul's laboratory using targeted recombination and a breeding colony was established at the London Health Sciences Center Research Vivarium (Simon, 1998). Wild-type (WT) mice (C57BL/6) were obtained from Jackson Laboratory, Bar Harbor, ME). Mice were bred and maintained according to policies outlined by the University of Western Ontario Council on Animal Care. Mice were housed in shoebox cages with 1-5 mice per cage in a room kept at 23 °C with 14 hours of light and 10 hours of dark and had unlimited access to food and water. For this study, male littermates (progeny of heterozygous (*Gja5*$^{+/-}$) parents) between the ages of 2-6 months were used after two generations of backcrossing with C57BL/6.

For the purpose of genotyping, a 0.5 cm tail clipping taken from individual mice was placed in 200 µl tail lysis buffer (100 mM Tris-HCl (pH8.5)/ 5 mM ethylenediaminetetraacetic acid (EDTA)/ 0.2% sodium dodecyl sulphate (SDS / 200Mm NaCl) containing 5µl of 0.1 mg/ml proteinase K (Sigma-Aldrich Canada Ltd., Oakville, ON) and heated at 56 °C overnight. Samples were subsequently heated to 95 °C for 5 minutes, centrifuged at 12000g for 10 minutes and supernatant was collected. Genotype was determined by polymerase chain reaction (PCR) applied to proteinase K-digested tail snips. A 270 base pair (bp) amplicon of the wild type allele was amplified using the primer sequence 50-TCT CTG ACT CCG AAA GGC AAG-30 (50 primer) and 50-TGG AGC CAC AGT TGC AAT GGT-30 (30 primer, from the region not targeted for deletion). In order to identify the knockout allele, a 50 primer to the neomycin resistance gene (which replaces the Cx40 coding region in the knockout) 50-GCA CGA GAC

TAG TGA GAC GTG-30 and the wild type -30 primers were used, resulting in a 470 bp amplicon. Each PCR mixture contained 20 mM Tris–HCl pH 8.4, 50 mM KCl, 3 mM $MgCl_2$, 0.2 mM dNTP's, 0.125 IU JumpStart^{TM} Taq Polymerase, 1 pM of all primers, 10% glycerol, 44% H_2O and 1ml tail clipping DNA solution in a 25-ml volume (Invitrogen Canada, Inc., Burlington, ON). The PCR was performed using a thermocycler (Eppendorf Mastercycler Gradient) programmed to these specifications: 94 °C for 10 minutes, followed by 30 cycles of 94 °C for 30 sec, 64 °C for 30 sec and 72 °C for 30 sec. The last (30^{th}) cycle was followed by 4-minutes soak at 72 °C. Samples were cooled to 4 °C and stored at -20°C until gel loading.

PCR products were size separated in 6% gel consisting of polyacrylamide (30% acrylamide/0.8% bisacrylamide stock), 10% (w/v) ammonium persulfate (APS), 0.05% (v/v) N,N,N', N –tetramethylethylenediamine (TEMED) (acrylamide, APS, and TEMED from Sigma-Aldrich, Canada Ltd., Oakville, ON), buffered in 50 × tris-actate EDTA (TAE: 89 mM tris base/89 mM glacial acetic acid/0.5M EDTA). Following electrophoresis for 2 hours at 90 V, gels were soaked for 5 minutes in 1μg/ml ethidium bromide in TAE. Cx40KO alleles were identified as one band at ~470 bp, whereas, WT alleles were identified as one band at ~270 bp. For heterozygous Cx40-deficient, both bands appeared simultaneously at ~270 bp and ~470 bp.

3.2 Isolation and culture of mouse microvascular endothelial cells (MMEC)

Protocol for isolation of MMEC, based on the procedure as previously described (Lidington et al., 2000, Bolon et al., 2005, 2007 & 2008), was approved by the Animal Use Subcommittee of the Council on Animal Care at the University of Western Ontario. *Griffonia simplicifolia* lectin (GS-I lectin; Sigma) was bound to Dynabeads (M-450, uncoated; Dynal). Approximately

1×10^8 beads were washed in 0.1 M borate buffer (pH 9.5) and rotated for 24 hours with GS-I lectin (0.2 mg/ml in 0.1 M borate buffer) at 4 °C. The beads were then washed and stored in phosphate buffer saline (PBS) containing 0.1% bovine serum albumin (BSA).

Mice weighing between 18-25 gm were anaesthetized with ketamine (80 mg/kg) plus xylazine (4mg/kg). Hind limb muscle of mice was excised and cut into ~0.5 mm fragments. The muscle fragments were digested in an enzyme solution containing trypsin (0.12 mg/ml; Sigma), collagenase (0.84 mg/ml; Sigma), bovine serum albumin (1.62 mg/ml; Sigma) and dispase (0.14 U/ml; Invitrogen) in Kreb's buffer (127mM NaCl, 4.6 mM KCl, 1.1 mM anhydrous $MgSO_4$, 1.2 mM KH_2PO_4, 8.3 mM D-glucose, 2mM pyruvate, 1.49mM creatine, 20mM taurine, 5mM D-ribose, 2 mM L-asparagine, 2mM L-glutamine, 1mM L-arginine and 0.5 mM uric acid in Millipure water). The digest solution taken in chambers was bubbled with 95% O_2 / 5% CO_2 at 37 °C for 30 minutes. After digestion, the solution was filtered through 100 µm mesh to remove undigested fragments. The filtrate was then washed with Dulbecco's Modified Eagle's Medium (DMEM, Sigma) base medium, pelleted by centrifugation and plated. The cells were grown in DMEM/F12 Ham nutrient supplemented with 20% fetal bovine serum (FBS; Sigma), endothelial growth supplement (50 µl/ml; Sigma), heparin (5U/ml; Leo Laboratories, Ajax, ON), L-glutamine (Gibco; Mississauga, ON) and antibiotic-mycotic solution (10 µl/ml, containing penicillin, streptomycin, amphotericin B, penicillin G1, and streptomycin sulfate (Gibco) at 37 °C in water-saturated air containing 5% CO_2.

Cells were grown to confluence (3-7 days), then lifted with trypsin-EDTA (purchased as 10×trypsin-EDTA and diluted to 4× in DMEM basal solution; Gibco), resuspended with ~1×10^8 GS-I coated Dynabeads in culture medium, and rotated for 10 minutes. The GS-I coated

magnetic beads, to which the endothelial cells were bound, were collected using a magnetic particle concentrator (Dynal, Lake Success, NY).

Once the collected endothelial cells reached confluence (3-7 days), they were passaged using 4× trypsin-EDTA. After 5-6 passages, the concentration of FBS in the medium was reduced from 20% to 5%. For electrophysiological experiments, monolayers of endothelial cells were grown on the12 mm diameter glass coverslips (VWR International; Mississauga, ON). Cells were used between passages 6 and 15, during which they maintained their phenotype (Bolon et al., 2008).

3.2.1 Endothelial Cell Characterization:

Endothelial cell phenotype was confirmed by the observation of von Willebrand Factor VIII as described previously (Wilson et al., 1996), showing purity near 100%.

Von Willibrand Factor VIII

Cold (-20 °C) methanol was applied to MMEC monolayers grown on glass coverslips. After 15 minutes, monolayers were rinsed 3 times with Dulbecco's phosphate buffered saline (PBS; Sigma). Monolayers were treated with 1% H_2O_2 in PBS for 15 minutes to remove exogenous peroxidase activity. The cells were blocked with 3% goat serum (in PBS) for 30 minutes and then incubated with rabbit anti-human von Willibrand factor VIII (1:100 in PBS; Sigma) for 2 hours at room temperature. Monolayers were rinsed 3 times with PBS and then incubated with horseradish peroxidase (HRPO)-conjugated goat anti-rabbit IgG antibody (1:100 in PBS; Sigma) for 1 hour. After washing, the cells were incubated with 3, 3-diaminodenzidine (DAB) solution

(0.06% DAB in PBS containing 0.012% H_2O_2; Boehringer Mannheim) until colour developed (1-5 minutes). The coverslips were mounted and examined under light microscopy.

3.3 Infecting endothelial cells using adenovirus

Adenovirus infection method was adopted to re-introduce Cx40 cDNA into Cx40 knock-out endothelial cells via recombinant adenovirus vector. Adenovirus carrying β-Gal (β-galactosidase) was also used as a negative control. Adenovirus is extensively used for the construction of vector systems because of its great packaging capacities, broad range of target cell infection, efficient viral infection and gene transfer (Walther and Stein, 2000). Our laboratory has previously attempted to transfect MMEC with Cx40 cDNA. Since this procedure yielded low transfection efficiency, the adenovirus infection approach was used instead.

3.3.1 Production of recombinant adenovirus:

Recombinant adenoviruses were cloned and supplied by Applied Biological Material Inc. (ABM; Richmond, B.C). Constructs of adenovirus carrying wild type Cx40 (Adv-Cx40), Cx40 with deleted carboxylic tail residues from 237 to 358 (AdV-$Cx40_{\Delta 237\text{-}358}$), Cx40 with deleted carboxylic tail residues from 345 to 358 (AdV-$Cx40_{\Delta 345\text{-}358}$) and β-gal (Adv-βgal) were produced by ABM Inc. with the titer value of 1×10^6 plaque forming units (pfu) / ml and stored in DMEM with 2.5% glycerol. On arrival at our facility, 2-3 aliquots of these viruses were made, properly labeled and discreetly stored at -80 °C. To carry out MMEC experiments with these viruses, the limited amount of virus supplied by ABM had to be amplified, purified and titrated in our laboratory.

3.3.2 Adenovirus amplification in HEK293 cells:

Human embryonic kidney 293 cells (HEK293) are used as host cells for viral amplification. These cells perform the production of recombinant virus stocks and generation of infectious viral particles by providing the essential *E1A* protein for efficient viral encapsidation (Graham et al., 1977). *E1A* gene is essential for virus replication and is deleted during the modifications of the adenoviral genome to create replication incompetent vectors (Steinwaerder et al., 2000). The HEK 293 cells are particularly suited as a packaging cell line as they are easy to transfect and produce high virus titers.

The procedure involved in the amplification of adenovirus was based on the instructions and guidance of Dr. Tianqing Peng, an expert in recombinant adenovirus production, handling and usage.

Phase I amplification in T25 flask: HEK293 cells were passaged regularly 2-3 times in 10% FBS in DMEM (293 media), prior to infection. These cells were cultured until the monolayer was 70% - 80% confluent. Subsequently, the cell culture media was replaced with 2-3 ml of new media in a T25 flask, to which 75 µl of crude viral stock was added. After 2 hours, culture was supplemented with additional 2-3 ml of 293 media. This optimum volume of the virus used was reached after a few trial experiments, as it was found to be sufficient for the cells to demonstrate the cytopathic effect (CPE) after 48 hours of infection. The CPE on adenovirus infected 293 cells causes rounding & swelling of cells and loss of cell-to-cell contact. During next 24 - 48 hour progress of infection was examined in short intervals. As the CPE was found to be nearly complete (i.e. most cells rounded but not yet detached from the flask), the cells were harvested cells by pipetting media in and out to thoroughly suspend the infected cells into the media. To achieve the maximal yield during the purification, it is critical to harvest the infected 293 cells

when most of the cells show cytopathic effects but not yet detached from the flask. Infected cells along with the medium were pelleted by centrifugation at 1000 g for 5 minutes and the supernatant was collected. The cells were lysed by three freeze/thaw cycles, to release the virus, and centrifuged at 3000 g for 10 minutes to pellet the cell debris. The pellet was discarded and the supernatant was saved for phase II amplification. If a large amount of cell debris was still visible, the supernatant was re-centrifuged.

Phase II amplification in T75 flasks: HEK293 cells were grown as monolayers in four T75 flasks in 293 culture media. The cells were cultured until the monolayers were ~ 60-70% confluent. The 293 cell culture media was then replaced with new media, 15ml per flask, to which 1 ml of viral supernatant, obtained in phase I amplification, was added to each of the T75 flask. 293 cells started to show the cytopathic effect (CPE) after 72 hours of infection. The morphological changes in adenovirus-infected 293 cells are same as discussed in phase I amplification procedure. During 3^{rd} to 5^{th} day post-infection, the monolayer was examined three to four times a day the CPE. Near the completion of the CPE, when the cells were rounded but not yet detached, the cells were harvested along the medium. Infected cells from all the four T75 flasks were pooled along with the medium and were pelleted by centrifugation at 1000 g for 5 minutes. All but 15 ml of the supernatant was discarded. The virus was released from the cells by three freeze/thaw cycles and centrifuged at 3000 g for 10 minutes to pellet the cell debris. The pellet was discarded and the supernatant was saved. If a large amount of cell debris was still visible, the supernatant was re-centrifuged. This viral supernatant was stored at -80°C until purified.

3.3.3 Adenovirus purification:

The concentrated viral supernatant obtained in phase II of amplification needed to be be purified to separate the virus from the cellular proteins and media components. This was achieved by using ViraBind™ Adenovirus Purification Mega Kit, supplied by Cell Biolabs, San Diego, CA (Catalog # VPK-101). Special purification filters to adsorb viral particles, 10 × wash buffer and 1 × elution buffer (25 mM Tris, pH 7.5, 2.5 mM $MgCl_2$, 1M NaCl) were also included in the kit along with the purification protocol.

Prior to application of the viral supernatant to the purification filter, the supernatant was clarified by passing through a 0.45 µm sterile filter. A syringe was attached to the purification filter, and 15 ml of 1× Wash Buffer was added to pre-rinse the filter. Slowly the viral supernatant was allowed to pass through the purification filter by gravity flow, and the flow-through was saved. To ensure maximal recovery, the flow-through was passed through the same filter again. When the flow through noticeably slowed down during loading viral sample or reapplying the first flow-through for the second time, gentle pressure was applied with syringe plunger. To ensure maximal virus binding, I tried to keep the flow rate at less than 10 ml/min, as the flow through was recommended at dropwise (3-5 ml/min).

The purification filter was thoroughly washed with 50 ml of 1× Wash Buffer using gravity flow or by gently applying moderate pressure with syringe plunger. The wash step was repeated twice, using 50 ml of 1× Wash Buffer each wash. A collection tube was positioned under the purification filter and 2 ml of 1× Elution Buffer was allowed to pass through (gravity flow or moderate pressure). It was noted that air bubbles possibly formed between syringe and filter would slow down the elution. To avoid them I pipetted the elution buffer a few times, taking care not stab the membrane filter. While applying moderate pressure, the flow rate was

critically kept slow (drop-wise) to ensure the maximal yield. 10% of glycerol was added to the purified virus. The purified virus solution was aliquoted into smaller volumes (150µl - 200 µl) and stored at -80 °C.

3.3.4 Immunotitration of adenovirus:

A particular challenge in the delivery of a gene by a viral vector is the accurate measurement of virus titer. Initially, I tried to measure virus-infected particles in culture by a plaque-forming unit assay (PFU) that scores the number of viral plaques as a function of dilution. This method was not only time-consuming (10 days) and required a long infection period but also suffered from a high degree of inter-assay variability and was affected by virus-cell interactions. These shortcomings were overcome by using QuickTiter™ Adenovirus Titer Immunoassay Kit, supplied by Cell Biolabs, San Diego, CA (catalog # VPK-109). This kit utilizes an antibody against adenovirus hexon proteins to visualize infected cells by immunocytochemistry staining (Peled, 2009). The hexon proteins are the largest and most abundant of the structural proteins in the adenovirus capsid, and they are distributed symmetrically to form capsid facets. In contrast to the 10-day infection of previously attempted plaque assay experiments, this method made possible to observe even a 2-day infection.

Reagents supplied in the QuickTiter™ Adenovirus Titer Immunoassay Kit included 1000 × anti-hexon antibody, 1000 × secondary antibody (HRP conjugate), 25 × 3, 3'-diaminobenzidine (DAB), 10 × diluents and AdV-β gal positive control (1.0×10^9 ifu/ml). Upon receipt, AdV-β gal positive control was stored at -80 °C. Other kit components were stored at -4 °C until their expiration dates.

Preparation of adenoviral samples: Immediately before infection, serially diluted viral samples were prepared (10^{-2}, 10^{-4}, 10^{-6}, 10^{-7} and 10^{-8}). Six sterile tubes were taken and labeled as #1 to

#6. Firstly, original viral sample was diluted 1:100 by adding 10 µl of viral sample to tube #1 containing 990 µl of culture medium (10^{-2}). 990 µl of culture medium was added to tubes # 2 and #3. Mixture from tube #1 was further diluted 1:100 by transferring 10 µl from it to tube #2 (10^{-4}). Similarly, the 1:100 dilution step was repeated from tube #2 to tube #3 (10^{-6}). 900 µl of culture medium was added to tubes # 4 and #5. Mixture from tube #3 was further diluted 1:10 by transferring 100 µl from it to tube #4 (10^{-7}). Similarly, the 1:10 dilution step was repeated from tube #4 to tube #5 (10^{-8}). Tube # 6 was used as a blank

Adenovirus infection: HEK 293 cells were harvested and re-suspended in 293 cell culture medium at ~2 x 10^5 cells/ml. Cells suspended volume of 500 µl was seeded in each well of a 24-well plate and incubated at 37 °C, 5% CO_2 for 3 - 4 hours until 30%-40% confluence is reached. Adenovirus titer assay is critically dependent of the firm attachment of cells. The cells looking thin and easy to come off during immunostaining steps would not yield consistent results. Subsequently, 300 µl of the media was aspirated from each well and replaced with equal volume of serially diluted adenoviral samples. Cell culture media without virus was taken as negative control. To ensure accuracy, each sample was performed in duplicate. Cells were incubated at 37 °C, 5% CO_2 and after ~2 hours additional 500 µl of the 293 media was added to each well. Incubation was continued for 2-6 days to study day-to-day progression of infection. Mostly, immunostaining of the infected cell was conducted on day 6 post-infection to study the maximum potential of the viruses to inflict cytopathic effects on the cells.

Preparation of reagents: 1× anti-hexon primary antibody solution was prepared by diluting the

1000× anti-hexon antibody 1:1000 in 1% BSA/PBS and was stored on ice. Similarly, 1000 × secondary antibody was also diluted using 1% BSA/PBS and was stored on ice. Prior to use, 1 × DAB was *freshly* prepared. Firstly, the 10× diluent was diluted 1:10 with double-distilled water (dd-H_2O), and 0.01% of H_2O_2 was added. Then the 25× DAB diluted to 1:25 with 1× diluents / H_2O_2 mixture was used immediately.

Immunostaining: This was done on day 3 and day 6 post-infection. Slowly the medium was removed from the wells by tilting the plate and aspirating from the edge. Infected 293 cells were fixed by gently adding 0.5 ml of cold methanol down the side of each well of the 24-well assay plate, taking care not to dislodge the cells, and then incubated for 20 minutes at -20 °C. The fixed cells were gently washed three times with 1× PBS (5 minutes each wash) and blocked for 1 hr with 1% BSA in PBS at room temperature on an orbital shaker. 0.25 ml of diluted 1× anti-Hexon antibody solution was added to each well and incubated for 1 hour at room temperature on an orbital shaker. The fixed cells were gently washed three times with 1× PBS (5 minutes each wash). 0.25 ml of diluted 1× secondary antibody solution (HRP-conjugated) was added to each well and incubated for 1 hour at room temperature on an orbital shaker. The fixed cells were gently washed five times with 1× PBS (5 minutes each wash) and 0.25 ml of freshly diluted 1× DAB working solution was added to each well and incubated for 20 - 30 minutes at room temperature on an orbital shaker. Adenovirus infected cells would show dark brown staining within 5 minutes. During incubation, excess DAB would start to form light precipitates in solution, and this would not affect the staining results. DAB was aspirated and cells were, finally, washed twice with 1× PBS before adding 1 ml of 1× PBS to each well. Number of

positive stained cells (brown) were counted in as higher a diluted well as they appear in, using a light microscope and 10× objective, and accounted for in the calculation of adenovirus titer.

Calculation of adenovirus titer: Using the known values for the number of positive stained cells, dilution factor (for the well in which stained cells were counted) and volume of virus used, the viral titer is derived, as inclusion forming units (ifu/ml), as:

$$\text{Viral titer (ifu/ml)} = \frac{\text{Number of positive stained cells} \times \text{dilution factor}}{\text{volume of virus (ml)}}$$

Multiplicity of infection (MOI):

$$\text{ifu/cell} = \frac{\text{Volume of virus used for infection (ml)} \times \text{viral titer}}{\text{number of cells/ml}}$$

3.4 Real-Time Polymerase Chain Reaction

Real-time PCR was used as a tool to detect the expression of Cx40 in wild type cells (used as positive control) and Cx40KO cells infected with AdV-Cx40, AdV-$Cx40_{\Delta 237\text{-}358}$ and AdV-$Cx40_{\Delta 345\text{-}358}$. At the same time, this method also re-confirmed the absence of Cx40 in Cx40KO cells (used as negative control).

3.4.1 RNA extraction:

Cells were grown as monolayers in the culture medium having 5% FBS. 2 ml of the medium is pipette out in a 35 mm culture dish and placed in the incubator. At ~70% confluence the Cx40KO cells were separately infected with AdV-Cx40, AdV-$Cx40_{\Delta 237\text{-}358}$ and AdV-$Cx40_{\Delta 345\text{-}358}$ at MOI of 50 ifu/cell and placed back in the incubator for another 24 hours (~100% confluence). Media was aspirated and lysed with 1ml of TRIZOL reagent (Sigma). Suspended lysed cells were transferred into a sterile sample tube and incubated for 5 minutes at room

temperature. 200 µl of chloroform was added. The samples were vigorously vortexed for 15 seconds and further incubated for 3 minutes at room temperature. The samples were centrifuged at 11,900 × g at 4 °C for 15 minutes. Following centrifugation, the mixture separated into lower red, phenol-chloroform phase, an interphase, and a colorless upper aqueous phase. RNA remained exclusively in the aqueous phase. The upper aqueous phase was carefully transferred without disturbing the interphase into a fresh tube. RNA was precipitated from the aqueous phase by mixing with 500 µl isopropyl alcohol (70%). The samples were incubated for 10 minutes at room temperature and centrifuged at 11,900 × g at 4 °C for 10 minutes. The precipitated RNA, often invisible before centrifugation, forms a gel-like pellet on the side and bottom of the tube. The supernatant was completely removed and the RNA pellet was washed with 70% ethanol. The samples were mixed well and centrifuged at 11,900 × g for another 10 minutes at 4 °C. RNA pellet was air-dried for 5-10 minutes and then dissolved in 30 µl of DEPC water (Sigma) by passing solution a few times through a pipette tip.

Spectrophotometric analysis:

5 µl of the RNA sample was further diluted in 95 µl of dd-H_2O. Using a 10 µl microcuvette, optical density of the sample was read at 260 nm and 280 nm to determine sample concentration and purity. (Note: The A_{260}/A_{280} ratio was above 1.6, as recommended).

3.4.2 DNAse treatment:

Purpose of this treatment is to purify the RNA sample of any DNA contamination. Adjusted volume of RNA sample consisting of 1 µg of RNA is transferred into a fresh sterile tube. 2 µl each of 10× PCR buffer (Sigma) and DNAse I (Sigma) was added to the RNA sample.

The total volume is then adjusted to 20 µl using DEPC water. This mixture was incubated for 15 minutes at room temperature. 2 µl of Stop Solution (Sigma) was added and heat inactivated at 70 °C for 10 minutes.

3.4.3 Reverse transcription:

All products for RT-PCR were purchased from Invitrogen. To 11 µl of the RNA sample, 1 µl of random primers (250ng/ml) and 1 µl of dNTP (10 mM) was added and heated at 65 °C for 5 minutes. After a quick chill spin, 4 µl of 5 × 1st Strand buffer and 2 µl of DTT (0.1M) were added and incubated for 2 minutes at 25 °C. 1 µl of Reverse Transcriptase SuperScript II is added and further incubated at 42 °C for 50 minutes. Heat inactivation is done at 70 °C for 15 minutes.

3.4.4 Real time polymerase chain reaction (PCR):

Quantitative measurement of RNA concentrations relies on real-time detection of amplified cDNA targets (amplicons) generated by successive rounds of PCR amplification. Amplicons are detected on the basis of fluorescence, which increases proportionally with the PCR product. Quantification is determined by comparing the number of cycles required per sample to cross a certain threshold of fluorescence (Ct). This threshold is set in the exponential phase of the reaction; such that the difference between samples in the number of cycles required crossing this threshold reflect the relative difference in the starting amount of the target sequence. For detection, the DNA intercalating minor groove-binding fluorophore SYBR Green is used, which only produces a strong signal when incorporated into double-stranded DNA (Figure 9A).

Following reverse transcription, PCR master mix is prepared which consisted of 2 µl of the cDNA template, 12.5 µl of SYBR Green and 1.0 µl of the primers specific to Cx40 (25 µmol). The forward and reverse sequences of the specified primers were: 5′ CTG GCT CAC TGT CCT GTT CA 3′ and 5′ GCA ACC AGG CTG AAT GGT AT 3′ respectively, resulting in an amplicon length of 112 base pairs (bp). β-actin was also amplified as a control for genomic DNA. The sequences for forward and reverse β-actin primers were : 5' ATC GTG GGC CGC TCT AGG CAC CA 3' and 5' GTT GGC CTT AGG GTT CAG GGG GG 3' respectively, resulting in an amplicon length of ~300 base pairs in the absence of contamination, and an additional amplicon of ~500 base pairs in the presence of genomic DNA contamination. Total volume of 250 µl of the PCR master mix was adjusted by adding remaining volume of dd-H_2O. All the samples were prepared in triplicate. The samples were run in the Real-time PCR machine using the following protocol:

– One cycle: 2 min hot start at 94 °C.

– 40 cycles: 30 s 94 °C

– 30 s 60 °C

Quantification of gene expression: The average Ct value for the Cx40 KO - β actin samples was subtracted from the average Ct value for the infected Cx40 KO samples. This value, referred to as ΔCt, in turn, was subtracted from the average value similarly acquired from control samples (WT). The value '*x*' obtained, referred to as ΔΔCt, raised to the power of 2 (i.e., 2^x) represented the fold-induction of gene expression (Figure 9A).

3.5 Immunocytochemistry

Immunocytochemical study was performed to demonstrate the successful re-introduction of Cx40 into the Cx40KO cells through the adenoviral infection. Wild type and Cx40KO cells were grown on glass cover slips (VWR Scientific, Mississauga, ON). At ~70% confluence, Cx40-KO cells were infected with AdV-Cx40 (MOI: 50 ifu/cell) and incubated for 24 hours. Cells were fixed with 4% paraformaldehyde at 4 °C for 20 minutes, rinsed with PBS, and prepared for immunostaining. The cells were blocked with washing buffer containing 2% BSA (wt/vol) for 1 hour, immunolabeled with anti-Cx40 antibody at 1:300 dilution) for 1 hour at room temperature, washed with PBS, and immunolabeled with Alexa 488-conjugated secondary antibody (1:500 dilution) for 1 hour at room temperature in the dark. Cells were washed in PBS, and the nuclei were stained with 0.1% Hoechst 33258 (Sigma) for 10 minutes followed by washes with PBS and dd-H_2O. Adv-Cx40-infected Cx40KO cells with only the secondary antibody were used as negative control. The cover slips were mounted on slides with Airvol (Air Products and Chemicals, Allentown, PA) before storage at 4 °C. The cells were imaged using a Zeiss LSM 510 META confocal microscope (Thornwood, NY). Fluorescent signals were captured after excitation with 488 and 730 nm laser lines. Digital images were prepared using Zeiss LSM and Adobe Photoshop 7.0 software.

3.6 Electrophysiology

3.6.1 Experimental set-up:

Experiments to detect electrotonic spread in cell monolayers were performed as previously described (Lidington et al., 2000, Rose et al., 2003, Bolon et al., 2005, 2007 & 2008).

A Narshige vertical microelectrode puller was used to prepare glass electrodes from filamented microcapillary tubing (World Precision Instruments (WPI), Sarasota, FL; Kwik-Fil # 1B100F-3). The un-pulled ends of the electrodes were immersed in a 1M KCl solution for a minimum of 12 hours. Capillary action drew the KCl solution into the electrode. After backfilling, the electrodes had resistance of 40-90 MΩ.

The electrodes were mounted on mechanical micromanipulators (Leica), which were connected to electrometers (WPI, INTRA 767) by chlorinated silver wires. All electrophysiology experiments were performed in a grounded static bath chamber. Monolayers were viewed through a Leica DMIRB inverted microscope with a 20% phase contrast objective. Since electrophysiology was done in room air (cell chamber heated to 37 °C), cells were covered by normoxic dialyzed serum medium (DSM; Sigma) including 25mM of N-[2-hydroxethyl] piperazine-N-[2-ethane sulfonic acid] (HEPES; Sigma), to maintain pH at 7.3.

Two independent electrodes were inserted into two cells within the monolayer (figure 5A). Once both the electrodes obtained and maintained the full cell membrane potential (E_m), a series of hyperpolarizing pulses of current (25 nA, 100 msec pulse width) were injected into the monolayer through one of the electrodes from a current source (WPI, A310 Accupulser connected to a W361 Stimulus Isolator). After 3-4 pulses, both the injecting and the recording electrodes were removed and repositioned at a new interelectrode distance. Three to four interelectrode distances were used for each recording. The deflections of the membrane potential were recorded on a Gould RS 3200 two-channel recorder. As the interelectrode distance increases, the magnitude of deflection of the E_m due to current injections at the recording electrode decreases (figure 5B). Through this relationship intercellular resistance (r_i), membrane resistance (R_m) and the space constant (λ) can be determined.

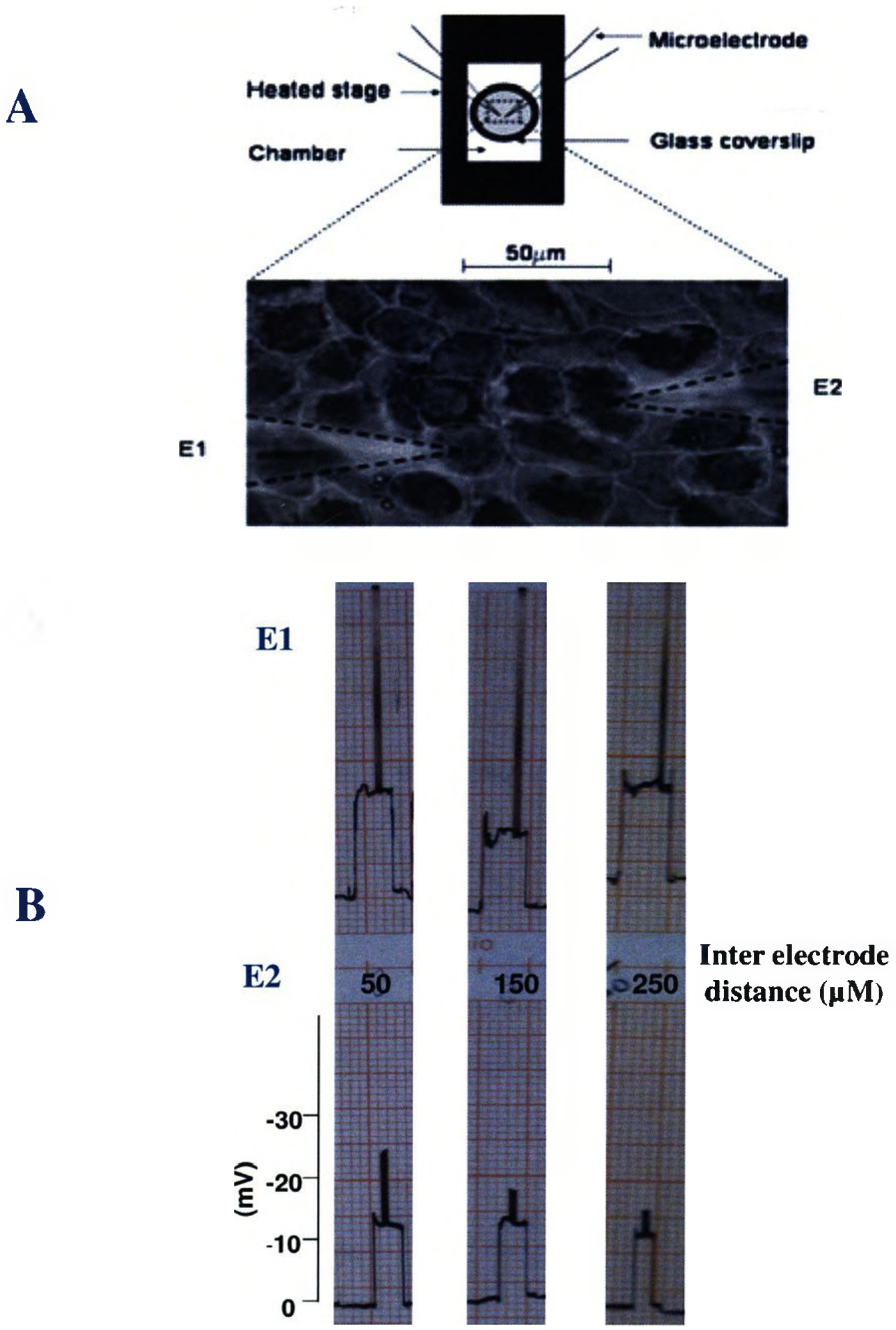

Figure 5. Electrophysiological setup for studying inter-endothelial electrical coupling. **(A)** A monolayer of cells grown on a glass coverslip placed in a culture medium-filled chamber on a heated microscope stage. Current injection microelectrode E1 and recording electrode E2 was inserted into two cells of the monolayer. **(B)** Examples of electrode E1 and E2 recordings from a control monolayer at interelectrode distances of 50, 150, and 250 μm.

3.6.2 Bessel function:

Within the monolayer, spread of current is predicted by a Bessel function: $\Delta Em(d) = (IoR_i / 2\pi t)\, K_o(x)$, where $\Delta Em(d)$ is the change in voltage at a given interelectrode distance (d), Io is the injected current, R_i is the resistivity of the intercellular pathway (including both cytoplasmic and junctional resistivity), t is the thickness of the monolayer, and x is the distance (d) divided by the space constant, λ. The spatial decay of the current is logarithmic for the interelectrode distances used (between 50 µm and 300 µm). Thus, a plot of voltage change (ΔEm) versus log interelectrode distance (d) produces a straight line through the experimental values. Intercellular resistivity (R_i) is proportional to the slope of this line and can be calculated after rearranging the Bessel function equation above, substituting the experimental slope for ΔEm (d) and the log portion of the Bessel function for $K_o(x)$. After calculation of (R_i), it is substituted into the equation of the Bessel function, and λ can be calculated. Intercellular resistance (r_i) is calculated by dividing R_i by the thickness of the monolayer (t). Membrane resistance (R_m) can be calculated from the equation of the space constant: $\lambda = (R_m t/2R_i)^{1/2}$. Calculations were done with the help of Matlab (The Math Works, Inc., 1999). Program details are shown in the Appendix B.

3.6.3 Treatment for LPS study:

Cells used for electrophysiology were of passages between 6 and 15 (Bolon et al., 2005, 2007 & 2008) and were grown as monolayers in culture medium, having 5% FBS, on glass coverslips. 4-5 glass coverslips were placed in 35 mm petri dish and 2 ml of culture medium was pipetted into it. The dishes were placed in a standard, normoxic incubator (37 °C in water-saturated air containing 5% CO_2). At ~70% confluence, Cx40KO cells were separately infected

with the recombinant adenovirus (AdV-Cx40 / AdV-Cx40$_{\Delta 237\text{-}358}$ / AdV-Cx40$_{\Delta 345\text{-}358}$ / AdV-β gal), 24 hours prior to the electrophysiology experiment, at the MOI of 50 ifu/cell. One hour prior to all experiments, the culture medium was replaced by dialyzed serum medium (DSM) for the duration of the experiment (FBS was replaced by 5% dialyzed serum). A standard concentration of LPS (10 μg/ml; Bolon, 2007 & 2008) was added to the dialyzed serum for 1 hour. Untreated cells were left for the equal duration with fresh DSM. Since electrophysiology was done in room air (cell chamber heated to 37 °C), cells were covered by dialyzed serum including 25 mM HEPES (i.e., to maintain pH at 7.3). For the LPS-treated cells, LPS (10 μg/ml) was added to the DSM+HEPES mix to maintain the effect of LPS during electrophysiology.

3.6.4 Treatment for H/R study:

Cells were grown, maintained and infected in the same way as discussed above. 1 hour prior to all experiments, the culture medium was replaced by dialyzed serum medium (DSM) for the duration of the experiment (FBS was replaced by 5% dialyzed serum). For H/R experiments, hypoxic DSM was prepared by bubbling with 100% N_2 for 5 minutes. Using a PO_2 microsensor (OxyLite, Oxford Optronix, UK), it was determined that the final PO_2 of the bubbled solution was less than 10 mmHg (~1%O_2). For hypoxia, cells were covered by ~ 2 mm thick layer of hypoxic DSM and placed into hypoxic incubator (5% CO_2, 0.1% O_2 and 94.9% N_2 at 37 °C). At the end of hypoxia (1 hour for all experiments), hypoxic medium was replaced with normoxic DSM for 5-15 minutes (i.e., duration of reoxygenation). The time of reoxygenation is accounted for while conducting electrophysiology. To the cells not exposed to H/R, fresh medium was added after 1 hour and left for another hour in the normoxic incubator.

3.6.5 Treatment for LPS+H/R study:

Cells were grown, maintained and infected in the same way as in the case of LPS and H/R studies. The culture medium was replaced by dialyzed serum medium (DSM) for the duration of the experiment (FBS was replaced by 5% dialyzed serum). For LPS+H/R, cells were covered by ~ 2 mm thick layer of hypoxic DSM with LPS (10 μg/ml) and placed into hypoxic incubator. At the end of hypoxia (1 hour for all experiments), hypoxic medium was replaced with DSM for 5-15 minutes (i.e., duration of reoxygenation). The time of reoxygenation is accounted for while conducting electrophysiology. To the cells not exposed to H/R+LPS, fresh medium (normoxic) was added after 1 hour and left for another hour in the normoxic incubator.

3.7 Data Analysis

The data are presented as mean ± standard error, n indicates the number of monolayers used per treatment group, MMEC were isolated from at least 3 different mice. Statistical significance was assessed using two-tailed Student's t -test. For experiments with more than one treatment group, ANOVA and t-test with Bonferroni correction was used. Significance was set to $p<0.05$.

Chapter 4 : Results

4.1 Genotyping of Cx40

Genotyping of the Cx40KO mice was determined by PCR, using the diluted tail clip digest. PCR products were size-separated on a gel and specially designed primers were used to detect Cx40KO allele which was identified by one band at ~470 bp. Where as, for wild type, a band appeared at ~270 bp and for heterozygous two bands appeared at ~470 bp and ~270 bp (Figure 6). Thus, the mouse in lane A (Fig.6) was identified as a Cx40KO mouse. Real-time PCR was also performed using RNA isolated from Cx40KO endothelial cells to re-confirm that the cells did not express the Cx40 transcript. Since most connexins do not have an intron within the coding region, the β- actin gene was amplified in order to test for the presence of genomic DNA. No signal for Cx40 was detected in Cx40KO samples by the end of 40 cycles.

Thus, the Cx40KO deficient genotype of these cells was confirmed. As well, Cx40 gene expression was detected in wild type cells indicating that endothelial cells of microvascular origin express this connexin *in vitro*.

4.2 Endothelial cell characterization

In order to ensure that the cells isolated were endothelial in nature, they were checked for several characteristics of endothelial cells. Endothelial cell cultures were obtained by selection with *Gryffonia symplicifolia* lectin-coated magnetic beads. This lectin attaches to α-D-galactosyl residues on the cell surface of mouse endothelial cells (Laitinen, 1987) allowing for specific selection of this cell type. A primary characteristic of endothelial cells is a 'cobblestone' morphology which is exhibited by both wild type and Cx40KO cells (Figure 7A) (Scott and

Bicknell, 1993). Positive stains obtained by von Willibrand factor VIII characterization procedure (Figure 7B) further confirmed the isolated cells to be endothelial in nature.

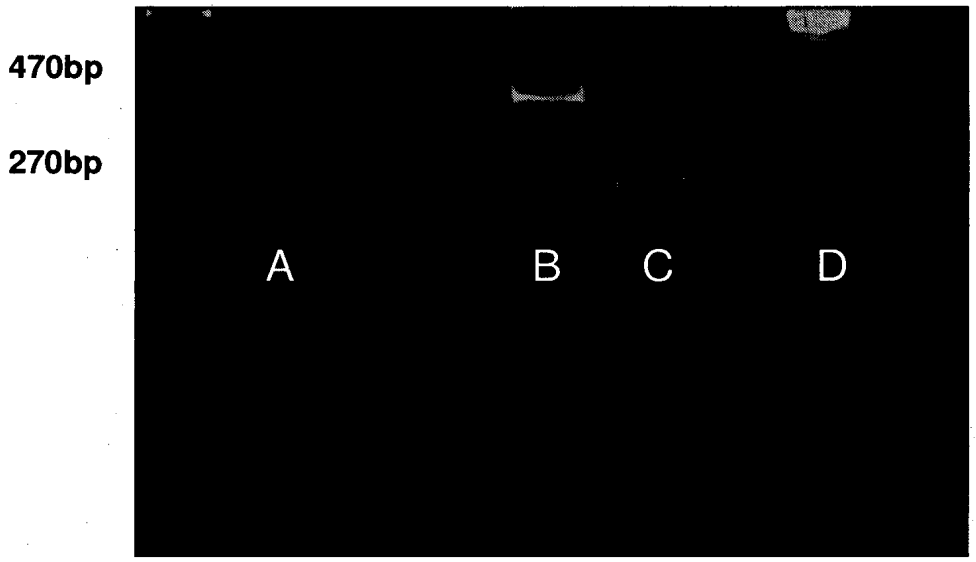

Figure 6. Genotyping of mice determined by the size-separation of the PCR products. Band appearing at 470 bp (A) and 270 bp (B) represented Cx40 and WT alleles respectively. Heterozygous were identified by both the bands appearing simultaneously at 470 bp and 270 bp (C). DNA ladder was added in the last well (D).

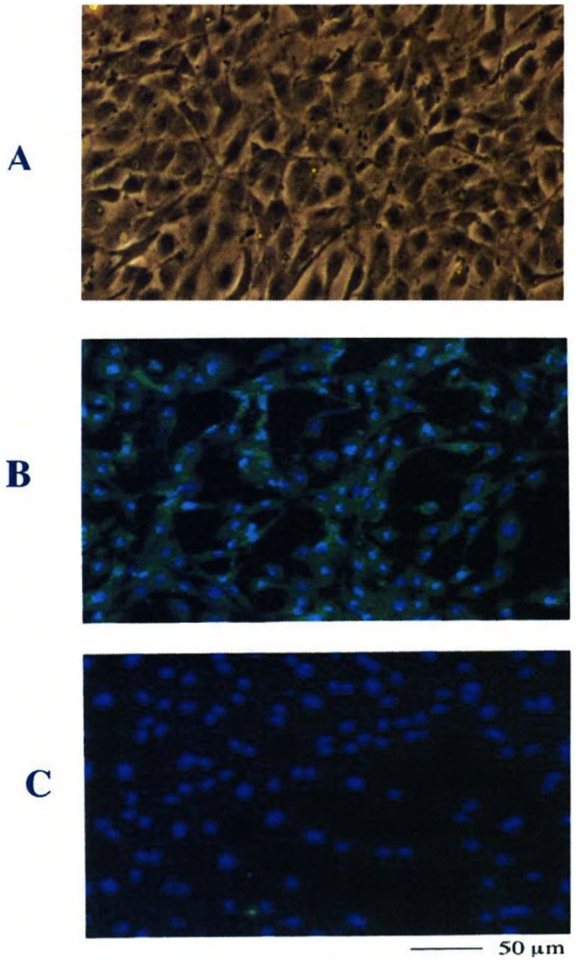

Figure 7. **(A)** Confluent monolayer of mouse microvascular endothelial cells grown on a coverslip seen under bright light illumination (cells at this confluence were used for electrophysiology). **(B)** Using a separate coverslip with cells, endothelial cell phenotype was identified with von Willebrand factor VIII antibody staining. **(C)** Control experiment using another coverslip. Here, cells were probed with the secondary antibody only, omitting the primary antibody (von Willebrand factor VIII Ab). Green fluorescence indicates positive von Willebrand factor VIII staining while blue fluorescence indicates cell nuclei highlighted with Hoechst stain.

4.3 Immunotitration of recombinant adenovirus

HEK 293 cells, infected with serially diluted adenovirus carrying Cx40 cDNA were immunostained using anti-hexon antibody and HRP-conjugated secondary antibody. Incubation with DAB substrate caused formation of dark brown stains representing the adenovirus - infected cells. These stains were viewed through a Leica DMIRB inverted microscope with a 20% phase contrast objective and images were captured in a camera attached to a port in the microscope. Number of positive stains was found to be correlated to the severity of infection, which in turn depended on the dilution factor. Large number of positive stained cells was detected in lesser diluted wells (150-200) i.e., for 10^{-2} and 10^{-4} dilutions (Figure 8). Lesser number of stains appearing in higher diluted wells, therefore, was counted in every field of view for the determination of titer value. No positive stains were found in the uninfected cells, used as negative control. AdV-β gal of the known titer value 10^{8} ifu/ml, which was readily available in our laboratory stock (stored at -80 °C) or other adenoviruses of Cx40 whose potency was already determined were used as positive controls.

5 -10 number of stains appeared in 10^{-7} dilution as a result of the infection using AdV-Cx40, AdV-$Cx40_{\Delta 237\text{-}358}$ and AdV-$Cx40_{\Delta 345\text{-}358}$. Immunotitration experiment in all the cases was done separately and on the 6^{th} day post-infection. The titer value, thus calculated, for all the above adenoviruses was 10^{8} ifu/ml.

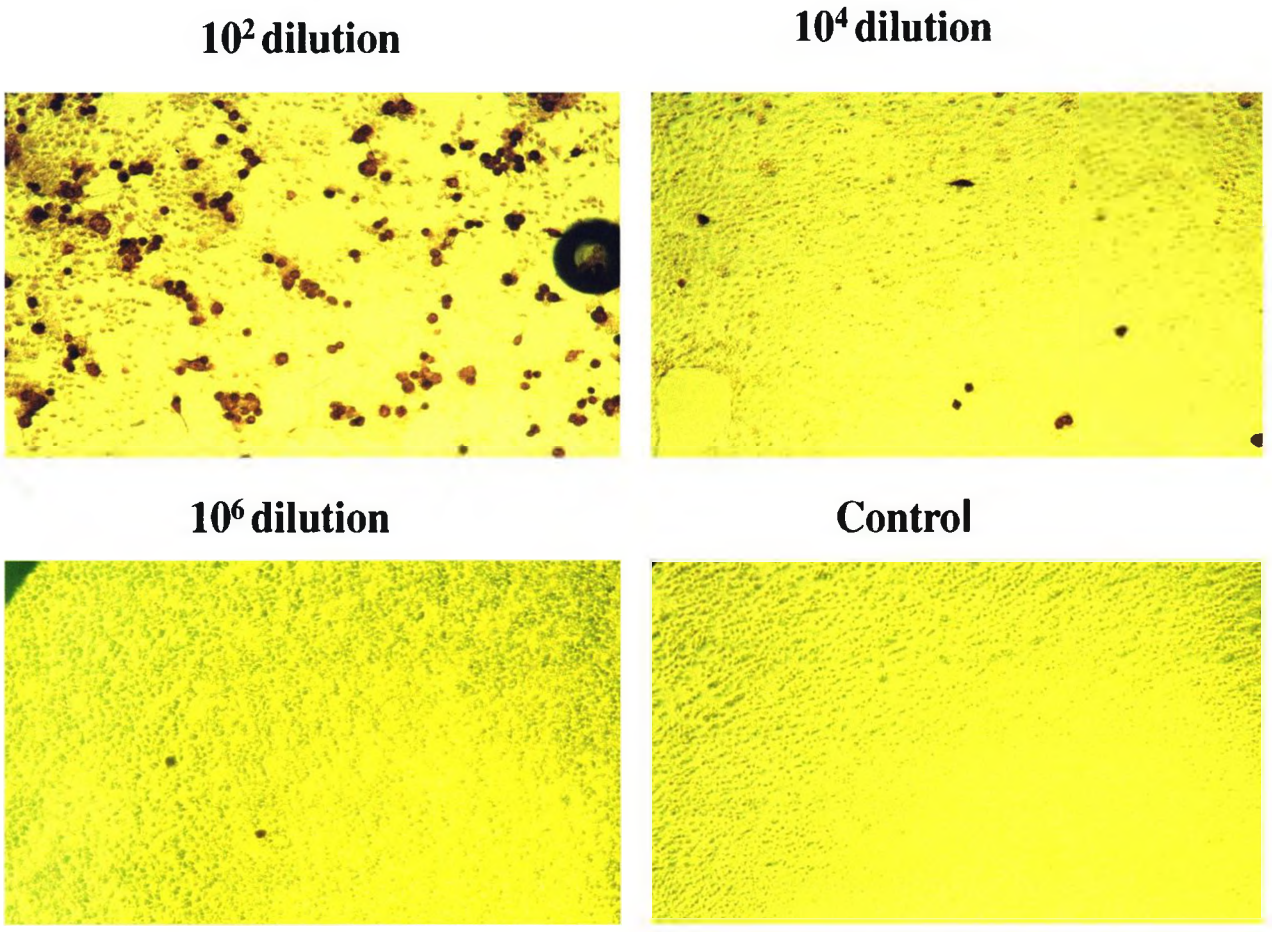

Figure 8. An example of determining adenovirus titer. HEK 293 cells were infected with AdV-Cx40 at indicated dilutions, and examined 6 days later for DAB-labeled anti-hexon antibody (brown stain). Based on the number of stained cells in the 10^6 dilution panel, the titer value was calculated as 6.6×10^6 ifu/ml.

4.4 Detection of Cx40 mRNA by Real-Time PCR

Cx40-cDNA samples (reverse transcribed from Cx40 mRNA), derived from Cx40KO cells separately infected with AdVCx40, AdV-Cx40$_{\Delta 237\text{-}358}$ and AdV-Cx40$_{\Delta 345\text{-}358}$, were subjected to amplification by real-time PCR and use of Cx40-specific primers. All samples studied were studied in triplicate. The relative expressions of Cx40 mRNA in the 3 different samples with respect to that of wild-type are discussed below.

4.4.1 AdV-Cx40 expression:

Figure 9A shows an example of determining a fold-increase in Cx40 mRNA in AdV-Cx40 - infected Cx40KO cells with respect to Cx40 mRNA expression in WT cells. Average ΔCt value representing the expression of Cx40 mRNA in AdV-Cx40 - infected Cx40KO cells relative to that of the constitutive β- actin was 14.95. ΔΔCt value, representing the relative Cx40 mRNA expression in the infected Cx40KO cells with respect to that of WT cells was calculated as 4.46. Thus, the fold increase of Cx40 mRNA in AdV-Cx40 - infected Cx40KO cells compared to the Cx40 mRNA in WT cells was determined as 22.0. No signal was detected for the expression of Cx40 mRNA in uninfected Cx40KO sample, re-confirming the absence of Cx40 in Cx40KO cells (Figure 9B, bar 1).

4.4.2 AdV-Cx40$_{\Delta 237\text{-}358}$ expression:

Average ΔCt value representing the expression of Cx40 mRNA in AdV-Cx40$_{\Delta 237\text{-}358}$ - infected Cx40KO cells relative to that of the constitutive β- actin was 15.28. ΔΔCt value, representing the relative Cx40 mRNA expression in the infected Cx40KO cells with respect to that of WT cells was calculated as 4.13. Thus, the fold increase of Cx40 mRNA in AdV-

$Cx40_{\Delta 237-358}$ - infected Cx40KO cells compared to the Cx40 mRNA in WT cells was determined as 17.5. No detection was recorded for mRNA samples from Cx40KO cells, taken as a negative control (Figure 9B, bar 2).

4.4.3 AdV-Cx40$_{\Delta 345-358}$ expression:

Average ΔCt value representing the expression of Cx40 mRNA in AdV-$Cx40_{\Delta 345-358}$ - infected Cx40KO cells relative to that of the constitutive β- actin was 15.79. ΔΔCt value, representing the relative Cx40 mRNA expression in the infected Cx40KO cells with respect to that of WT cells was calculated as 3.61. Thus, the fold increase of Cx40 mRNA in AdV-$Cx40_{\Delta 345-358}$ - infected Cx40KO cells compared to the Cx40 mRNA in WT cells was determined as 12.2. No signal was detected for the expression of Cx40 mRNA in uninfected Cx40KO sample (Figure 9B, bar 3).

4.5 Detection of Cx40 protein in infected Cx40KO cells:

Immunochemistry study showed a large number of Cx40 gap junction plaques in AdV-Cx40 - infected Cx40KO cells (Figure 10D). Moreover, the degree of expression of Cx40 was found to be far greater in the infected cells than in the WT cells (Figure 10A). No stains for Cx40 were seen in Cx40KO cells (Figure 10B) as well as in Cx40-infected Cx40KO cells with only the secondary antibody (Figure 10C). The nuclei of the cells stained with 0.1% Hoechst cells were immunolabeled with anti-Cx40 antibody and Alexa 488-conjugated secondary antibody.

1

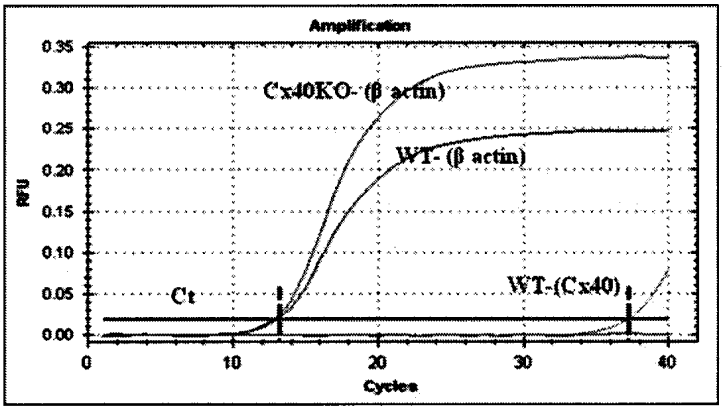

2

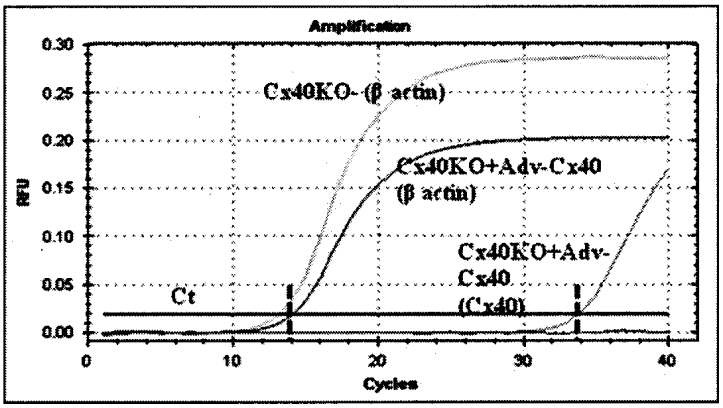

Calculating Cx40 – mRNA expression (Example)

	Average Ct		
	β -actin	Cx40	ΔCt
WT	13	37	24 (A)
Cx40KO+ Adv-Cx40	14	34	20 (B)

(A) – (B) i.e. 24 – 20 = ΔΔ Ct

Fold Increase = $2^{\Delta\Delta Ct}$ (i.e. 2^4) relative to WT

= **16**

Figure 9A. Determination of fold-increase of Cx40-mRNA in infected Cx40KO cells relative to that of WT cells by real-time PCR. As an example, calculation of Cx40 mRNA expression in AdV-Cx40 - infected Cx40KO cells is shown on the right. **Panel 1:** Relative detection of Cx40 cDNA with respect to that of β-actin in WT cells and in Cx40 KO cells. For WT cells, the Ct value for Cx40 was 37, while the Ct value for the reference protein β-actin was 13 (these Ct values are also shown in the upper row of the table). For Cx40 KO cells, the Ct value for β-actin was 13, but Cx40 mRNA was not detected (i.e., lack of detection is seen by the horizontal line parallel to x-axis, situated just above x-axis). **Panel 2:** Relative detection of Cx40 cDNA with respect to that of β-actin in AdV-Cx40 - infected Cx40KO cells, and also in Cx40 KO cells. In Adv-Cx40-infected Cx40KO cells, the Ct value for Cx40 was 34, while the Ct value for β-actin was 14 (these Ct values are shown also in the bottom row of the table). Below the table, based on the Ct values in the table, a computation is shown to determine the fold-increase of Cx40-mRNA in infected Cx40KO cells relative to that in WT cells.

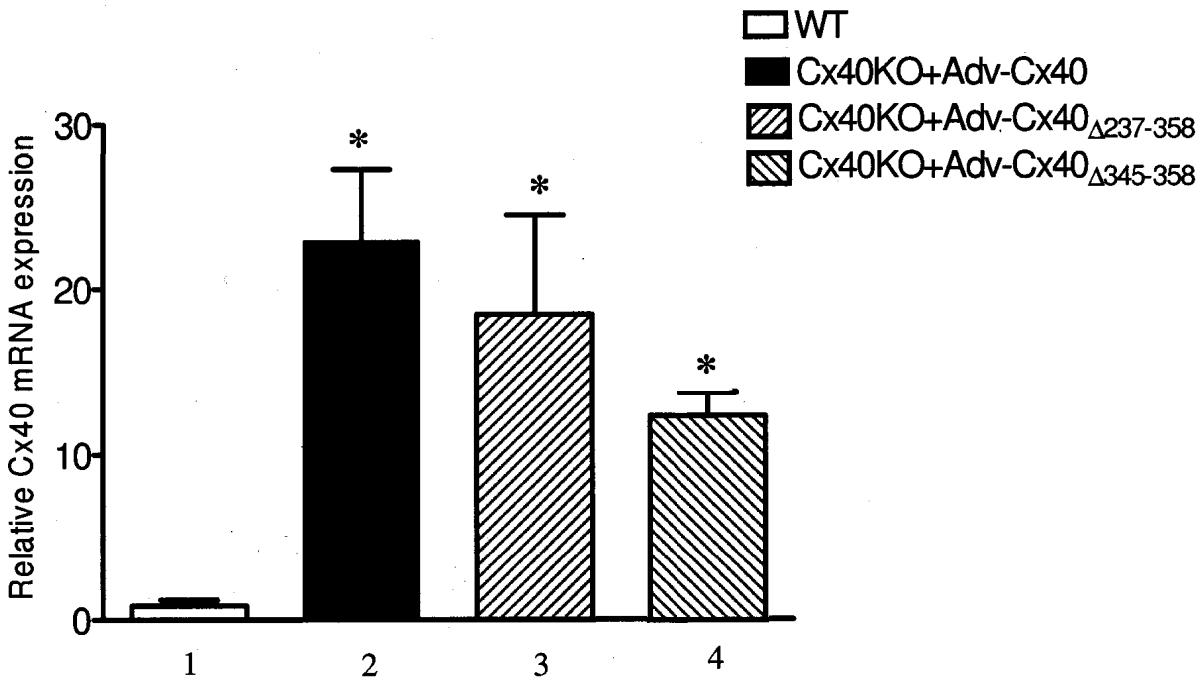

Figure 9B. Cx40 mRNA expression in WT cells is set to 1.0 (bar 1). Cx40 mRNA expression in Cx40KO cells infected with AdV-Cx40 (bar 2), AdV-$Cx40_{\Delta 237\text{-}358}$ (bar 3) and AdV-$Cx40_{\Delta 345\text{-}358}$ (bar 4) are shown as fold increases relative to Cx40 mRNA expression in WT cells (n=3 for all groups). * indicates significant difference from the control group (WT), $p < 0.05$.

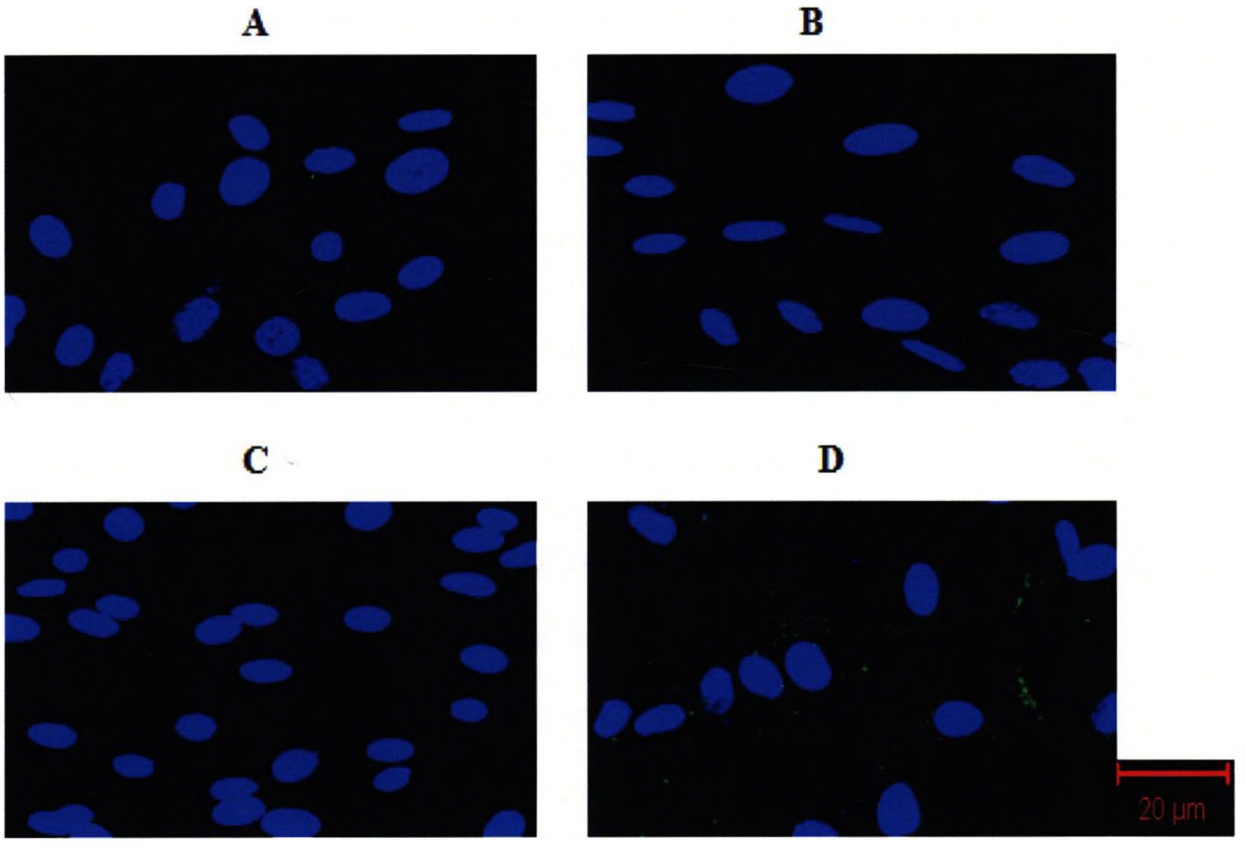

Figure 10. Detection of Cx40 protein by immunocytochemistry. Endothelial cell nuclei are stained with Hoechst (blue). The presence of Alexa 488-labeled anti-Cx40 antibody (used to detect Cx40 protein) is identified by punctuate staining of florescence (green). **(A)** WT cells. **(B)** Cx40 KO cells. **(C)** AdV-Cx40 - infected Cx40KO cells with only the secondary antibody. **(D)** AdV-Cx40 - infected Cx40KO cells with both primary and secondary antibody. AdV-Cx40 concentration used: MOI= 50 ifu /cell.

Bar represents 20 µm.

4.6 Effect of LPS on electrical coupling in MMEC and role of Cx40

LPS exposure (10 μg/ml, 1 hour) or infection of adenoviruses did not result in any visual morphological changes in the appearance of cell monolayers in all the experiments, before or during the electrophysiological recordings. The baseline resting E_m for WT (-13.5 ± 6.5 mV, n=6), Cx40KO (-12.7± 4.1, n=22), Cx40KO/AdV-Cx40 (-13.2 ± 6.0, n=16), Cx40KO/ AdV-Cx40$_{\Delta 236\text{-}358}$ (-12.7 ± 3.3, n=8) and Cx40KO/AdV-Cx40$_{\Delta 345\text{-}358}$ (- 14.1 ± 4.2, n=11) remained consistent in all the experiments. The values of E_m in these monolayers did not change significantly after the exposure to LPS.

4.6.1 WT and Cx40KO cells:

In the WT cells monolayer, LPS significantly increased the intercellular resistance, r_i, indicating the reduced electrical coupling (Figure 11, Table 1). However, there was no increase in resistance in Cx40KO cells after LPS treatment (Figure 12, bars 1 and 2). These findings correlated with the data reported by our lab (Bolon et al., 2007). LPS did not affect the membrane resistivity, R_m, in WT cells, which also remained unchanged in Cx40KO cells after LPS treatment. However, the space constant, λ, significantly decreased in both the WT and Cx40KO cells after their exposure to LPS (Table 1).

4.6.2 Adenovirus - infected Cx40KO cells:

AdV-Cx40-infected Cx40KO cells: Infection of Cx40KO cells monolayer by AdV-Cx40 did not alter its r_i compared to the Cx40KO cells. However, r_i increased significantly in the AdVCx40 - infected Cx40KO cells after their exposure to LPS (Figure 12, bars 3 and 4). Though R_m remained unchanged in the infected cells compared to the control, λ was found to have decreased

considerably in all the experiments in response to LPS (Table 1). These findings suggest a major role of Cx40 in the LPS-induced reduction of intercellular electrical coupling. The results not only remained consistent with the previously reported data by our lab (Bolon et al., 2007), but also demonstrated a successful infection procedure, using the recombinant adenoviruses, by which Cx40 was re-incorporated into Cx40KO cells.

AdV-Cx40$_{\Delta 236\text{-}358}$ – infected Cx40KO cells: Unlike in the case of AdV-Cx40 infection, Cx40KO cells monolayer when infected with adenovirus carrying carboxylic tail-truncated Cx40, interestingly, showed no change in the intercellular electrical coupling after its treatment with LPS (Figure 12, bars 5 and 6). The results implicate the carboxylic tail of Cx40 in the LPS-induced reduction in r_i. The R_m and λ values, in these cells monolayers, did not differ much after the LPS treatment (Table 1).

AdV-Cx40$_{\Delta 345\text{-}358}$ – infected Cx40KO cells: This experiment was conducted to further probe for the region in the carboxylic tail of Cx40 instrumental in the LPS-signaling pathway. Cx40KO cells were infected with the adenovirus carrying Cx40 without the end portion of its carboxylic tail (lacking residues from 345 to 358) and subjected to LPS treatment. The r_i remained unaltered, post-LPS exposure, in these infected cells (Figure 12, bars 7 and 8). The values for R_m and λ remained unchanged after the LPS treatment (Table 1). The findings indicate that the deleted region of the Cx40 carboxylic tail is crucial in the overall functionality of Cx40, in LPS-triggered increase in intercellular resistance.

4.7 Effect of H/R on electrical coupling in MMEC and role of Cx40

Hypoxia (1 hour) followed by abrupt reoxygenation did not change the morphological appearance of the cells monolayers in all the experiments, before or during the electrophysiological recordings. The baseline resting E_m for WT cells (-13.5 ± 6.5 mV, n=6), Cx40KO cells (-12.7± 4.1, n=22), AdV-Cx40 - infected Cx40KO cells (-13.2 ± 6.0, n=16), AdV-$Cx40_{\Delta 236-358}$ - infected Cx40KO cells (-12.7 ± 3.3, n=8) and AdV-$Cx40_{\Delta 345-358}$ - infected Cx40KO cells (- 14.1 ± 4.2, n=11) remained consistent in all the experiments. The values of E_m in these monolayers did not change significantly after the exposure to H/R.

4.7.1 WT and Cx40KO cells:

In the WT cells monolayer, H/R reduction in electrical coupling between the cells was evident by the significant increase in r_i (Figure 13, bars 1 and 2). In contrast, there was no increase in resistance in Cx40KO cells after their exposure to H/R (Figure 14, bars 1 and 2). These results were found to be consistent with the findings previously reported by our lab (Bolon et al., 2005). Membrane resistivity was not affected by H/R in the WT as well as Cx40KO cells monolayers. Space constant (λ), on other hand, significantly decreased in both the WT and Cx40KO cells after their exposure to H/R (Table 1).

4.7.2 Adenovirus - infected Cx40KO cells:

AdV-Cx40 - infected Cx40KO cells: Significant increase in r_i was recorded in the Cx40KO cells monolayers infected with AdV-Cx40 and exposed to H/R. This increase in r_i was not observed in the infected Cx40KO cells not subjected to H/R (Figure 14, bars 2 and 3). R_m values obtained for the cells monolayers remained unaltered regardless of the H/R treatment. However,

λ was seen to be greatly reduced in AdV-Cx40 - infected Cx40KO under the influence of H/R (Table 1). These findings provide evidence that Cx40 is the target gap junction protein in the H/R signaling process leading to the reduced electrical coupling between the cells, thus confirm the previously published work in this regard (Bolon et al., 2005).

AdV-Cx40$_{\Delta 236\text{-}358}$ – infected Cx40KO cells: Unlike in the case of the AdV-Cx40 infection, the infection of Cx40KO cells with adenovirus carrying Cx40 devoid of its carboxylic tail did not result in the increase in r_i after H/R treatment when compared to the r_i in the infected cells in the absence of H/R (Figure 14, bars 4 and 5). This indicates a key role of Cx40 carboxylic tail in H/R signaling pathway, similar to that of LPS response. R_m, throughout the experiments, was not affected by H/R. The stimulus, however, significantly reduced λ in all the experimented cells monolayers (Table 1).

AdV-Cx40$_{\Delta 345\text{-}358}$ – infected Cx40KO cells: Electrical coupling between Cx40KO cells infected with AdV-Cx40$_{\Delta 345\text{-}358}$ did not differ from that of Cx40KO uninfected cells. The coupling still remained unchanged after the infected cells were subjected to H/R, suggesting that the end region of the carboxylic tail of Cx40 is responsible for the reduced intercellular resistance in response to H/R (Figure 14, bars 5 and 6). No significant difference in R_m was recorded in the infected cells before or after the H/R treatment. However, λ was greatly reduced in these cells in response to H/R (Table 1).

4.8 Effect of LPS+H/R on electrical coupling in MMEC and role of Cx40

Combined effect of LPS (10 μg/ml) and hypoxia (1 hour) followed by reoxygenation did not have any effect on the morphological appearance of the cell monolayers, thus deemed suitable for the electrophysiological experiments. The baseline resting E_m for WT cells(-13.5 ± 6.5 mV, n=6), Cx40KO cells (-12.7± 4.1, n=22), AdV-Cx40 – infected Cx40KO cells (-13.2 ± 6.0, n=16), AdV-Cx40$_{\Delta 236\text{-}358}$ – infected Cx40KO cells (-12.7 ± 3.3, n=8) and AdV-Cx40$_{\Delta 345\text{-}358}$ – infected Cx40KO cells (- 14.1 ± 4.2, n=11) remained consistent in all the experiments. The values of E_m in these monolayers did not change significantly after the exposure to LPS + H/R.

4.8.1 WT and Cx40KO cells:

Though the intercellular resistance (r_i) recorded for LPS+H/R was more than the one under the influence of LPS or H/R alone (Figure 13, bars 1 and 3), the magnitude of increase in r_i revealed that the effect was, moreover, additive rather than synergistic. Cx40KO cells failed to record any change in the measure of electrical coupling after LPS+H/R treatments (Figure 15, bars 1 and 2). The results confirmed the findings previously reported by our lab (Bolon et al., 2008). R_m values recorded for all the control experiments did not change in response to LPS+H/R treatments. However, λ was shown to be significantly reduced by the stimuli (Table 1).

4.8.2 AdV-Cx40 - infected Cx40KO cells:

Electrical coupling between Cx40KO cells treated with LPS and subsequently exposed to H/R did not change when compared to the control cells. In contrast, Cx40KO cells infected with AdV-Cx40, and subjected to LPS+H/R treatments resulted in increase in r_i, which was more than the r_i observed in the experiments involving LPS or H/R, individually (Figure 15, bars 3 and 4).

Throughout all the experiments, R_m values between control and treated cells were consistently similar. At the same time, λ values were seen to be largely reduced by LPS+H/R treatment compared to the control (Table 1). The results fall in line with the previously reported findings (Bolon et al., 2008) that Cx40 is responsible in the increased reduction of intercellular electrical coupling, perhaps due to an additive effect of LPS and H/R.

4.8.3 Comparison between the effect of LPS, H/R and LPS+H/R in WT cells and in AdV-Cx40 - infected Cx40KO cells:

The value of intercellular resistance (r_i) in the WT cells as well as Adv-Cx40-infected Cx40KO cells after LPS+H/R treatment (Figure 16, bars 4 and 8 respectively) was larger than r_i after LPS and H/R treatment alone (Figure 16, bars 2, 3, 6 and 7) . However, the magnitude of increase in r_i in WT cells and Adv-Cx40-infected Cx40KO cells, after LPS+H/R treatment, relative to control (Figure 17, bars 4 and 8, respectively) was not different from the computed sum of increases in r_i after LPS and H/R treatments alone (Figure 17, bars 3 and 7, respectively). This indicates that LPS+H/R treatment exerts an additive effect rather than a synergic effect on the increase of r_i.

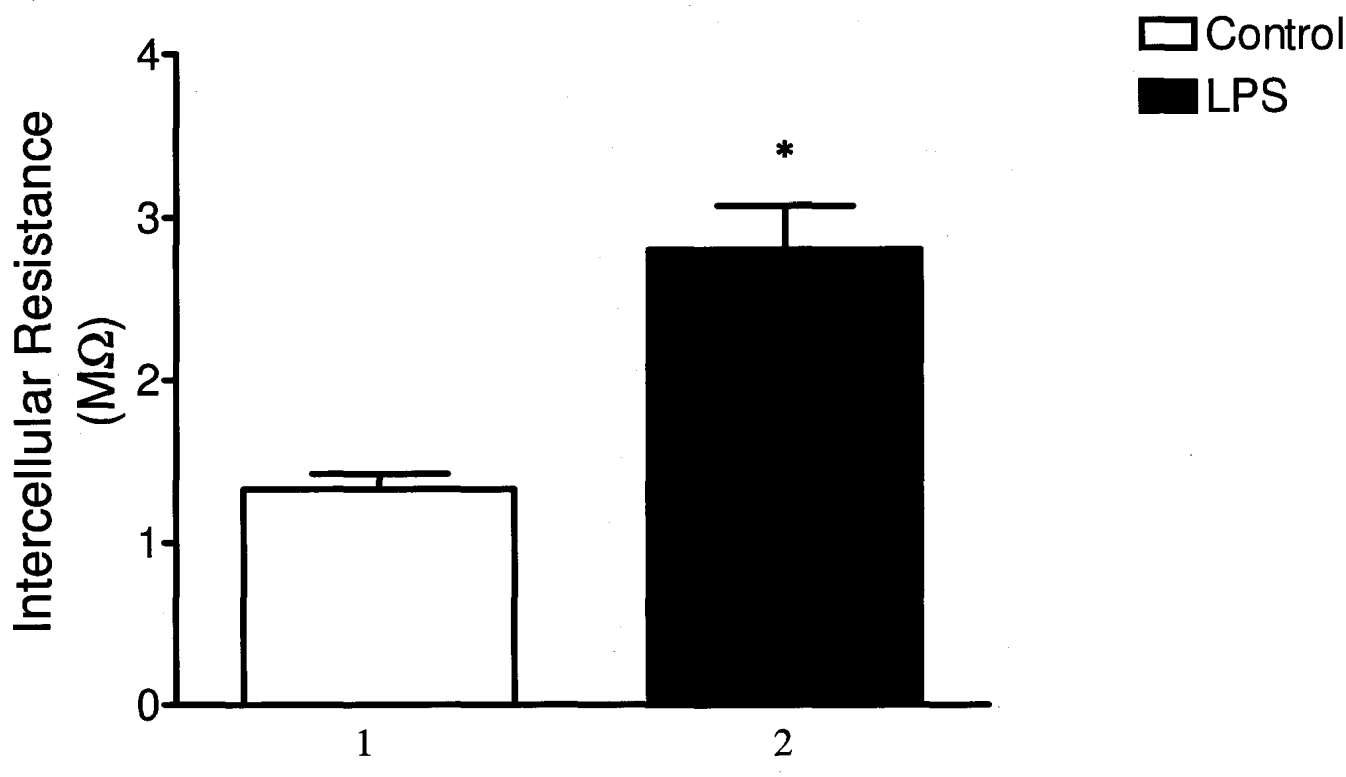

Figure 11. LPS (10 μg/ml, 1 hour) exposure increased intercellular resistance (an inverse measure of electrical coupling) in WT cells, indicating that LPS reduced electrical coupling in the cell monolayer. * indicates significant difference from the appropriate control group, $p < 0.05$, $n = 6$ monolayers for bar 1 and $n = 10$ for bar 2 ('n' values in both the groups were derived from 3 mice).

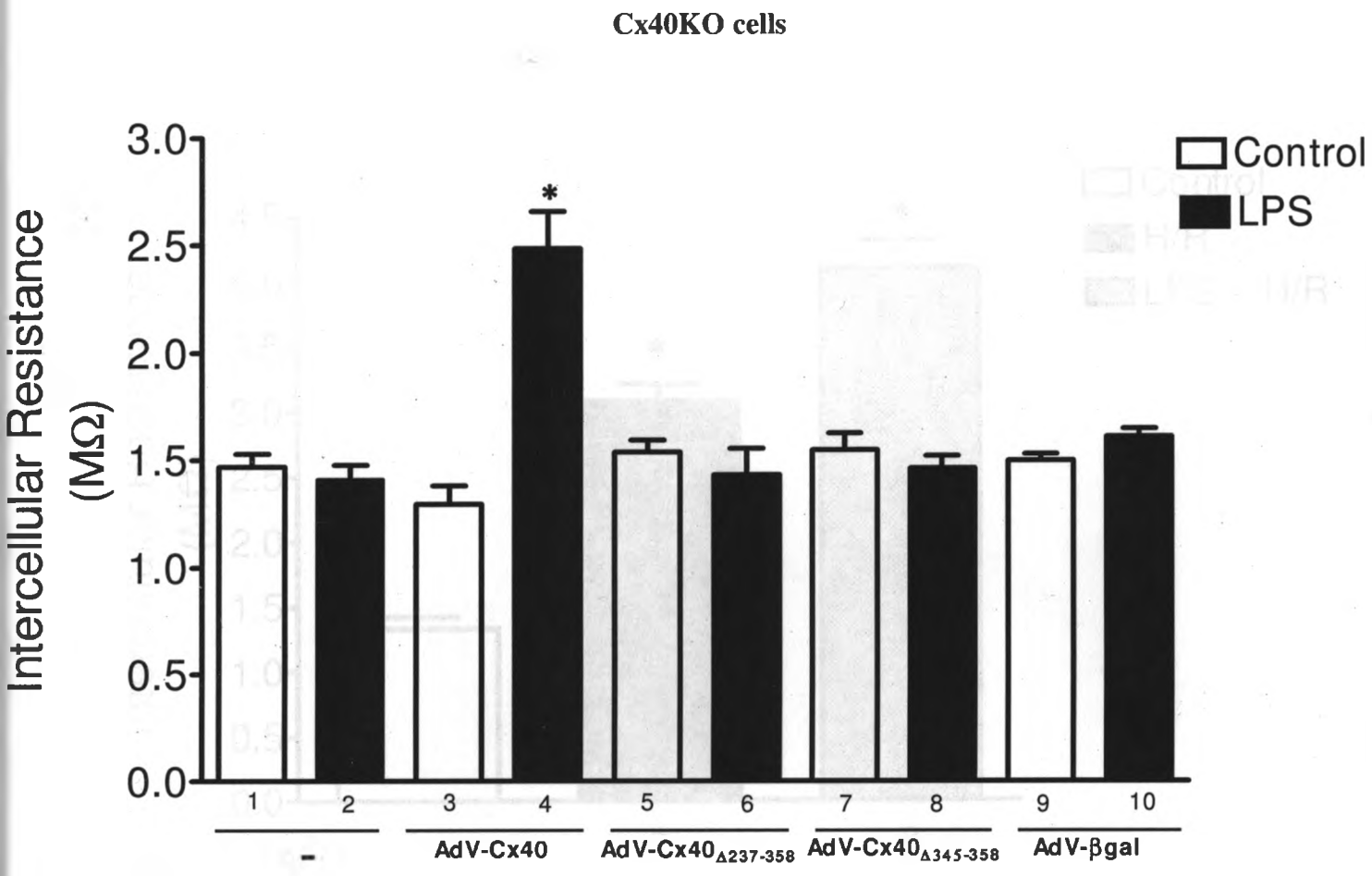

Figure 12. Effect of LPS (10 µg/ml, 1 hour) on intercellular resistance in non-infected Cx40 KO cells, Cx40 KO cells infected with AdV-Cx40, AdV-$Cx40_{\Delta 237-358}$, AdV-$Cx40_{\Delta 345-358}$ and AdV-βgal. (MOI of all the adenoviruses was 50 ifu/cell). LPS increased resistance only in Cx40 KO cells infected with AdV-Cx40 (i.e., mimicking the response in WT cells). Cx40KO cells, Cx40KO cells infected with Cx40 without its carboxylic tail and without the end region of its carboxylic tail showed no response. * indicates difference from appropriate control at $p< 0.05$, n = 22 (7 mice), n = 10 (5 mice), n = 16 (6 mice), n = 16 (4 mice), n = 8 (3 mice), n = 6 (4 mice), n = 11 (5 mice), n = 6 (3 mice), n=3 (2 mice) and n=3 (2 mice) for bars 1 to 10 respectively.

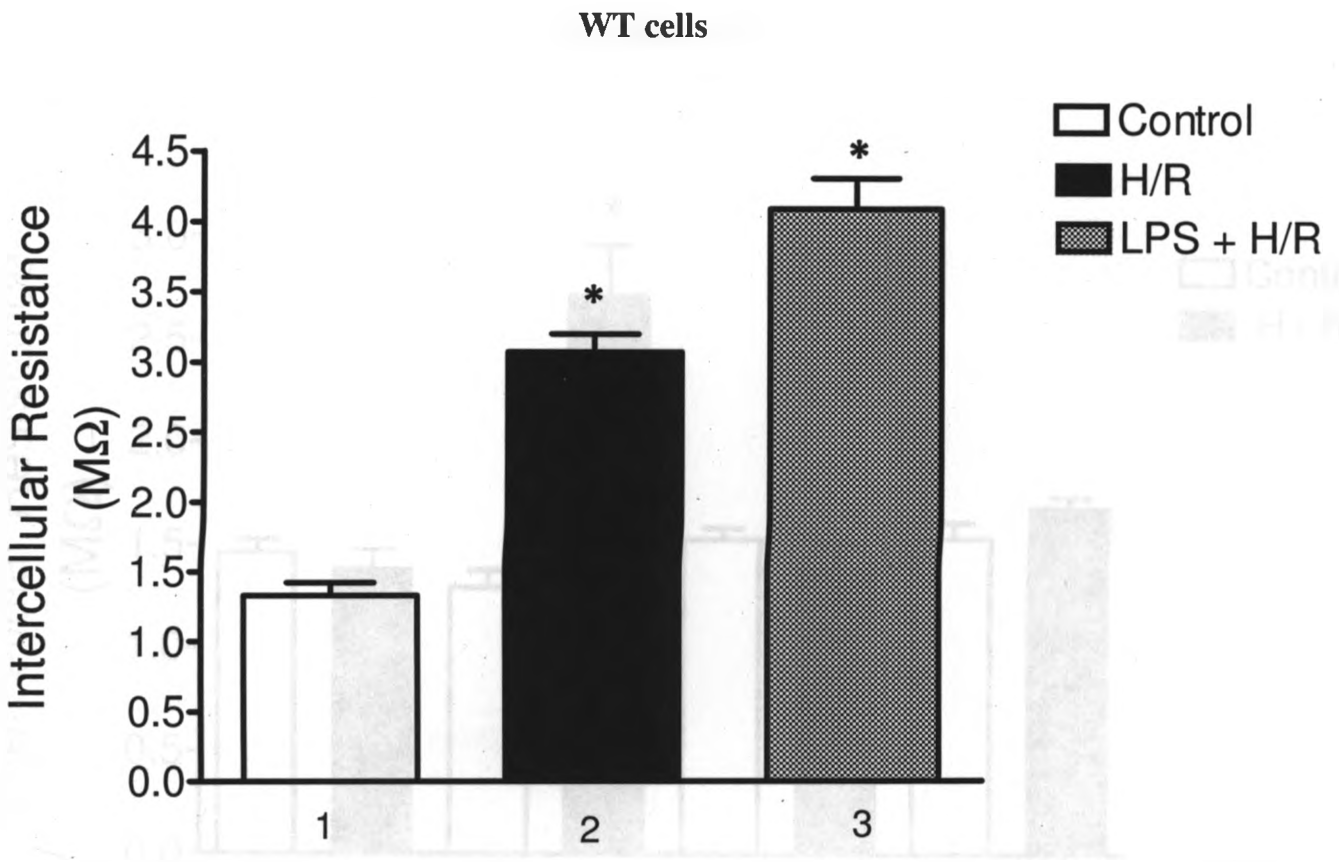

Figure 13. Effects of hypoxia (H; 0.1 % O_2, 1 hour) followed by reoxygenation (R; 20% O_2, 5-15 minutes) and H/R + LPS (10 μg/ml, 1 hour) on intercellular resistance in wild-type cells. H/R is shown to increase intercellular resistance in the wild-type cells. Larger increase in resistance is seen in WT cells concurrently treated with LPS+H/R. * indicates significant difference from the control group (bar 1), $p < 0.05$. n = 6 (3 mice), n = 4 (2 mice) and n = 4 (2 mice) for bars 1, 2 and 3 respectively.

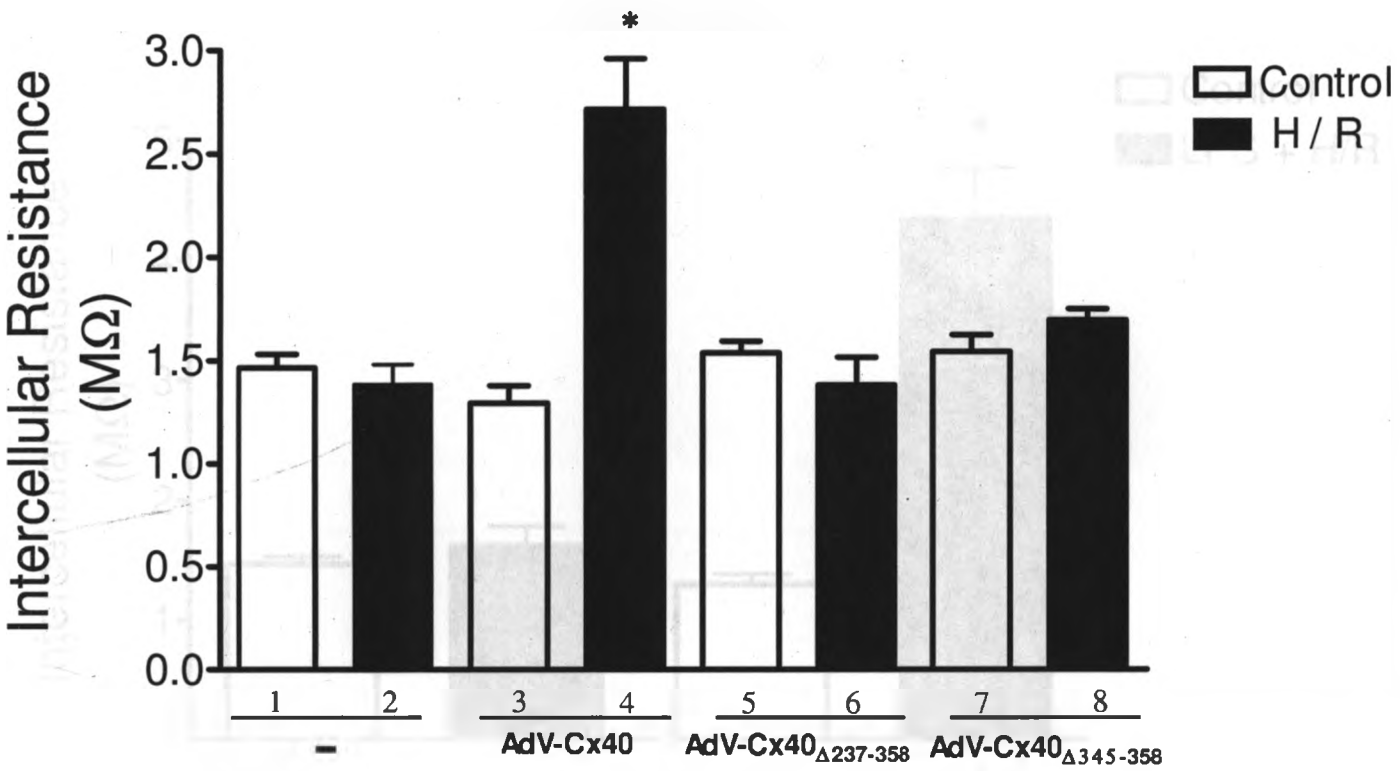

Figure 14. Effect of hypoxia (H; 0.1 % O_2, 1 hour) followed by reoxygenation (R; 20% O_2, 5-15 minutes) on intercellular resistance in non-infected Cx40 KO cells, Cx40 KO cells infected with AdV-Cx40, AdV-Cx40$_{\Delta 237\text{-}358}$ and AdV-Cx40$_{\Delta 345\text{-}358}$ (MOI of all the adenoviruses was 50 ifu/cell). H/R increased resistance only in Cx40 KO cells infected with AdV-Cx40 (i.e., mimicking the response in WT cells). Cx40KO cells, Cx40KO cells infected with Cx40 without its carboxylic tail and without the end region of its carboxylic tail showed no response. * indicates significant difference from appropriate control at $p< 0.05$, n = 22 (7 mice), n = 11 (5 mice), n = 16 (6 mice), n = 8 (3 mice), n = 8 (3 mice), n = 4 (3 mice), n = 11 (5 mice) and n = 6 (3 mice) for bars 1 to 8 respectively.

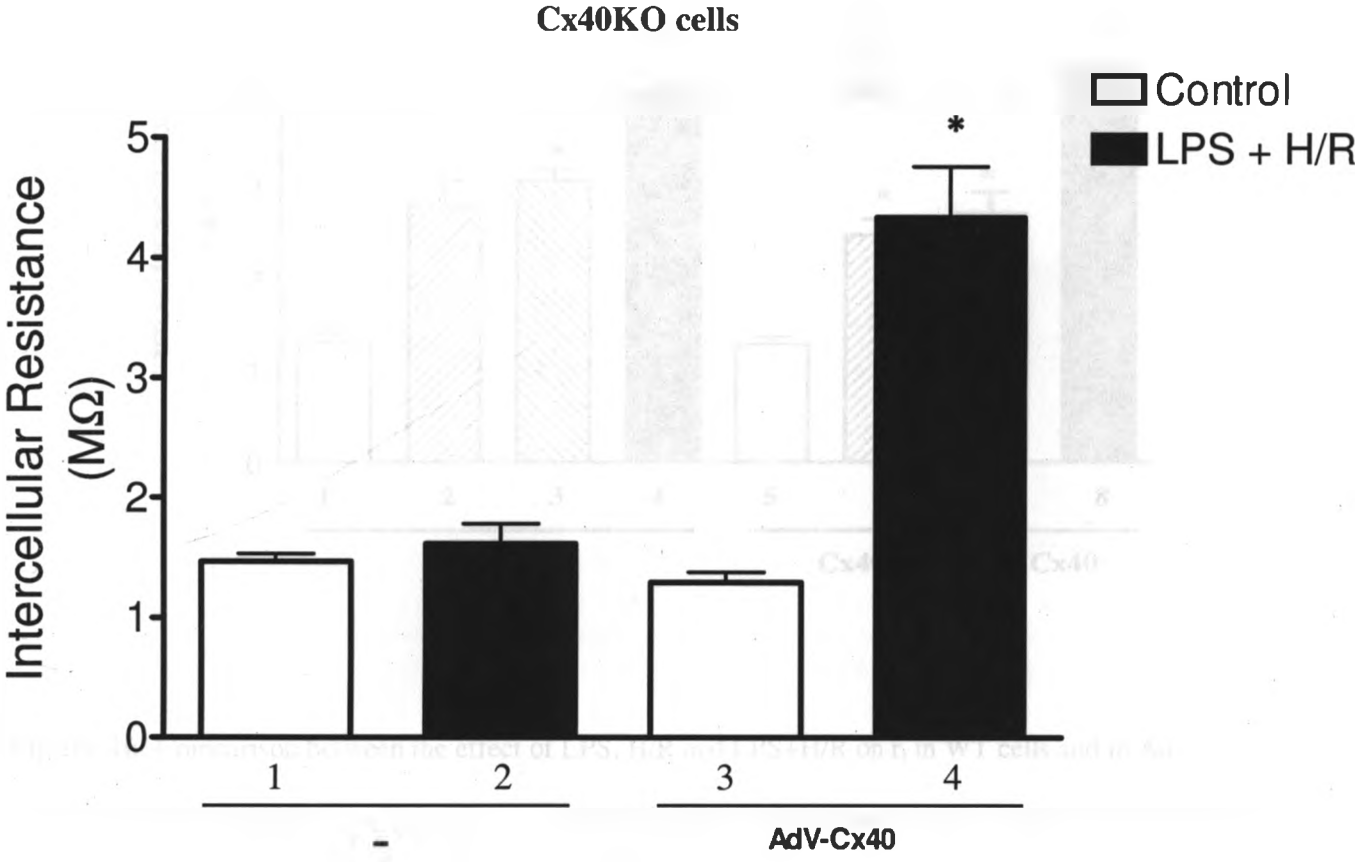

Figure 15. Concurrent effect of LPS + H/R on intercellular resistance in non-infected Cx40 KO cells and Cx40 KO cells infected with AdV-Cx40 at MOI of 50 ifu/cell. LPS+H/R increased resistance only in Cx40 KO cells infected with AdV-Cx40 (i.e., mimicking the response in WT cells). Cx40KO cells, Cx40KO cells infected with Cx40 without its carboxylic tail and without the end region of its carboxylic tail showed no response. * indicates difference from appropriate control at $p < 0.05$, n = 22 (7 mice), n = 5 (3 mice), n = 16 (6 mice), n = 7 (3 mice) for bars 1 to 4 respectively.

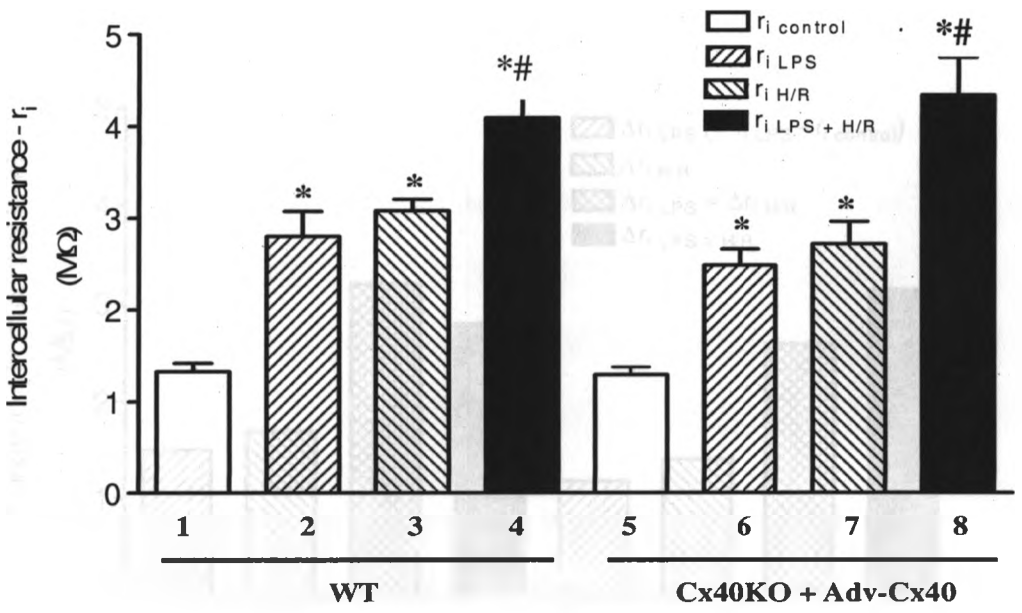

Figure 16. Comparison between the effect of LPS, H/R and LPS+H/R on r_i in WT cells and in Adv-Cx40 - infected Cx40KO cells. Values of r_i recorded for LPS+H/R treatment in these cells was more than the r_i recorded for LPS or H/R treatment alone. * indicates difference from appropriate control bar 1, # difference of data in bar 4 from bar 2 or 3, or difference of data in bar 8 from bar 6 or 7. n = 6 (3 mice), n=10 (3 mice), n=4 (2 mice), n=4 (2 mice), n=16 (6 mice), n=16 (4 mice), n=8 (3 mice) and n=7 (3 mice) in groups 1-8, respectively, $p< 0.05$.

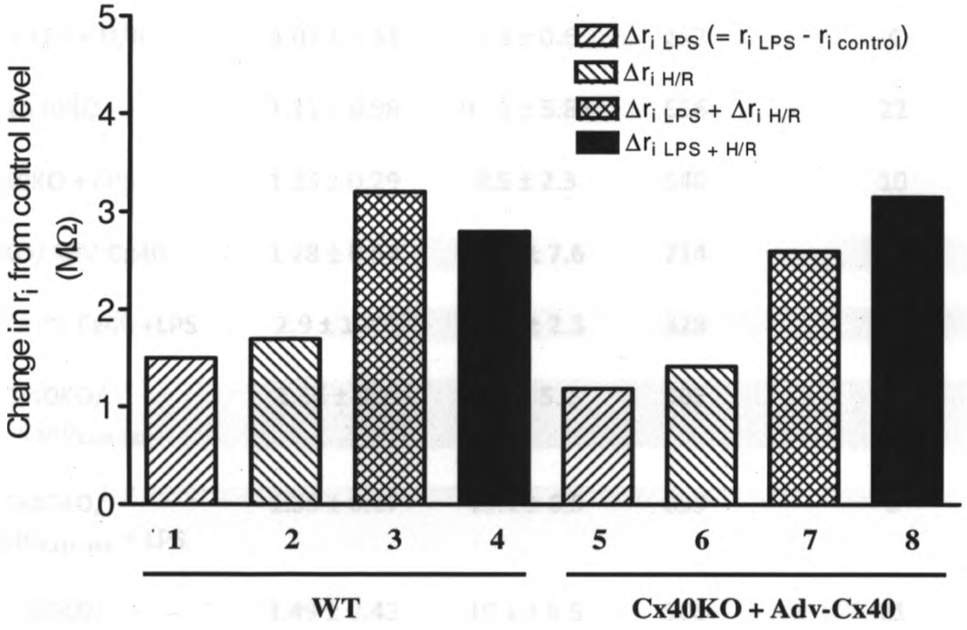

Figure 17. Using the average r_i values shown in Figure 16, Figure 17 shows increase in r_i relative to control, in WT cells and Adv-Cx40 - infected Cx40KO under the influence of LPS, H/R and LPS+H/R. Effect of LPS+H/R on the increase in r_i in both the cell types (bars 4 and 8) apprears not different from the computed sum of increases in r_i after discreet treatment of LPS and H/R (bars 3 and 7).

Cell monolayer	r_i (MΩ)	R_m (kΩ cm^2)	λ (μm)	n (monolayers)	No. of mice
WT	1.33 ± 0.33	7.6 ± 1.7	542	6	3
WT + LPS	3.08 ± 1.25	9.2 ± 3.4	306	10	3
WT + H/R	3.06 ± 0.32	7.68 ± 1.77	278	4	2
WT + LPS + H/R	4.02 ± 0.51	9.3 ± 0.6	257	4	2
Cx40KO	1.11 ± 0.98	9.45 ± 5.85	556	22	7
Cx40KO + LPS	1.35 ± 0.29	8.5 ± 2.3	540	10	5
Cx40KO/AdV-Cx40	1.28 ± 0.54	11.5 ± 7.6	714	16	6
Cx40KO/AdV-Cx40 +LPS	2.9 ± 1.47	12.9 ± 2.3	328	16	4
Cx40KO/ AdV-$Cx40_{\Delta 236-358}$	1.56 ± 0.2	9.6 ± 5.2	502	8	3
Cx40KO/ AdV-$Cx40_{\Delta 236-358}$ + LPS	1.35 ± 0.27	10.1 ± 6.5	659	6	4
Cx40KO/ AdV-$Cx40_{\Delta 345-358}$	1.49 ± 0.43	10.1 ± 6.5	566	11	5
Cx40KO/ AdV-$Cx40_{\Delta 345-358}$ + LPS	1.43 ± 0.21	7.45 ± 1.95	436	6	3
Cx40 + H/R	1.29 ± 0.35	10.05 ± 4.2	684	11	5
Cx40KO/AdV-Cx40 +H/R	3.13 ± 1.1	13.1 ± 4.7	313	8	3
Cx40KO/ AdV-$Cx40_{\Delta 236-358}$ + H/R	1.41 ± 0.29	11.0 ± 6.6	621	4	3
Cx40KO/ AdV-$Cx40_{\Delta 345-358}$ + H/R	1.68 ± 0.2	7.55 ± 0.8	632	6	3
Cx40 + LPS + H/R	1.59 ± 0.44	7.72 ± 1.42	588	5	3
Cx40KO/ AdV-Cx40 + LPS + H/R	4.08 ± 1.47	10.5 ± 5.4	257	7	3

Table 1 (previous page). Electrophysiological data representing the values of intercellular resistance, ri, membrane resistivity(-Rm) and space constant (-λ) for WT and Cx40KO (infected and uninfected with adenoviruses) cell monolayers, with and without the treatment of LPS, H/R and LPS+H/R. *n* values (cell lines) and total number of monolayers used in each group is also shown.

Chapter 5 : Discussion

5.1 Key Findings and review of rationale

In the present study, I succeeded for the first time in infecting the MMEC with various adenoviruses. I also show, for the first time, the crucial role of Cx40 carboxylic tail in the reduced electrical coupling between MMEC after LPS, H/R and LPS+H/R treatment. As we have previously reported that PKA-dependent Cx40 phosphorylation of serine residues is instrumental in the regulation of GJIC (Bolon et al., 2008), the findings of this project indicated that these serine residues targeted by LPS-, H/R- and LPS+H/R-induced signaling are present in the serine-rich end region of the Cx40 carboxylic tail (residues 345-358). These data also indicate that LPS, H/R and LPS+H/R signaling targets either the same serine residue/s or, one or more of the five serine residues (345-358) present in close proximity to each other in the end region of the Cx40 carboxylic tail (Figure 2).

LPS being a major constituent of the bacteria causing sepsis (Bone, 1991) and I/R being associated with impaired microvascular blood flow during sepsis (De Backer et al., 2002), the effect of LPS and H/R at the molecular level, leading to reduced GJIC, was worth investigating. Though the role of certain Cx40 serine residues in reduced electrical coupling in MMEC after LPS and H/R treatment has previously been reported by our lab (Bolon et al., 2008), the question that still remained as to whether those serine residues reside in the carboxylic tail of Cx40, has been answered in the findings. Since, we also asked if LPS, H/R and LPS+H/R signaling targets common serine residues, the key findings of my thesis was also able to address this query.

5.2 Methodological considerations

5.2.1 Difficulties faced during adenovirus preparation:

Procedural aspects involving adenovirus amplification in HEK293 cells, titration & purification and successful infection of MMEC has been quite a challenge throughout the project, requiring modifications in the corresponding protocols and help from Dr. Tianqing Peng.

Periodical inspection of the progress of cytopathic effect of the virus during the amplification procedure and critical judgment to harvest the infected HEK293 cells in time were the key elements in obtaining the virus of high potency. Drop-wise filtration and careful elution of viral supernatant during the purification procedure required a great deal of patience and skillful approach. Before resorting to the use of QuickTiter™ Adenovirus Titer Immunoassay Kit (as recommended by Dr. Tianqing Peng) for accurately measuring virus titer, I had attempted several times doing plaque-forming unit assay (PFU) that is expected to score number of viral plaques as a function of dilution. Unfortunately, this PFU assay method was not only time-consuming (10 days) and required a long infection period but also, inexplicably, suffered from a high degree of inter-assay variability. Instead of the PFU approach I used the IFU approach utilizing the QuickTiter™ Adenovirus Titer Immunoassay Kit. This kit uses an antibody against adenovirus hexon proteins to visualize infected cells by immunocytochemistry staining, to permit determination of the titer virus infectivity.

Since the titration is the last of the procedures involved in the preparation of virus for infecting MMEC, any lapse in the preceding procedures would require the starting of the complete process all over again.

5.2.2 Trouble spots in electrophysiology

Achieving the full and steady resting potential for both the electrodes is one of the criteria for the valid electrophysiological recordings. During the course of my electrophysiology experiments, meeting this criterion has been an intimidating challenge until I was able to rightly attribute the shortcoming to the electrodes' tips with inconsistent length and thickness. Long and thin electrodes with sharp-pointed tips are considered ideal in order to reduce damage to a cell during insertion. Changing the electrodes repeatedly in quick successions during the experiments would rectify the problem, but only temporarily. Replacing of the over-used heating element of the puller with the new ones helped resolving the issue to a large extent. Moreover, increasing the acute angle of the electrode to the cell surface helped making a much perfect impalement, which otherwise at a lesser acute angle would scrape the cell surface and accumulate cell debris into the electrode tip. Deposition of salt over time on the outer surface of the electrode holders (half-cells) or worn-out rubber septum of the half-cell would badly effect the conduction of electric current through the electrodes. Thus, good functioning of electrodes also necessitated regular maintenance of the electrode holders or replacing with a new one as needed.

In the event of unstable resting E_m and/or intra-experimental variability in E_m values, the potential factors involved were thoroughly verified and tackled so as to generate valid electrophysiological recordings.

5.3 Comparison of the present data with the literature

5.3.1 Effect of LPS treatment on r_i:

The observed increase in r_i following 1 hour LPS exposure in MMEC (~100% increase in WT cells and ~70% increase in Cx40KO cells infected with AdVCx40) is consistent with our

previously reported 100% increase (Bolon et al., 2007) and 60% increase (Lidington et al., 2000) in r_i following 1 hour LPS exposure in the wild-type MMECs and RMECs respectively. Reported reduction in dye coupling after 30 minutes of LPS between human umbilical vein endothelial cells and human umbilical vein smooth muscle cells (Hu & Cotgreave, 1997) also falls in line with the present findings. No significant change in r_i in Cx40KO cells separately infected with AdV-Cx40$_{\Delta 236\text{-}358}$ and AdV-Cx40$_{\Delta 345\text{-}358}$, and treated with LPS, indicates that the serine residues in the end region of the carboxylic tail are the potential targets in the LPS-induced signaling.

5.3.2 Effect of H/R treatment on r_i:

Similar to the LPS study, our findings of H/R-induced increase in r_i in MMEC (100% increase in WT and 85% increase in Cx40KO cells infected with AdVCx40) are consistent with our previously reported 100% increase (Bolon et al., 2005) and 32 % increase (Rose et al., 2005) in r_i in the wild-type MMECs and RMECs respectively. Our data are also consistent with the effect of long-term H/R (12–16 hours hypoxia plus 1–2 hours reoxygenation), which reduced coupling in both HUVEC (Zhang et al., 1999, 2000a and 2000b) and rat cortical astrocytes (Martinez and Saez, 2000). As in the case of LPS study, unaltered values of r_i in AdV-Cx40$_{\Delta 236\text{-}358}$ - , and AdV-Cx40$_{\Delta 345\text{-}358}$ - infected Cx40KO cells, subjected to H/R, implicate one or more of the 5 serine residues present in the end region of Cx40 carboxylic tail as potential sites of dephosphorylation in the H/R-induced signaling pathway.

5.3.3 Effect of LPS+H/R treatment on r_i :

Increase in r_i, in LPS+H/R treatment in Cx40KO cells infected with AdV-Cx40 was, moreover, the sum of the increase in r_i following H/R or LPS stimulus alone. This findings, reflecting the additive effect of the concurrent LPS+H/R stimulation, are also consistent with the *in vivo* studies in which shock/resuscitation - induced oxidative stress exaggerated LPS responsiveness with excessive generation of proinflammatory molecules (Powers et al., 2006; Cuschieri and Maier, 2007). Similar to the effect of LPS or H/R signaling, LPS+H/R signaling seems to target serine residues present in the end region of Cx40 carboxylic tail.

5.4 Effect of LPS, H/R, and LPS+H/R treatment on R_m and λ

I observed that LPS-, H/R-, and LPS+H/R - induced changes in membrane resistivity, R_m, and space constant, λ, were not always consistent, because of the low *n* value per experiment. To assess the overall effect of each stimulus on R_m and λ, I separately pooled all the data derived from control and treated groups (infected and uninfected cell monolayers). On the basis of these data, I found that LPS, H/R or LPS+H/R treatment did not affect R_m, indicating that the treatment-induced change in spatial decay of injected current along the monolayer was mainly due to the change in intercellular resistance, rather than due to change in current leakage from the intra- to extra-cellular space (i.e., a change in leakage would be expected to result from a change in transmembrane resistivity R_m). However, the values for λ were significantly decreased after LPS and/or H/R treatment.

5.5 Proposed signaling pathways

The carboxyl terminal domain contains the most pronounced sequence diversity among different connexins, as well as a large number of potential phosphorylation sites. Previous investigations have examined the possibility that differential phosphorylation by intracellular protein kinases plays a major role in regulating the specific functions of connexins. This thesis examined and confirmed the role of Cx40 carboxylic tail in GJIC in a model of sepsis comprising of LPS and H/R stimuli. Although the role of Cx40 carboxylic tail in the regulation of gap junction activity is previously reported (Stergiopoulos et al., 1999; Anumonwo et al., 2001; Moreno et al., 2002), the present study identifies for the first time the specific region in Cx40 carboxylic tail, having the serine residues which are potential phosphorylation site for PKA, in control of intercellular electrical coupling. However, the precise mechanisms of LPS-, H/R and LPS+H/R signaling pathways resulting in reduced coupling are not yet understood. But it is known that regardless of the difference in initiation of their pathways, these stimuli seem to share a common end-point as PKA-dependent serine dephosphorylation of Cx40 (Bolon et al., 2008), involving the serine residues that are present in the end region of its carboxylic tail (345-358).

In the context of the key findings and based on the relevant research published, some of the possible signaling pathways that may help in understanding the potential mechanisms are proposed as follows.

5.5.1 Potential role of protein-protein interaction:

Intrinsically disordered structure of Cx40 carboxylic tail as characterized by the use of NMR (Bouvier et al., 2008) seems to play an important role in protein-protein interaction,

protein modification and cell signaling events, including phosphorylation (Dunker and Obradovic, 2001). Protein–protein interactions are key elements in building functional protein complexes, among which second PDZ domain (PDZ-2) of zonula occludens (ZO)-1 is most common (Herve et al., 2007).

Structural change in the Cx40 carboxylic tail has been reported to occur upon binding to ZO-1 and domain of c-Src (plasma membrane-associated tyrosine kinase) (Bouvier et al., 2008). Interestingly, the region in Cx40 carboxylic tail shown to be modified by the binding of ZO-1 (residues 333-355) largely corresponds to the one, identified by us in the present study (residues 345-358), comprising of serine residues functional in the regulation of GJIC under the effect of LPS and/or H/R. Unlike in Cx40, the binding of c-Src and ZO-1 to Cx43 carboxylic tail are interdependent, since c-Src can disrupt the Cx43/ZO-1 interaction, leading to the down-regulation of GJIC (Toyofuku et al., 2001, Duffy et al., 2004). Based on the findings of the thesis it can be hypothesized that LPS-, H/R- and LPS+H/R-induced, PKA-dependent serine dephosphorylation of Cx40 at residues 345-358 is necessary to dissociate the Cx40CT/ZO-1 interaction, resulting in reduced electrical coupling.

5.5.2 'Particle-receptor' model in support of Cx40 function:

The carboxyl terminal acts as an independent domain ("binding particle") that upon intracellular acidification recognizes and noncovalently binds to a specific peptide sequence at or near the pore (acting as a receptor for the particle), thus closing the channel. This would suggest that at least two regions of the molecule act in concert to bring about acidification-induced uncoupling (Morley et al., 1996). Diminished pH sensitivity in carboxylic tail-truncated Cx40 was restored by coexpression of its carboxylic tail region suggesting that the carboxylic tail

domain was able to interact directly or indirectly with the pore-forming region of Cx40 to restore pH sensitivity. Thus acidification may cause gap junction channel closure and loss of functional synchronization between cells (Delmar et al., 1994, Saffitz et al., 1995). Among vascular connexins, only the carboxylic tails of Cx40 and Cx43, and not of Cx37 and Cx45, are shown to play a role in pH-sensitive channel gating (Stergiopoulos et al., 1999).

Though the molecular mechanisms mediating this process are not yet understood it can be postulated that during sepsis, LPS-induced lactic acidosis (Kellum et al., 2003), and H/R-induced intracellular $Ca2^{+}$ and H^{+} overload (Strenbergen et al., 1987; Dekker et al., 1996) may facilitate the model of acidification-induced uncoupling following 'Particle-receptor' hypothesis. Moreover, since intracellular acidosis has been shown to suppress PKA-mediated phosphorylation of Cx43 (Imanaga et al., 2002; Matsumura et al., 2006), it was suggested that PKA-mediated phosphorylation of Cx43 is affected by the ionic strength of H^{+}. Similar conditions of increase in acidosis under the effect of LPS and /or H/R may result in reduced PKA-dependent Cx40 phosphorylation of serine residues in the end region of its carboxylic tail, resulting in uncoupling of cells.

5.5.3 pH-dependent hetero-domain interaction:

Compared to homomeric channels, the regulation of heteromeric channels are more complex. Hetero-domain interaction (in which, regulatory domain of one connexin interacts with a homomeric channel formed by a different isoforms) between connexins has been reported as the basis for regulation of heteromeric channels (Stergiopoulos et al., 1999). Cx43 carboxylic tail co-expressed with Cx40 without its carboxylic tail, or vice-versa, was shown to rescue pH-sensitive channel gating of the heteromeric channel. Not only that the hetero-domain interactions

were observed to be more effective at closing the channel in response to acidification than the homo-domain interactions, they were specifically effective in-between Cx40 and Cx43. This suggests that the possible co-expression of Cx40 and Cx43 in mouse endothelium (Isakson et al., 2006), may involve hetero-domain interaction between the connexins in order to regulate closure of acidification- induced heteromeric channel.

Sepsis cause increase in intracellular acidosis (Fall and Szerlip, 2005) which also suppresses PKA-mediated phosphorylation (Matsumura et al., 2006). Hence, in the light of present study it can be suggested that the reduced PKA activity during the effect of LPS and/or H/R leads to the dephosphorylation of serine residues in the end region of Cx40 carboxylic, rendering Cx40 in-sensitive to pH-dependent channel gating. Thus hetero-domain interaction involving Cx43 might take place to rescue the pH-sensitivity of Cx40, eventually closing the heteromeric gap junction channel.

5.6 Implications

Impaired arteriolar conducted response in sepsis is attributed mainly to the electrical uncoupling of microvascular endothelial cell (Segal, 2005), involving closure of gap junction channels present between them (Goodenough et al., 1996). Understanding the role and regulation of gap junction protein responsible for reduced coupling in sepsis is prerequisite to addressing the issue of microvascular blood flow impairment in the disease state. Adding to the fact that Cx40 is targeted in the reduced electrical coupling between MMEC in sepsis in PKA-dependent manner (Bolon et al., 2008), this study for the first time determined the region in the carboxylic tail of Cx40 (345-358) that is targeted to produce the effect. Episodes of I/R associated with sepsis has been shown to aggravate microvascular impairment due to excessive generation of

proinflammatory molecules (Powers et al., 2006; Cuschieri and Maier, 2007). Findings of the thesis, based on electrophysiological studies, can well explain this increased impairment of vascular function at sub cellular level.

Cx40 are found to co express with Cx43 in cardiac tissues (Severs et al., 2001). Effect of episodes of I/R due to compromised blood flow during myocardial infarction can be studied in the light of the present study, taking into account the key role of Cx40 carboxylic tail in reduced electrical coupling between cells and closure of heteromeric gap junction channel under the effect of H/R.

5.7 Future directions

Indeed, the key findings of this project have the potential to launch new research avenues pertaining to pathophysiological state of sepsis. Also, already reported observations in vascular dysfunction during sepsis may be subjected to re-examination in context of intercellular electrical coupling and the role of Cx40 carboxylic tail.

Since any (or all) of the 5 serine residues among the last 17 residues in the Cx40 carboxylic tail are thought to play a key role in reduced electrical coupling in MMEC during sepsis, further dissection on this end region of the tail can be performed to determined the specific serine residue/s that produce the effect.

Since the increased intracellular acidosis, as during sepsis (Fall and Szerlip, 2005), is known to reduce PKA-dependent phosphorylation, as seen in Cx43 (Matsumura et al., 2006), the effect of change in pH on the PKA-dependent phosphorylation of Cx40 could be tested out. If the reduced pH under the effect of LPS suppresses PKA activity, as in the case of Cx43, thus resulting in dephosphorylation of serine residues in the end region of Cx40 carboxylic tail, then

the modulation of pH can be used as a tool to counteract the eventual reduction in electrical coupling during sepsis. This may also help in regulating pH-sensitive channel gating due to homo-domain and/or hetero-domain interactions involving Cx40 with other isoforms.

The role of serine residues in the end region of Cx40 carboxylic tail (345-358) could also be studied in the context of myocardial contractility and the pathophysiology of arrhythmia in ischemic heart, as both Cx43 and Cx40 are important for cell coupling in the beating heart.

References

Alexander, D. B., Goldberg, G. S. (2003) Transfer of biologically important molecules between cells through gap junction channels. *Curr Med Chem.*, **10**, 2045–2058.

Ambrosio, G., Tritto, I. (1999) Reperfusion injury: experimental evidence and clinical implications. *Am. Heart J.* **138**, S69–S75.

Anumonwo, J. M., Taffet, S. M., Gu, H., Chanson, M., Moreno, A. P., Delmar, M.,(2001) The carboxyl terminal domain regulates the unitary conductance and voltage dependence of connexin40 gap junction channels. *Circ. Res.*, **88**, 666–673.

Arditi, M., Zhou, J., Torres, M., Durden, D. L., Stins, M., Kim, K. S. (1995) Lipopolysaccharide stimulates the tyrosine phosphorylation of mitogen-activated protein kinases p44, p42, and p41 in vascular endothelial cells in a soluble CD14-dependent manner. Role of protein tyrosine phosphorylation in lipopolysaccharide-induced stimulation of endothelial cells. *J Immunol*, **155**, 3994-4003.

Armour, J., Tyml, K., Lidington, D., Wilson, J. X.. (2001) Ascorbate prevents microvascular dysfunction in the skeletal muscle of the septic rat. *J Appl Physiol*, **90**, 95–803.

Azarnia, R., Reddy, S., Kmiecik, T. E., Shalloway, D., Loewenstein, W. R. (1988) The cellular src gene product regulates junctional cell-to-cell communication. *Science*, **239**, 398- 401.

Barchowsky, A., Williams, M. E., Benz, C. C. (1994) Oxidant - sensitive protein phosphorylation in endothelial cells. *Free Radic. Biol. Med.* **16**, 771-777.

Bateman, R. M., Jagger, J. E., Sharpe, M. D., Ellsworth, M. L., Mehta, S., Ellis, C. G. (2001) Erythrocyte deformability is a nitric oxide-mediated factor in decreased capillary density during sepsis. *Am J Physiol Heart Circ Physiol*, **280**, H2848–H2856.

Bauer, P.R. (2002) Microvascular responses to sepsis: clinical significance. *Pathophysiology*, **8**, 141-148.

Beardslee, M., Laing, J., Beyer, E., & Saffitz, J. (1998) Rapid turnover of connexin43 in the adult rat heart. *Circulation Research*, **83**, 629–635.

Bennett, M. V. (1994) Connexins in disease, *Nature*, **368**, 18-19.

Berthoud, V. M., Beyer, E. C., Kurata, W. E., Lau, A. F., Lampe, P. D. (1997) The gap junction protein connexin 56 is phosphorylated in the intracellular loop and the carboxyl- terminal region. *European Journal of Biochemistry*, **244**, 89-97.

Blom, N., Sicheritz-Ponten, T., Gupta, R., Gammeltoft, S., Brunak, S. (2004) Prediction of posttranslational glycosylation and phosphorylation of proteins from the amino acid sequence. *Proteomics*, **4**, 1633–1649.

Bolon, M.L., Ouellette, Y., Li, F., Tyml, K. (2005) Abrupt reoxygenation following hypoxia reduces electrical coupling between endothelial cells of wild-type but not connexin40 null mice in oxidant- and PKA-dependent manner. *FASEB J.*, **19,** 1725-1727.

Bolon M. L., Kidder, G. M., Simon, A. M., Tyml, K. (2007) Lipopolysaccharide reduces electrical coupling in microvascular endothelial cells by targeting connexin40 in a tyrosine-, ERK1/2-, PKA-, and PKC-dependent manner. *J Cell Physiol.*, **211,** 159-166.

Bolon, M. L., Peng, T., Kidder, G. M., Tyml, K. (2008) Lipopolysaccharide plus hypoxia and reoxygenation synergistically reduce electrical coupling between microvascular endothelial cells by dephosphorylating connexin40. *J Cell Physiol*, **217** (2), 350-359.

Bone, R. C. (1991). Gram-negative sepsis. Background, clinical features, and intervention. *Chest,***100**, 802–808.

Bouvier , D., Kieken, F., Kellezi, A., Sorgen, P. L. (2008) Structural Changes in the Carboxyl Terminus of the Gap Junction Protein Connexin40 Caused by the Interaction with c-Src and Zonula Occludens-1. *Cell Communication and Adhesion*, **15**, 107–118.

Brad, L. U., Kyung-Sun, K., Hye-Youn, C., James, E. T.(1997) Hydrogen peroxide inhibits gap junctional intercellular communication in glutathione sufficient but not glutathione deficient cells. *Carcinogenesis*, **18**, 37- 42.

Butterweck, A., Gergs, U., Elfgang, C., Willecke, K., Traub, O. (1994) Immunochemical characterization of the gap junction protein connexin45 in mouse kidney and transfected human HeLa cells. *J. Membr. Biol.* **141,** 247–256.

Boerma, E. C., van der Voort, P. H. J., Spronk, P. E., Ince, C. (2007) Relationship between sublingual and intestinal microcirculatory perfusion in patients with abdominal sepsis. *Crit Care Med*, **35**, 1055–1060.

Bruzzone, R., Haefliger, J. A., Gimlich, R. L., Paul, D. L. (1993) Connexin40, a component of gap junctions in vascular endothelium, is restricted in its ability to interact with other connexins. *Mol Biol Cell.* **4**, 7-20.

Bruzzone, R., White, T. W., Paul, D. L. (1996) Connections with connexins: the molecular basis of direct intercellular coupling. *Eur. J. Biochem.*, **238**, 1-27.

Calero, G., Kanemitsu, M., Taffet, S. M., Lau, A. F., Delmar, M. (1998) A 17mer peptide interferes with acidification-induced uncoupling of connexin43. *Circ. Res.*, **82**, 929-935.

Chanson, M., Scerri, I., uter, S. (1999) Defective regulation of gap junctional coupling in cystic fibrosis pancreatic duct cells. *J. Clin. Invest.* **103,** 1677–1684.

Cipolle, M. D., Pasquale, M., Cerra, F.B. (1993) Secondary organ dysfunction. From clinical perspectives to molecular mediators. *Crit. Care Clin,* **9**, 261-298.

Clauss, S. B., Walker, D. L., Kirby, M. L., Schimel, D., Lo, C. W. (2006) Patterning of coronary arteries in wildtype and connexin43 knockout mice. *Dev Dyn,* **235**, 2786–2794.

Cottrell, G. T., Lin, R., Warn-Cramer, B. J., Lau, A. F., Burt, J. M. (2003) Mechanism of v-Src- and mitogen-activated protein kinase-induced reduction of gap junction communication. *Am. J. Physiol., Cell Physiol,,* **284**, C511– C520.

Crow, D. S., Beyer, E. C., Paul, D. L., Kobe, S. S., Lau, A. F. (1990) Phosphorylation of connexin43 gap junction protein in uninfected and Rous sarcoma virus-transformed mammalian fibroblasts. *Molecular and Cellular Biology*, **10**, 1754–1763.

Cryer, H. M., Garrison, R. N., Kaebnick, H. W., Harris, P. D., Flint, L. M. (1987) Skeletal microcirculatory responses to hyperdynamic Escherichia coli sepsis in anaesthetized rats. *Arch Surg*, **122**, 86–92.

Cuschieri, J., Maier, R. V. (2007) Oxidative stress, lipid rafts, and macrophage reprogramming. *Antioxid. Redox Signal*, **9**, 1485 – 1497.

Darrow, B. J., Fast, V. G., Kleber, A. G., Beyer, E. C., Saffitz, J. E. (1996) Functional and structural assessment of intercellular communication. Increased conduction velocity and enhanced connexin expression in dibutyryl cAMP-treated cultured cardiac myocytes. *Circ. Res.* **79,** 174–183.

Davies, P. F., Shi, C., dePaola, N., Helmke. B. P., Polacek, D. C. (2001) Hemodynamics and the focal origin of atherosclerosis: a spatial approach to endothelial structure, gene expression, and function. *Ann NY Acad Sci,* **947**, 7–16.

De Backer, D., Creteur, J., Preiser, J. C., Dubois, M. J., Vincent, J. L. (2002) Microvascular blood flow is altered in patients with sepsis. *Am. J. Respir. Crit. Care Med.* **166**, 98-104.

Dekker, L. R., Fiolet, J. W., van Bavel, E. (1996) Intracellular $Ca2^{+}$, intercellular electrical coupling, and mechanical activity in ischemic rabbit papillary muscle. Effects of preconditioning and metabolic blockade. *Circ. Res.*, **79**, 237-246.

Delmar, M., Liu, S., Morley, G. E., Ek, J. F., Anumonwo, J. M. B., Taffet, S. M. (1994) Toward a molecular model for the pH regulation of intercellular communication in the heart. *Cardiac Electrophysiology*. From Cell to Bedside. D. P. Zipes and J. Jalife, editors. W. B. Saunders, Philadelphia. 135-143.

de Wit, C., Roos, F., Bolz, S. S. (2000) Impaired conduction of vasodilation along arterioles in connexin-40 deficient mice. *Circ. Res*, **86**, 649-655.

de Wit, C., Roos, F., Bolz, S. S., Pohl, U. (2003) Lack of vascular connexin 40 is associated with hypertension and irregular arteriolar vasomotion. *Physiol Genomics,* **13**, 169 -177.

de Wit, C., Hoepfl, B., Wolfle, S. E. (2006a) Endothelial mediators and communication through vascular gap junctions. *Biol Chem*, **387**, 3–9.

de Wit, C., Hoepfl, B., Wolfle, S. E. (2006b) Connexin – dependent communication within the vascular wall: contribution to the control of arteriolar diameter. *Adv. Cardiol*, **42**, 268 - 283.

Dietrich, H. H. (1989) Effect of locally applied epinephrine and norepinephrine on blood flow and diameter in capillaries of rat mesentery. *Microvasc. Res.*, **38,** (2), 125-135.

Dietrich, H. H. & Tyml, K. (1992) Capillary as a communicating medium in the microvasculature. *Microvasc. Res.*, **43**, 87-99.

Dimon-Gadal, S., Gerbaud, P., Keryer, G., Anderson, W., Evain-Brion, D.,Raynaud, F. (1998) In vitro effects of oxygen-derived free radicals on type I and type II cAMP-dependent protein kinases. *J. Biol. Chem.* **273,** 22833–22840.

Dora, K. A., Doyle, M. P., Duling, B. R. (1997) Elevation of intracellular calcium in smooth muscle causes endothelial cell generation of NO in arterioles. *Proc Natl Acad Sci USA,* **94**, 6529–6534.

Dora, K. A., Xia, J., Duling, B. R. (2003) Endothelial cell signaling during conducted vasomotor responses. *Am J Physiol Heart Circ Physiol*, **285**, H119–H126.

Duffy, H. S., Delmar, M., Spray, D. C. (2002) Formation of the gap junction nexus: binding partners for connexins, *J. Physiol. (Paris),* **96**, 243 – 249.

Duffy, H. S., Ashton, A. W., O'Donnell, P., Coombs, W., Taffet, S. M., Delmar, M., Spray, D.C. (2004). Regulation of connexin43 protein complexes by intracellular acidification. *Circ. Res.* **94**, 215-222.

Dunham, B., Liu, S., Taffet, S., Trabka-Janik, E., Delmar, M., Petryshyn, R., Zheng, S., Perzova, R., Vallano, M. L. (1992) Immunolocalization and expression of functional and nonfunctional cell-to-cell channels from wild-type and mutant rat heart connexin43 cDNA. *Circ. Res*, **70,** 1233-1243.

Dunker, A. K., Obradovic, Z. (2001) The protein trinity--linking function and disorder. *Nat Biotechnol.* **19**, 805-806.

Elfgang, C., Eckert, R., Lichtenberg-Fraté, H., Butterweck, A., Traub, O., Klein, R. A., Hülser, D. F., Willecke, K. (1995) Specific permeability and selective formation of gap junction channels in connexin-transfected HeLa cells. *J Cell Biol.***129**, 805-817.

Ellis, C. G., Bateman, R. M., Sharpe, M. D., Sibbald, W. J., Gill, R. (2002) Effect of a maldistribution of microvascular blood flow on capillary O(2) extraction in sepsis. *Am J Physiol Heart Circ Physiol,* **282**, H156–164.

Emerson, G. G., Segal S. S. (2000a) Endothelial cell pathway for conduction of hyperpolarization and vasodilation along hamster feed artery. *Circ Res*, **86**, 94–100.

Emerson, G. G., Segal, S. S. (2000b) Electrical coupling between endothelial cells and smooth muscle cells in hamster feed arteries: role in vasomotor control *Circ Res.***87**(6):427-428.

Emerson, G. G., Segal, S. S. (2001) Electrical activation of endothelium evokes vasodilation and hyperpolarization along hamster feed arteries. *Am J Physiol Heart Circ Physiol.* **280**:H160–H167.

Ertel, W., Kremer, J. P., Kenney, J., Steckholzer, U., Jarrar, D., Trentz, O., Schildberg, F. W. (1995) Downregulation of proinflammatory cytokine release in whole blood from septic patients. *Blood*, **85**, (5), 1341-1347.

Evans, W. H., Ahmad, S., Diez, J. (1999) Trafficking pathways leading to the formation of gap junctions. Gap junction–mediated intercellular signaling in health and disease. *Novartis Found Symp*, **219**, 44-54.

Evans, W. H., Martin, P. E.(2002) Gap junctions: structure and function (review). *Mol Membr Biol.*, **19**, 121–136.

Evans, W. H., De Vuyst, E., Leybaert, L. (2006) The gap junction cellular internet: connexin hemichannels enter the signaling limelight. *Biochem J.*, **397**, 1–14.

Falk, M. M., Buehler, L. K., Kumar, N. M., Gilula, N. B. (1997) Cell-free synthesis and assembly of connexins into functional gap junction membrane channels. *EMBO J*, **16**, 2703–2716.

Falk, M. M., Gilula, N. B. (1998) Connexin membrane protein biosynthesis is influenced by polypeptide positioning within the translocon and signal peptidase access. *J. Biol. Chem*, **273**, 7856– 7864.

Fall, P. J., Szerlip, H. M. (2005) Lactic acidosis: from sour milk to septic shock. *J Intensive Care Med.*, **20**, 255-271.

Figueroa, X. F., Paul, D. L., Simon, A. M., Goodenough, D. A., Day, K. H., Damon, D. N., Duling, B. R. (2003) Central role of connexin40 in the propagation of electrically activated vasodilation in mouse cremasteric arterioles in vivo. *Circ. Res.*, **92**, 793 – 800.

Figueroa, X. F., Isakson, B. E., Duling, B. R. (2004) Connexins: gaps in our knowledge of vascular function. *Physiology (Bethesda)*, **19**, 277–284.

Figueroa, X. F., Isakson, B. E., Duling, B. R. (2006) Vascular gap junctions in hypertension. *Hypertension* **48**, 804-811.

Figueroa, X. F., Duling, B. R. (2008) Dissection of two Cx37-independent conducted vasodilator mechanisms by deletion of Cx40: electrotonic versus regenerative conduction. *Am J Physiol Heart Circ Physiol*, **295**, H2001- H2007.

Fishman, G. I., Moreno, A. P., Spray, D. C., Leinwand, L. A. (1991) Functional analysis of human cardiac gap junction channel mutants. *Proc. Natl. Acad. Sci. USA*, **88**, 3525-3529.

Gabriels, J. E., Paul, D. L. (1998) Connexin43 is highly localized to sites of disturbed flow in rat aortic endothelium but connexin37 and connexin40 are more uniformly distributed. *Circ Res*, **83**, 636-643.

Goodenough, D. A., Goliger, J. A., Paul, D. L. (1996) Connexins, connexons, and intercellular communication. *Annu Rev Biochem.*, **65**, 475-502.

Goodenough, D. A., Paul, D. L. (2003) Beyond the gap: functions of unpaired connexon channels, *Nat. Rev., Mol. Cell Biol.* **4**, 285– 294.

Graham, F. L., Smiley, J., Russell, W. C. (1977) Characteristics of a human cell line transformed by DNA from human adenovirus type 5. *J Gen Virol*, **36**, 59-74.

Grandel, U., Grimminger, F. (2003) Endothelial responses to bacterial toxins in sepsis. *Crit Rev Immunol*, **23**, (4), 267-99.

Gustafsson, F., Holstein-Rathlou, N. (1999) Conducted vasomotor responses in arterioles: characteristics, mechanisms and physiological significance. *Acta Physiol Scand*, **167**, 11–21.

Haas, T. L., Duling, B. R. (1997) Morphology favors an endothelial cell pathway for longitudinal conduction within arterioles. *Microvasc Res*, **53**, 113–120.

Haefliger, J. A., Nicod, P., Meda, P. (2004) Contribution of connexins to the function of the vascular wall. *Cardiovasc Res.*, **62**, 345-356.

Haefliger, J. A., Krattinger, N., Martin, D., Pedrazzini, T., Capponi, A., Doring, B., Plum, A., Charollais, A., Willecke, K., Meda, P. (2006) Connexin43-dependent mechanism modulates renin secretion and hypertension. *J. Clin. Invest* **116**, 405-413.

Harris, A. L. (2001) Emerging issues of connexin channels: biophysics fills the gap. Q. *Rev. Biophys*, **34**, 325- 472.

Hastie, L. E., Patton, W. F., Hechtman, H. B., and Shepro, D. (1997) H2O2-induced filamin redistribution in endothelial cells is modulated by the cyclic AMP-dependent protein kinase pathway. *J. Cell. Physiol.* **172,** 373–381.

Hertlein, B., Butterweck, A., Haubrich, S., Willecke, K., Traub, O. (1998) Phosphorylated carboxyl terminal serine residues stabilize the mouse gap junction protein connexin45 against degradation. *J. Membrane Biol*, **162**, 247-257.

Hertlein, B., Butterweck, A., Haubrich, S., Willecke, K., and Traub, O. (1998) Phosphorylated carboxyl terminal serine residues stabilize the mouse gap junction protein connexin45 against degradation. *Membr. Biol.* **162,** 247–257.

Hervé, J. C., Bourmeyster, N., Sarrouilhe, D., Duffy, H.S. (2007) Gap junctional complexes: from partners to functions. *Prog Biophys Mol Biol.*, **94**, 29-65.

Hess, M. L., Manson, N. H. (1984) Molecular oxygen: friend and foe. The role of the oxygen free radical system in the calcium paradox, the oxygen paradox and ischemia/reperfusion injury. *J. Mol. Cell. Cardiol.* **16**, 969–985.

Horn, K. D. (1998) Evolving strategies in the treatment of sepsis and systemic inflammatory response syndrome (SIRS). *QJM* , **91**, 265-277.

Hua, C., David, G. H. (2000) Endothelial Dysfunction in Cardiovascular Diseases: The Role of Oxidant Stress. *Circ.Res,* **87**, 840 - 844.

Hille, B. (2003) Ionic Channels of Excitable Membranes, Sinauer Associates, Sunderland, MA.

Hjerrild M, Stensballe A, Rasmussen T. E., Kofoed, C. B., Blom, N., Sicheritz-Ponten, T., Larsen, M.R., Brunak, S., Jensen, O. N., Gammeltoft, S. (2004) Identification of phosphorylation sites in protein kinase A substrates using artificial neural networks and mass spectrometry. *J Proteome Res*, **3**, 426-33.

Hunter, T. (1998) The Croonian Lecture 1997. The phosphorylation of proteins on tyrosine: its role in cell growth and disease. *Philos. Trans. R. Soc. Lond. B.*, **353**, 583- 605.

Imanaga, I., Hirosawa, N., Hai, L., Sakamoto, Y., Matsumura, K., Mayama, T. (2002). Phosphorylation of connexin43 and regulation of cardiac gap junction. In: DeMello W. C ; Janse M. J, eds. Heart Cell Coupling and Impulse Propagation in Health and Disease. *Boston: Kluwer Academic Publishers*, 185-205.

Isakson, B. E., Duling, B. R. (2005) Heterocellular contact at the myoendothelial junction influences gap junction organization. *Circ Res.* **97**, 44 -51.

Isakson, B. E., Damon, D. N., Day, K. H., Liao, Y., Duling, B. R. (2006) Connexin40 and connexin43 in mouse aortic endothelium: evidence for coordinated regulation. *Am J Physiol. Heart Circ. Physiol.*, **290**, H1199-H1205.

John, S., Cesario, D., Weiss, J. N. (2003) Gap junctional hemichannels in the heart. *Acta Physiol. Scand*, **179**, 23–31.

Jongen, W. M., Fitzgerald, D. J., Asamoto, M., Piccoli, C., Slaga, T. J., Gros, D., Takeichi, M., Yamasaki. (1991) Regulation of connexin 43-mediated gap junctional intercellular communication by Ca^{2+} in mouse epidermal cells is controlled by E-cadherin. *J. Cell Biol*, **114**, 545-555.

Johnson, L., Noble, M., Owen, D. (1996) Active and inactive protein kinases: structural basis for regulation.*Cell,*, **85**, 149–158.

Johnson, L., Lowe, E., Noble, M., Owen, D. (1998) The Eleventh Datta Lecture. The structural basis for substrate recognition and control by protein kinases. *FEBS Lett.*, **430**, 1–11.

Jones, D. P. (2006) Redefining oxidative stress. *Antioxid Redox Signal,* **9**, 1865-1879.

Jordan, K., Solan, J. L., Dominguez, M., Sia, M., Hand, A., Lampe, P. D., Laird, D. W. (1999) Trafficking, assembly, and function of a connexin43 - green fluorescent protein chimera in live mammalian cells. *Mol. Biol. Cell,* **10**, 2033-2050.

Kanemitsu, M. Y., and Lau, A. F. (1993) Epidermal growth factor stimulates the disruption of gap junctional communication and connexin43 phosphorylation independent of 12-0-tetradecanoylphorbol 13-acetate-sensitive protein kinase C: the possible involvement of mitogen-activated protein kinase. *Mol. Biol. Cell* **4,** 837–848.

Kanno, Y., Enamoto, T., Shiba, Y., Yamasaki, H. (1984) Protective effect of cyclic AMP on tumor promoter-mediated inhibition of cell–cell communication (electrical coupling). *Exp. Cell Res*, **152**, 31- 37.

Kellum, J. A., Song, M., Li, J. (2003) Lactic and hydrochloric acids induce different patterns of inflammatory response in LPS-stimulated RAW 264.7 cells. *Am J Physiol Regul Integr Comp Physiol.*, **286**, R686-692.

Khadaroo, R. G., Kapus, A., Powers, K. A., Cybulsky, M. I., Marshall, J. C., Rotstein, O. D.(2003) Oxidative stress reprograms lipopolysaccharide signaling via Src kinase-dependent pathway in RAW 264.7 macrophage cell line. *J Biol Chem,* **278**, 47834 – 47841.

Kirchhoff, S., Kim, J. S., Hagendorff, A., Thonnissen, E., Kruger, O., Lamers, W. H., Willecke, K. (2000) Abnormal cardiac conduction and morphogenesis in connexin40 and connexin43 double-deficient mice. *Circulation Research,* **87**, 399-405.

Kolibaba, K., Druker, B. (1997) Protein tyrosine kinases and cancer. *Biochim. Biophys. Acta,* **1333**, F217–F248.

Koval, M., Harley, J. E., Hick, E., Steinberg, T. H. (1997) Connexin46 is retained as monomers in a trans-Golgi compartment of osteoblastic cells. *J. Cell Biol*, **137**, 847– 857.

Kruger, O., Plum, A., Kim, J. S., Winterhager, E., Maxeiner, S., Hallas, G., Kirchhoff, S., Traub, O., Lamers, W. H.,Willecke, K.(2000) Defective vascular development in connexin 45-deficient mice. *Development,* **127**, 4179-4193.

Kukreja, R. C., Kontos, H. A., Hess, M. L., Ellis, E. F. (1986) PGH synthase and lipoxygenase generate superoxide in the presence of NADH or NADPH. *Circ Res,* **59**, 612–619.

Kumar, N. M., Gilula, N. B. (1996) The gap junction communication channel. *Cell,* **84**: 381-388.

Kwak, B. R., Hermans, M. M. P., De Jonge, H. R., Lohmann, S. M., Jongsma, H. J., and Chanson, M. (1995) *Mol. Biol. Cell* **6,** 1707–1719.

Kwak, B. R., Jongsma, H. J., (1996) Regulation of cardiac gap junction channel permeability and conductance by several phosphorylating conditions. *Mol. Cell. Biochem.* **157**, 93-99.

Laird, D. W., Puranam, K. L., Revel, J. P. (1991) Turnover and phosphorylation dynamics of connexin43 gap junction protein in cultured cardiac myocytes. *Biochemistry Journal*, **273**, 67-72.

Laird, D. W., Castillo, M., Kasprzak, L. (1995) Gap junction turnover, intracellular trafficking, and phosphorylation of connexin43 in brefeldin A-treated rat mammary tumor cells. *J. Cell Biol*, **131** 1193– 1203.

Laitinen, L. (1987) Griffonia simplicifolia lectins bind specifically to endothelial cells and some epithelial cells in mouse tissues. *Histochem J,* **19**, 225-234.

Lam, C., Tyml, K., Martin, C., Sibbald, W. (1994). Microvascular perfusion is impaired in a rat model of normotensive sepsis. *J Clin Invest*, **94**, 2077–2083.

Lampe, P. D. (1994). Analyzing phorbol ester effects on gap junction communication: A dramatic inhibition of assembly. *Journal of Cell Biology*, **127**, 1895–1905.

Lampe, P. D., Lau, A. F. (2000) Regulation of gap junctions by phosphorylation of connexins, *Arch. Biochem. Biophys.* **384**, 205– 215.

Lampe, P. D., Lau, A. F. (2004) The effects of connexin phosphorylation on gap junctional communication. *Int. J. Biochem. Cell Biol*, **(36)**, 1171–1186.

Larson, D. M., Haudenschild, C. C., Beyer, E. C. (1990) Gap junction messenger RNA expression by vascular wall cells. *Circ Res.* **66**, 1074-1080.

Lau, A. F., Kurata, W. E., Kanemitsu, M. Y., Loo, L. W., Warn-Cramer, B. J., Eckhart, W., Lampe, P. D., (1996) Regulation of connexin43 function by activated tyrosine protein kinases. *J. Bioenerg. Biomembr.* **28**, 359-368.

Li, J. M., Shah, A. M. (2004) Endothelial cell superoxide generation: regulation and relevance for cardiovascular pathophysiology. *Am. J. Physiol. Regul. Integr. Comp. Physiol.*,**287**, R1014–R1030.

Lidington, D., Ouellette, Y., Tyml, K. (2000) Endotoxin increases intercellular resistance in microvascular endothelial cells by a tyrosine kinase pathway. *J Cell Physiol*, **185**, 117–125.

Lidington, D., Li, F., Tyml, K. (2007) Deletion of neuronal NOS prevents impaired vasodilation in septic mouse skeletal muscle. *Cardiovasc Res*, **74**, 151–158.

Lin, R., Martyn, K. D., Guyette, C. V., Lau, A. F., Warn-Cramer, B. J. (2006) v-Src tyrosine phosphorylation of connexin43: regulation of gap junction communication and effects on cell transformation. *Cell Commun. Adhes*, **13**, 199–216.

Locke, D., Liu, J., Harris, A. L. (2005) Lipid rafts prepared by different methods contain different connexin channels, but gap junctions are not lipid rafts. *Biochemistry,* **44**, 13027-13042.

Martinez, A. D., Saez, J. C. (2000) Regulation of astrocyte gap junctions by hypoxia / reoxygenation. *Brain Res. Brain Res. Rev.* **32**, 250–258.

Martinez, A. D., Hayrapetyan, V., Moreno, A. P., Beyer, E. C. (2002) Connexin43 and connexin45 form heteromeric gap junction channels in which individual components determine permeability and regulation. *Circ. Res*, **90**, 1100 - 1107.

Maass, K., Ghanem, A., Kim, J. S., Saathoff, M., Urschel, S., Kirfel, G., Grummer, R., Kretz, M., Lewalter, T., Tiemann, K. (2004) Defective epidermal barrier in neonatal mice lacking the C-terminal region of connexin43. *Mol. Biol. Cell,* **15**, 4597-4608.

Masamichi, N., Satoru, F., Ikuo, M., Kazuhiko, M., Sei-Itsu, M. (2000) Hypoxia – reoxygenation inhibits gap junctional communication in cultured human umbilical vein endothelial cells. *Endothelium*, **7**, 279 - 286.

Matsumura, K., Mayama, T., Lin, H., Sakamoto, Y., Ogawa, K., Imanaga, I. (2006) Effects of cyclic AMP on the function of the cardiac gap junction during hypoxia. *Exp. Clin. Cardiol.*, **11**, 286-293.

McCord, J. M., Roy, R. S., Schaffer, S. W. (1985) Free radicals and myocardial ischemia. The role of xanthine oxidase. *Adv. Myocardiol.* **5**, 183-189.

Mellander, S., Johansson, B. (1968) Control of resistance, exchange and capacitance functions in the peripheral circulation. *Pharmacol. Rev.*, **20**, 117-196.

Meyer, R.A., Laird, D.W., Revel, J.P., Johnson, R.G. (1992) Inhibition of gap junction and adherens junction assembly by connexin and A-CAM antibodies. *J. Cell Biol*, **119**, 179-189.

Michiels, C., Arnould, T., Remacle, J. (2000) Endothelial cell responses to hypoxia: initiation of a cascade of cellular interactions. *Biochim.Biophys.Acta*, **1497**, 1-10.

Moorby, C. (2000) A connexin 43 mutant lacking the carboxyl cytoplasmic domain inhibits both growth and motility of mouse 3T3 fibroblasts. Mol. Carcinog. **28**, 23–30.

Moreno, A. P., Chanson, M., Elenes, S., Anumonwo, J., Scerri, I., Gu, H., Taffet, S.M., Delmar, M., (2002) Connexin43 and connexin45 form heteromeric gap junction channels in which individual components determine permeability and regulation. *Circ. Res.*, **90**, 450-457.

Morley, G. E., Taffet, S. M., Delmar, M. (1996) Intramolecular Interactions Mediate pH Regulation of Connexin43 Channels *Biophysical Journal*, **70**, 1294-1302.

Motterlini, R., Kerger, H., Green, C. J., Winslow, R. M., Intaglietta, M. (1998) Depression of endothelial and smooth muscle cell oxygen consumption by endotoxin. *Am J Physiol*, **275**, H776-H782.

Mottet, D., Dumont, V., Deccache, Y., Demazy, C., Ninane, N., Raes, M., and Michiels, C. (2003) Regulation of hypoxia-inducible factor-1alpha protein level during hypoxic conditions by the phosphatidylinositol 3-kinase/Akt/glycogen synthase kinase 3β pathway in HepG2 cells. *J. Biol. Chem.* **278,** 277–231.

Musil, L. S., Beyer, E. C., Goodenough, D. A. (1990) Expression of the gap junction protein connexin43 in embryonic chick lens: Molecular cloning, ultrastructural localization, and post-translational phosphorylation. *Journal of Membrane Biology*, **116**, 163–175.

Mueller, C. F. H., Laude, K., McNally, J. S., Harrison, D. G. (2005) Redox mechanisms in blood vessels. *Arterioscler Thromb Vasc Biol*, **25**, 274–278.

Musil, L., Goodenough, D. A. (1993) Multisubunit assembly of an integral plasma membrane channel protein, gap junction connexin43, occurs after exit from the ER. *Cell*, **74**, 1065- 1077.

Nguyen, H. B., Smith, D. (2007) Sepsis in the 21st century: Recent definitions and therapeutic advances. *Am J Emerg Med* **25**, 564–571.

Oh, S. Y., Grupen, C. G., Murray, A. W. (1991) Phorbol ester induces phosphorylation and downregualtion of connexin 43 in WB cells. *Biochim. Biophys. Acta*, **1094**, 243-245.

Paul, D. L (1986) Molecular cloning of cDNA for rat liver gap junction protein, *J. Cell Biol.* **103**, 123-134.

Peled, M., Shaish, A., Katav, A., Greenberger, S., Barshack, I., Tal, R., Bangio, L., Breitbart, E., Harats, D. (2009) Systemic administration of a conditionally replicating adenovirus, targeted to angiogenesis, reduced lung metastases burden in cotton rats. *Clin Cancer Res.*, **15**, 1664-1673.

Peng, T., Lu, X., Feng, Q. (2005) Pivotal role of gp91phox-containing NADH oxidase in lipopolysaccharide - induced tumor necrosis factor-alpha expression and myocardial depression. *Circulation*, **111**, 1637–1644.

Peracchia, C., Wang, X. G., Peracchia, L. L. (2000) Behavior of chemical- and slow voltage-sensitive gating of connexin channels: the "cork" gating hypothesis, in: Peracchia, C. (Ed.), Gap junctions, molecular basis of cell communication in health and disease, Academic Press, San Diego, CA, 271-295.

Piper, R. D., Pitt-Hyde, M., Li, F., Sibbald, W. J., Potter, R. F. (1996) Microcirculatory changes in rat skeletal muscle in sepsis. *Am J Respir Crit Care Med*, **154**, 931–937.

Pittman, R. N. (2005) Oxygen transport and exchange in the microcirculation. *Microcirculation*, **12**, 59-70.

Pohlman, T. H., Harlan, J. M. (2000) Adaptive responses of the endothelium to stress. *J. Surg. Res.* **89**, 85-119.

Powers, K. A., Szaszi, K., Khadaroo, R. G., Tawadros, P. S.,Marshall, J. C., Kapus, A., Rotstein, O. D. (2006) Oxidative stress generated by hemorrhagic shock recruits Toll-like receptor 4 to the plasma membrane in macrophages. *J Exp Med*, **203**, 1951–1961.

Rabadan-Diehl, C., Dahl, G., Werner, R. (1994) A connexin-32 mutation associated with Charcot-Marie-Tooth disease does not affect channel formation in oocytes. *FEBS Lett.* **351**,90-94.

Reed, K. E., Westphale, E. M., Larson, D. M., Wang, H. Z., Veenstra, R. D., Beyer, E. C. (1993) Molecular cloning and functional expression of human connexin37, an endothelial cell gap junction protein. *J Clin Invest*, **91**, 997-1004.

Rose, K., Ouellette, Y., Bolon, M., Tyml, K. (2005) Hypoxia/reoxygenation reduces microvascular endothelial cell coupling by a tyrosine and MAP kinase dependent pathway. *J Cell Physiol*, **204**, 131-138.

Reaume, A. G., de Sousa, P. A., Kulkarni, S., Langille, B. L., Zhu, D., Davies, T. C., Juneja, S. C., Kidder, G.M., Rossant, J. (1995) Cardiac malformation in neonatal mice lacking connexin43. *Science,* **267**, 1831–1834.

Rignault, S., Haefliger, J. A., Gasser, D., Markert, M., Nicod, P., Liaudet. L., Waeber, B., Feihl, F. (2005) Sepsis up-regulates the expression of connexin 40 in rat aortic endothelium. *Crit Care Med*, **33**, 1302-1310.

Robin, C. Looft-Wilson, Geoffrey, W., Payne, Segal, S. S. (2004) Connexin expression and conducted vasodilation along arteriolar endothelium in mouse skeletal muscle. *J Appl Physiol* **97**, 1152–1158, 2004.

Ruch, R. J., Klaunig, J. E. (1988) Inhibition of mouse hepatocyte intercellular communication by paraquat – generated oxygen free radicals. *Toxicol. Appl. Pharmacol.*, **94**, 427 - 436.

Sandow, S. L., Looft-Wilson, R., Doran, B., Grayson, T. H., Segal, S. S., Hill, C.E. (2003) Expression of homocellular and heterocellular gap junctions in hamster arterioles and feed arteries. *Cardiovasc Res.*, **60**, 643-653.

Saez, J. C., Nairn, A. C., Czernik, A. J., Spray, D. C., Hertzberg, E. L., Greengard, P., and Bennett, M. V. L. (1990) Phosphorylation of connexin 32, a hepatocyte gap-junction protein, by cAMP-dependent protein kinase, protein kinase C and Ca2+/calmodulin-dependent protein kinase II.*Eur. J. Biochem.* **192,** 263–273.

Saez, J. C., Nairn, A. C., Czernik, A. J., Spray, D. C., Hertzberg, E. L. (1993) Rat connexin43: regulation by phosphorylation in heart. In: Hall, J.E., Zampighi, G.A., Davies, R.M. (Eds.), *Progress in Cell Research*, **3**, 275-281.

Saez, J. C., Martinez, A. D., Branes, M. C., Gonzalez, H. E. (1998) Regulation of gap junctions by protein phosphorylation. *Braz. J. Med. Biol. Res,* **31**, 593 - 600.

Saez, J. C., Berthoud, V. M., Branes, M. C., Martinez, A. D., Beyer, E. C. (2003) Plasma membrane channels formed by connexins: their regulation and functions. *Physiol Rev,* **83**:1359–1400.

Saffitz, J. E., Davis, L. M., Darrow, B. J., Kanter, H. L., Laing, J. G., Beyer, E. C. (1995) The molecular basis of anisotropy: role of gap junctions. *J. Cardiovasc. Electrophysiol.*, **6**, 498-510.

Scott, P.A., Bicknell, R. (1993) The isolation and culture of microvascular endothelium. *J Cell Sci.*, **105**, 269-273.

Secomb, T. W., Pries, A. R. (2002) Information transfer in microvascular networks. *Microcirculation*, **9**, 377-387.

Segal, S. S., Duling, B. R. (1986) Flow control among microvessels coordinated by intercellular conduction. *Science*, **234**, 868–870.

Segal, S. S. (1991) Microvascular recruitment in hamster striated muscle: role for conducted vasodilation. *Am J Physiol,* **261**, H181-189.

Segal, S. S., Jacobs, T. L. (2001) Role for endothelial cell conduction in ascending vasodilatation and exercise hyperaemia in hamster skeletal muscle. *J Physiol.* **536**, 937–946.

Segal, S. S. (2005) Regulation of blood flow in the microcirculation. *Microcirculation,* **12**, 33- 45.

Seko, Y., Tobe, K., Takahashi, N., Kaburagi, Y., Kadowaki, T., Yazaki, Y. (1996) Hypoxia and hypoxia/reoxygenation activate Src family tyrosine kinases and p21ras in cultured rat cardiac myocytes. *Biochem. Biophys. Res. Commun.* **226,** 530–535.

Semenza, G.L. (1999) Perspectives on oxygen sensing. *Cell*, **98**, 281 – 284.

Severs, N. J., Rothery, S., Dupont, E., Coppen, S. R., Yeh, H. I., Ko, Y. S., Matsushita T, Kaba, R,. Halliday D. (2001) Immunocytochemical analysis of connexin expression in the healthy and diseased cardiovascular system. *Microsc. Res. Tech.*, **52**, 301-322.

Shah, M. M., Martinez, A. M., Fletcher, W. H. (2002) The connexin43 gap junction protein is phosphorylated by protein kinase A and protein kinase C: In vivo and in vtitro studies. *Mol. Cell. Biochem*, **238**, 57- 68.

Simon, A. M., Goodenough, D. A., Paul, D. L. (1998) Mice lacking connexin40 have cardiac conduction abnormalities characteristic of atrioventricular block and bundle branch block. *Curr Biol*, **8**, 295-298.

Simon, A.M., Goodenough, D. A. (1998b) Diverse functions of vertebrate gap junctions. *Trends Cell Biol.*, **8**, (12):477-83.

Simon, A. M., McWhorter, A. R.(2002) Vascular abnormalities in mice lacking the endothelial gap junction proteins connexin37 and connexin40. *Dev Biol,* **251**, 206–220.

Simon, A. M., McWhorter, A. R., Chen, H., Jackson, C. L., Ouellette, Y. (2004) Decreased Intercellular communication and connexin expression in mouse aortic endothelium during lipopolysaccharide-induced inflammation. *J Vasc Res*, **41**, 323–333.

Sohl G., Willecke, K. (2003) An update on connexin genes and their nomenclature in mouse and man. *Cell Commun Adhes*, **10**, 173–180.

Solan, J. L., Lampe, P. D. (2008) Connexin 43 in LA-25 cells with active v-src is phosphorylated on Y247, Y265, S262, S279/282, and S368 via multiple signaling pathways. *Cell Commun. Adhes,* **15**, 75–84.

Song, H., Tyml, K. (1993) Evidence for sensing and integration of biological signals by the capillary network. *Am.J.Physiol*, **265**, H1235-H1242.

Steinwaerder, D. S., Carlson, C. A., Lieber, A. (2000) DNA replication of first-generation adenovirus vectors in tumor cells. *Hum Gene Ther.*, **11**, 1933-1948.

Stergiopoulos, K., Alvarado, J. L., Mastroianni, M., Ek-Vitorin, J. F., Taffet, S. M., Delmar, M., (1999) Hetero-domain interactions as a mechanism for the regulation of connexin channels. *Circ. Res.* **84**, 1144–1155.

Strenbergen, C., Murphy, E., Levy, L., London, R. E. (1987) Elevation in cytosolic free calcium concentration early in myocardial ischemia in perfused rat heart. *Circ Res.*, **60**, 700-707.

TenBroek, E., Lampe, P. D., Taffet, S., Reynhout, J., Martyn, K., Kurata, W. E., Lau, A. F., Johnson, R. G. (1998) *in* Gap Junctions (Werner, R., Ed.), pp. 215–219, IOS Press, Amsterdam.

TenBroek, E. M., Lampe, P. D., Solan, J. L., Reynhout, J. K., Johnson, R.G. (2001) Ser364 of connexin43 and the upregulation of gap junction assembly by Camp. *J. Cell Biol*, **155**, 1307–1318.

Thomas, M. A., Huang, S., Cokoja, A., Riccio, O., Staub, O., Suter, S., Chanson, M. (2002) Interaction of connexins with protein partners in the control of channel turnover and gating, *Biol. Cell,* **94**, 445- 456.

Toyofuku, T., Akamatsu, Y., Zhang, H., Kuzuya, T., Tada, M., Hori, M. (2001) c-Src regulates the interaction between connexin-43 and ZO-1 in cardiac myocytes. *J. Biol. Chem.*, **276**, 1780-1788.

Traub, O., Look, J., Paul, D., Willecke, K. (1987) Cyclic adenosine monophosphate stimulates biosynthesis and phosphorylation of the 26 kDa gap junction protein in cultured mouse hepatocytes. *Eur.J. Cell Biol.* **43,** 48–54.

Traub, O., Look, J., Dermietzel, R., Brummer, F., Hulser, D., Willecke, K. (1989) Comparative characterization of the 21-kDa and 26-kDa gap junction proteins in murine liver and cultured hepatocytes. *Journal of Cell Biology*, **108**, 1039 -1052.

Traub, O., Eckert, R., Lichtenberg-Frate, H., Elfgang, C., Bastide, B., Scheidtmann, K.H., Hulser, D.F., Willecke, K. (1994) Immunochemical and electrophysiological characterization of murine connexin40 and -43 in mouse tissues and transfected human cells. *Eur.J.Cell Biol.* **64**, 101 – 112.

Trzeciak, S., McCoy, J. V., Phillip Dellinger, R., Arnold, R. C., Rizzuto, M., Abate, N. L., Shapiro, N. I., Parrillo, J. E., Hollenberg, S. M. (2008) Early increases in microcirculatory perfusion during protocol-directed resuscitation are associated with reduced multi-organ failure at 24 h in patients with sepsis. *Intensive Care Med.*, **34**, 2210-7

Tyml, K., Wang, X., Lidington, D., Ouellette, Y. (2001) Lipopolysaccharide reduces intercellular coupling in vitro and arteriolar conducted response in vivo. *Am J Physiol Heart Circ Physiol*, **281**, H1397–H1406.

Ulloa, L., Brunner, M., Ramos, L., Deitch, E.A. (2009) Scientific and clinical challenges in sepsis. *Curr Pharm Des*, **15**, (16), 1918-1935.

Valiunas, V., Beyer, E. C., Brink, P. R. (2002) Cardiac gap junction channels show quantitative differences in selectivity. *Circ. Res.* **91**, 104-111.

van Kempen, M. J., Jongsma, H. J. (1999) Distribution of connexin37, connexin40 and connexin43 in the aorta and coronary artery of several mammals. *Histochem Cell Biol*, **112**, 479-486.

van Rijen, H. V., van Veen, T. A., Hermans, M. M., Jongsma, H. J. (2000) Human connexin40 gap junction channels are modulated by cAMP. *Cardiovasc. Res.* **45,** 941–951.

van Veen, T. A., van Rijen, H. V., Jongsma, H. J. (2000) Electrical conductance of mouse connexin45 gap junction channels is modulated by phosphorylation. *Cardiovasc. Res.* **46,** 496–510.

Vincent, J. L., De Backer, D. (2005) Microvascular dysfunction as a cause of organ dysfunction in severe sepsis, *Crit Care*, **9,** S9–S12.

Walker, D. L., Vacha, S. J., Kirby, M. L., Lo, C. W. (2005) Connexin43 deficiency causes dysregulation of coronary vasculogenesis. *Dev Biol,* **284**, 479–498.

Walther, W., Stein, U. (2000) Viral vectors for gene transfer: a review of their use in the treatment of human diseases. Drugs, **60**, 249-271.

Warn-Cramer, B. J., Cottrell, G. T., Burt, J. M., Lau, A. F. (1998) Regulation of connexin-43 gap junctional intercellular communication by mitogen-activated protein kinase. *J. Biol. Chem*, **273**, 9188– 9196.

Warn-Cramer, B. J., Lau, A. F. (2004) Regulation of gap junctions by tyrosine protein kinases. *Biochim. Biophys. Acta*, **1662**, 81–95.

Welsh, D. G., Segal, S. S. (1998) Endothelial and smooth muscle cell conduction in arterioles controlling blood flow. *Am J Physiol*, **274**, H178–H186.

Werner, R., Levine, E., Rabadan-Diehl, C., and Dahl, G. (1991) *Proc. R. Soc. Lond. B. Biol. Sci.* **243,** 5-11.

White, T.W. (2003) Non-redundant gap junction functions. *News Physiol Sci,* **18**, 95–99.

Willecke, K., Eiberger, K., Degen, J., Eckardt, D., Romualdi, A., Guldenagel, M., Deutsch, U., Sohl, G. (2002) Structural and functional diversity of connexin genes in the mouse and human genome, *Biol. Chem.* **383**, 725–737.

Wilson, J. X., Dixon, S. J., Yu, J., Nees, S., Tyml, K. (1996) Ascorbate uptake by microvascular endothelial cells of rat skeletal muscle. *Microcirculation*, **3**, 211–221.

Wolfle, S. E., Schmidt, V. J., Hoepfl, B., Gebert, A., Alcolea, S., Gros, D., de Wit, C. (2007) Connexin45 cannot replace the function of connexin40 in conducting endothelium-dependent dilations along arterioles. *Circ Res,* **101**, 1292–1299.

Wolin, M. S., Ahmad, M., Gupte, S. A. (2005) Oxidant and redox signaling in vascular oxygen sensing mechanisms: Basic concepts, current controversies, and potential importance of cytosolic NADPH. *Am J Physiol Lung Cell Mol Physiol,* **289**, L159–L173.

Wolin, M. S. (2009) Reactive oxygen species and the control of vascular function. *Am J Physiol Heart Circ Physiol*, **296**, H539-49.

Wu, F., Wilson, J. X., Tyml, K. (2003) Ascorbate inhibits iNOS expression and preserves vasoconstrictor responsiveness in skeletal muscle of septic mice. *AmJ Physiol Regul Integr Comp Physiol*, **285**, R50–R56.

Yamamoto, Y., Klemm, M. F., Edwards, F. R., Suzuki, H.(2001) Intercellular electrical communication among smooth muscle and endothelial cells in guinea-pig mesenteric arterioles. *J Physiol.* **535**:181–195.

Yang, Z., Bochsler, P. N., Carroll, R. C., Carter, C. D., Khemlani, L. S., Breider, M. A. (1994) Signal transduction pathways of bacterial lipopolysaccharide-stimulated bovine vascular endothelial cells. *Inflammation*, **18**, 221–233.

Yashiro, Y., Duling, B. R. (2000) Integrated Ca^{2+} signaling between smooth muscle and endothelium of resistance vessels. *Circ Res* **87**, 1048–1054.

Yogo, K., Ogawa, T., Akiyama, M., Ishida, N., Takeya, T. (2002) Identification and functional analysis of novel phosphorylation sites in Cx43 in rat primary granulosa cells. *FEBS Lett*, **531**, 132- 136.

Zhang, Y. W., Morita, I., Nishida, M., Murota, S. I. (1999) Involvement of tyrosine kinase in the hypoxia/ reoxygenation – induced gap junctional communication abnormality in cultured human umbilical vein endothelial cells. *J.Cell. Phys*, **180**, 305 – 313.

Zhang, Y. W., Morita, I., Zhang, L., Shao, G., Yao, X. S., and Murota, S. (2000a) Screening of anti-hypoxia/reoxygenation agents by an in vitro method. Part 2: Inhibition of tyrosine kinase activation prevented hypoxia/reoxygenation-induced injury in endothelial gap junctional intercellular communication. *Planta Med.* **66,** 119–123.

Zhang, Y. W., Morita, I., Shao, G., Yao, X. S., and Murota, S. (2000b) Screening of anti-hypoxia / reoxygenation agents by an in vitro model. Part 1 : Natural inhibitors for protein tyrosine inase activated by hypoxia/reoxygenation in cultured human umbilical vein endothelial cells. *Planta Medica*, **66**, 114-118.

Zheng-Fischhofer, Q., Ghanem, A., Kim, J. S., Kibschull, M., Schwarz, G., Schwab, J. O., Nagy, J., Winterhager, E., Tiemann, K.,Willecke, K. (2006) Connexin31 cannot functionally replace connexin43 during cardiac morphogenesis in mice. *J Cell Sci,* **119**, 693–701.

Zhou, L., Kasperek, E. M., & Nicholson, B. J. (1999) Dissection of the molecular basis of pp60 (v-Src) induced gating of connexin 43 gap junction channels. *Journal of Cell Biology*, **144,** 1033-1045.

Appendix A:

Criteria used for electrophysiological recordings

In order for a recording to be considered valid the following conditions were obeyed:

1) For both electrodes:

a. The resting membrane potential (E_m) was at least -7 mV and relatively steady (it did not fluctuate more than 2 mV around its mean value).

b. The E_m values of all the recordings within the same experiment were comparable.

c. If the electrode was dislodged prematurely from a cell, it was returned and was attempted to re-insert it into the same cell. If the same E_m was not achieved after re-insertion, the entire recording from the cell was discarded.

2) If current was pulsed when the injecting electrode was not in a cell, and there was a deflection in the recording electrode, then the recording was discarded.

3) If the deflection from an injection that was far away from the recording electrode was bigger than the one closer, or vice versa, the recording was discarded.

4) Recording was considered void if obtained while the electrode resistance was outside the range of 40-90 MΩ.

5) On a given day, only the confluent monolayers with comparable cell density and distribution among and between the control and treated group of cells were selected.

6) Measurements at the edge of the coverslip was avoided in order to ensure that only two-dimensional spread of current was measured.

7) Impalements between different interelectrode distances were done not in a straight line to ensure that any current spread occurred through gap junctions and not through the hole created by the previous impalement/s.

8) Appropriate number of monolayer-covered glass coverslips was simultaneously prepared and randomly assigned to control and treatment groups in order to overcome the possibility of variability in baseline intercellular resistance (e.g., reflecting experiment-to-experiment-variability)

9) If the r^2 value of the linear regression of the deflections versus log (d) was not equal to or greater than 0.80, then the recording was discarded.

10) Positive values of ΔE_m, if obtained, were considered as artifact due to bad electrode and the corresponding recording was discarded.

Appendix B:

MATLAB program used for r_i, R_m and lambda calculations

The following MATLAB program analyzes electrophysiological data collected from monolayers according to the Bessel function model (Shiba, 1971). This program was written by Dr. Hanif Ladak (Department of Medical Biophysics, UWO).

```
function [Ri, ri, lambda, Rm, log10d100, v100, intercept, slope, r2] =
         calcri ( fname, I0, t )
```

---

calcRi Calculates intercellular resistivity (R_i), intercellular resistance (r_i), space constant (lambda), membrane specific resistance (R_m), voltage at interelectrode distance of d=100 um (v100 mV) and log10(d100), as well as slope and intercept of line fitted to v versus log10(d) and the coefficient of determination (r^2).

calcRi(fname) where fname is a string enclosed in single quotes (e.g., 'data.txt') that indicates the file in which d versus v data are stored. The file should be a simple ASCII (i.e., text) file containing one pair of d versus v values per line separated by spaces, e.g., d1v1,d2v2,...dNvN.

When calcRi is called with only a file name, the default values of I0=50e-9 A and t=1.9e-4 cm are used.

calcRi(fname, I0, t) allows the user to specify different values of I0 (in A) and t (in cm).

[Ri, ri, lambda, Rm, log10d100, v100, intercept, slope, r2] = calcRi (fname)
or
[Ri, , lambda, Rm, log10d100, v100, intercept, slope, r2] = calcRi (fname, I0, t)

Return variables in R_i, r_i, etc.

Created by Hanif M. Ladak, March 2002.

***Constants**

```
um2cm = 1.0e-4;                    * 1 um = 1e-4cm
bslope =  -1.43773;                * Slope of Bessel function
binter = 0.112707;                 * Intercept of Bessel function
d100 = 100;                        * Interelectrode distance of 100 um
```

***Check if enough inputs entered**

```
if nargin < 1,
   error ('Forgot to specify name of data file');
end
```

*If include optional arguments of I0 ot t, must include both

```
if nargin == 2,
   error ('Not enough arguments');
end
```

***Use default values of I0 & t?**

```
if nargin ==1,
   IO = 50e-9;                     * Injected current in Amps
    t = 1.9e-4;                    * Thickness of monolayer in cm
end
a = IO/(2*pi*t);                   * Factor for calculations
```

***Read in data**

```
data = load (fname, 'ascii');
d = data (:,1);
logd = log10 (d);
v = data (:,2);
figure
plot (logd, v, 'b')
xlabel ('Log_{10} (d), in um', 'fontweight', 'bold')
ylabel ('v (mv)', 'fontweight', 'bold)
```

***Fit straight line to v vs. logd data**

```
p = polyfit (logd, v, 1);      * p(1) = slope of line, p(2) = intercept
slope = p(1);
intercept = p(2);
```

***Plot fitted line**

```
vfitted = polyval(p, logd);
```

```
hold on, plot(logd, vfitted, 'r'), hold off
legend( 'Data', 'Fittted line')
```

***Calculate coefficient of determination**

```
Dev = v - mean(v);                  * deviations
SST = sum( dev.^2 );                * total variation to be accounted for
Resid = v - vfitted;                * residuals
SSE = sum( resid.^2);               * variation NOT accounted for
r^2 = 1 - SSE/SST;                  * Coefficient of determination
```

***Calculate Ri, ri**

```
Ri = slope/(bslope*a);
ri = Ri/t;
```

***Calculate lambda from value of v at d=100 um**

```
V100 = polyval(p, log10d100);
KO = v100/(a*Ri);                   * Solve for KO(x)
X = 10^( (KO - binter)/bslope );
```

***Calculate membrane specific resistance**

```
Rm = 2 * Ri * lambda^2/t;           * in ohm.um^2
Rm = Rm * um2cm^2;                  * Convert to ohm.cm^2
```

***Display Results**

```
fprintf(1,'Ri (intercellular resistivity) = %f ohm.cm\n', Ri);
fprintf(1,'ri (intercellular  resistance) = %f ohms\n',   ri);
fprintf(1,'Space constant (lambda) = %f \n', lambda);

fprintf(1,'Rm(Membrane specific resistance) = %f ohm.cm^2\n', Rm);

fprintf(1, 'Intercept of straight-line fit to v vs log10(d) = %f\n',
intercept);

fprintf(1,'Slope of straight-line fit to v vs log10(d) = %f\n',
slope);

fprintf(1,'Coefficient of determination, i.e., R squared, = %f\n',
r2);

fprintf(1,'(log10(d), v100) = (%f um, &f mv)\n', log10(d100), v100);
```